UNIVERSITY OF LEEDS

Towards Tasks Autonomy in Robotic Magnetic Endoscopy

Lavinia Barducci

Submitted in accordance with the requirements for the degree of Doctor of Philosophy in Robotics

The University of Leeds

Faculty of Engineering

School of Electronic and Electrical Engineering

May 2022

Intellectual Property and Publication Statements

The candidate confirms that the work submitted is her own, except where work which has formed part of jointly authored publications has been included. The contribution of the candidate and the other authors to this work has been explicitly indicated below. The candidate confirms that appropriate credit has been given within the thesis, where reference has been made to the work of others.

Chapter 2 includes work from a jointly authored publication:
- Fundamentals of the gut for capsule engineers, by Lavinia Barducci, Joseph C. Norton, Sunandita Sarker, Sayeed Mohammed, Ryan Jones, Pietro Valdastri, & Benjamin S Terry, Progress in Biomedical Engineering volume 2, (2020).

Lavinia Barducci worked on the design of the work, the writing and on the design of the figures. Joseph C. Norton worked on to the design and the writing of the work. Sunandita Sarker gave a substantial contribution to the writing of the work. Sayeed Mohammed contributed to the writing and to the design of the figures. Ryan Jones gave substantial contributions to the conception of the work and to the revision of the manuscript. Pietro Valdastri substantively revised the manuscript. Benjamin Terry substantially contributed to the conceptualization of the work and to the revision of the manuscript.

Chapter 4 includes work from two jointly authored publications:
- Magnetic Levitation for Soft-Tethered Capsule Colonoscopy Actuated With a Single Permanent Magnet: A Dynamic Control Approach, by Giovanni Pittiglio*, Lavinia Barducci*, James W. Martin, Joseph C. Norton, Keith L. Obstein, & Pietro Valdastri, IEEE Robotics and Automation Letters volume 4, pages 1224-1231 (2019). G.P. and L.B. co-led the paper.

Giovanni Pittiglio* and Lavinia Barducci* worked on the conceptualization of the work, on the design and validation of experiments and on the writing. James W. Martin gave a contribution to the realization of the experiments and to the writing. Joseph C. Norton contributed to the writing. Keith L. Obstain contributed on clinical perspective, identification of clinical needs. Pietro Valdastri contributed to the

conception of the work and to the revision of the manuscript.

- Adaptive Dynamic Control for Magnetically Actuated Medical Robots, by Lavinia Barducci*, Giovanni Pittiglio*, Joseph C. Norton, Keith L. Obstein, & Pietro Valdastri, IEEE Robotics and Automation Letters volume 4, pages 3633-3640 (2019). G.P. and L.B. co-led the paper.

Lavinia Barducci * and Giovanni Pittiglio * worked on the conceptualization of the work, on the design and validation of the experiments and on the writing. Joseph C. Norton worked on the design and validation of the experiment and contributed to the writing. Keith L. Obstain contributed on clinical perspective, identification of clinical needs. Pietro Valdastri contributed to the conception of the work and to the revision of the manuscript.

Chapter 5 includes work from a jointly authored publication:
- Active Stabilization of Interventional Tasks utilizing a Magnetically Manipulated Endoscope, by Lavinia Barducci, Bruno Scaglioni, James W. Martin, Keith L. Obstein, & Pietro Valdastri, Frontiers in Robotics and AI volume 2, (2022).

Lavinia Barducci worked on the conceptualization of the work, on the experiments and on the writing. Bruno Scaglioni gave a contribution to the design and to the writing of the work. James Martin contributed to the writing of the work. Keith L. Obstein contributed on clinical perspective, identification of clinical needs and critical elements of the task, verification of the accuracy of the clinical aspect of the discussion, critical review and revision of the manuscript. Pietro Valdastri contributed to the conception of the work and to the revision of the manuscript.

An asterisk indicates (co-)leadership.

Signed 

Abbreviations

AGC advanced gastric cancer

AI Artificial Intelligence

BD benign disease

CD Crohn's Disease

CE Capsule Endoscope

CR Continuum robot

CRC Colorectal Cancer

DK Direct Kinematics

DoF Degrees-of-Freedom

EE End Effector

EGC early gastric cancer

EPM External Permanent Magnet

FE Flexible Endoscope

FMEA Failure Mode and Effect Analysis

GI Gastrointestinal

GUI Graphical User Interface

IBD Inflammatory Bowel Disease

IBS Inflammatory Bowel Syndrome

IMU Inertial Measurement Unit

IPM Internal Permanent Magnet

LFT Linear-Fractional transformation

LPV Linear Parameter Varying

LTI Linear Time Invariant

MFE Magnetic Flexible Endoscope

MHRA Medicines and Healthcare products Regulatory Agency

MIMO Multiple-Input Multiple-Output

PID Proportional-Integral-Derivative

ROS Robotic Operating System

UC Ulcerative Colitis

WCE Wireless Capsule Endoscope

Contents

List of Figures

List of Tables

Chapter 1

Introduction

Over the past few decades, technological advances that have enabled the development of innovative medical devices and techniques [1], have drastically changed health-care procedures. Endoscopy and minimally invasive surgeries, such as laparoscopy and natural orifice transluminal endoscopic surgery [2] are the most successful examples of this. By using these devices, surgeons can inspect patients' bodies through natural orifices, leading to a reduction in blood loss, recovery time, and postoperative trauma in comparison to procedures that involve cutting the patient to provide a means to inspect inside the body. Nevertheless, the use of these kind of instruments/procedures can be challenging from the surgeon's perspective because of differences in ergonomic control, sensory feedback, dexterity, and intuitiveness [3].

These limitations combined with the constant drive towards better and improved medical procedures, have pushed the research towards the development of robotic-assisted medical devices. This has enabled physicians to perform surgeries with greater precision, flexibility and control, speeding up procedure completion time and, at the same time, diminishing complications for the patient [4]. Since their inception [5], medical robots have been continuously evolving and the release of the da Vinci Surgical System (Intuitive Surgical, Inc. Sunnyvale, CA, USA) further heightened the interest in this field.

One of the most recent developments in the field was the emergence of flexible and Continuum robots (CRs). While the majority of medical robotic systems in use today rely on rigid instruments with dexterous wrists at the tip, characterized by a low number of Degrees-of-Freedom (DoF) [6] and a consequent restriction in movement capability, CRs are able to generate smooth

curvilinear motions exhibiting infinite DoFs. Therefore, these innovative devices have the potential to reach further into the body with reduced tissue trauma for the patient [6]. In particular, endoluminal procedures have proven effective in reducing the invasiveness of both the diagnosis and the treatment of diseases. These procedures have been successfully introduced in the gastroscopy and colonoscopy (gastro-intestinal tract), bronchoscopy (bronchi), Ear Nose and Throat surgery, intravascular and cardiac operations, to mention a few.

In the context of autonomous robotic systems, control, modelling and sensing stand at the core of the design process whether it is standard rigid-link, flexible or CR. The lack of accurate or appropriate sensing mechanisms, in certain situations, has led researchers to distinguish between different types of control loops. Open-loop, which is based on model inversion, and closed-loop, based on robot actuator feedback control and combined feed-forward control. The last two classes differ in being model-based and model-free [7]. This dissertation presents different classes of closed-loop controllers, which can be applied to both flexible endoscopes and CRs.

1.1 Gastro-Intestinal Endoscopy

Digestive diseases are numerous and potentially severe. The most common of these are the Inflammatory Bowel Syndrome (IBS) and the Inflammatory Bowel Disease (IBD). Moreover, according to the International Agency for Research on Cancer [8, 9], cancer is the leading cause of death in the 21st century. Colorectal Cancer (CRC) is the third most common disease worldwide. The CRC starts with a small, benign mass, named polyp which, if identified in its early stages, can be removed with a survival rate of almost 90%. On the other hand, the survival rate drops drastically to less than 10%, when CRC is diagnosed in its later stages. For this reason early prevention is fundamental.

Several procedures are employed for examining the Gastrointestinal (GI) tract, such as gastroscopy for the inspection of the esophagus and stomach and colonoscopy for the colon. The colonoscope is a Flexible Endoscope (FE), that allows for visual inspection of the colon, tissue biopsies and polyps removal. However, the aged design of FEs requires lengthy and expensive training for the clinicians which has led to a shortage of gastroenterologists with respect to the high demand. In addition, issues around the invasiveness of FEs, due to the aged design and the method of actuation, cause tissue stretching and, thus, discomfort for the patient. This discourages patients from attending this potentially life-saving procedure [10]. Therefore, de-

spite the widespread adoption of the conventional FEs, the demand for less invasive, innovative procedures has increased [11, 12].

Robotic endoscope solutions claim to overcome the main limitation of conventional FEs. The adoption of robotic endoscopic procedures, which aim to reduce pain and discomfort for the patient, generally lead to a reduction in the need for sedation and recovery time. This results in a increase in the number of patients inclined to undergo endoscopic procedures.

In particular, magnetically actuated robots have been investigated in the last two decades [12, 13] with the main advantage of potential miniaturization and minimal invasiveness. The concept of magnetic endoscopy consists of using either coil-based systems [14–20], rotating permanent magnet-based systems [21, 22] or permanent magnet-based systems [23–27]. The permanent magnet-based devices have the advantage of compact size and low energy consumption. On-the-other-hand, the lack of direct control over the intensity of the magnetic field and its gradient leads to reduced controllability of the system. Therefore, the choice of suitable control techniques, relative to the specific task to be performed, is crucial.

The work in this thesis makes use of a single permanent magnet attached to the End Effector (EE) of a robotic manipulator. Magnetic forces and torques are used, in this context, to steer and navigate a magnetic endoscope through the GI tract. However, due to the non-intuitive nature of the magnetic fields, the implementation of an intelligent and suitable control approach is necessary. The work in this thesis seeks to overcome this issue.

1.2 Motivation

The need to explore innovative, less-invasive technologies and autonomy in medical robots motivated the work of different groups of researchers. In particular, in the colonoscopy field, preliminary studies have confirmed the promise of new technologies [23], such as the magnetic robotic colonoscopy [25]. However, performance of these new medical robots is limited by the complexity related to the control of the robots. My research was therefore motivated by the need to enhance the usability of the system by pursuing more sophisticated control techniques. The development of these new technologies would improve the performance of these systems, hopefully aiding their transfer into a clinical setting in the near future.

The first section of this dissertation presents a comprehensive literature review on the GI tract.

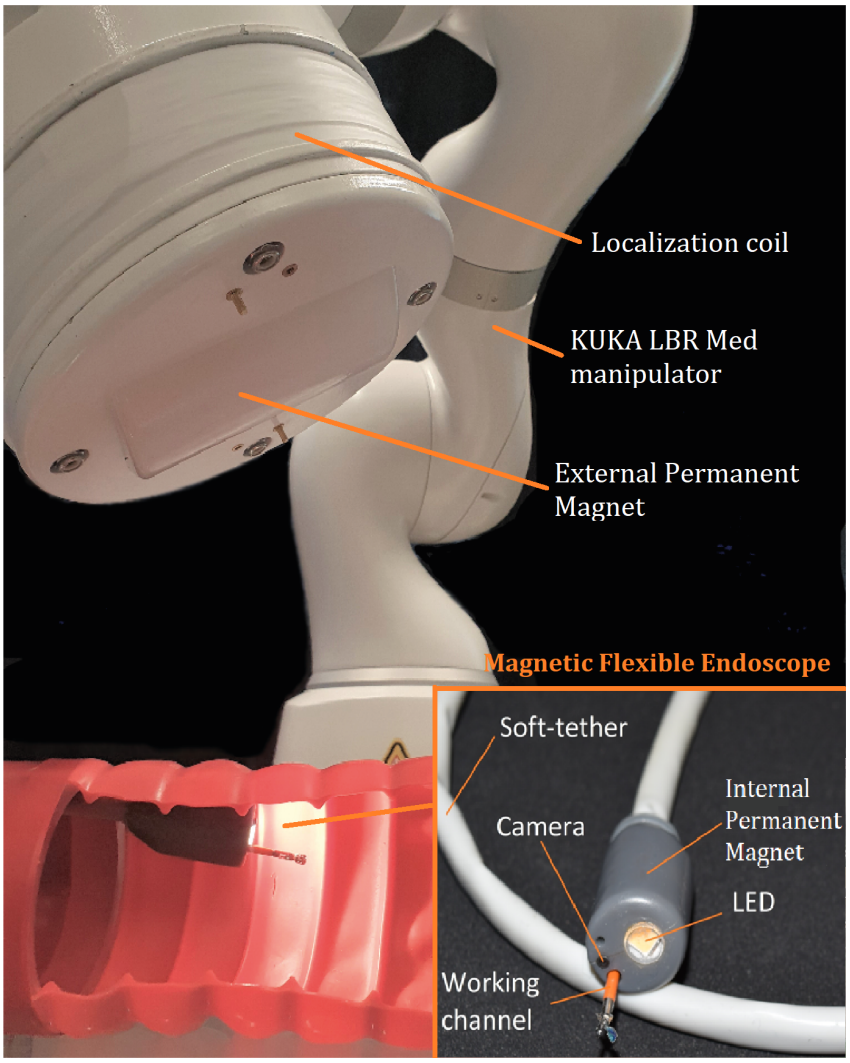

Figure 1.1: Overview of the Magnetic Flexible Endoscope system.

This work was motivated to provide engineers in the field with a broad reference manual comprehensive of the main anatomical, biological, chemical and mechanical characteristics of the GI environment. This literature review allows researchers to understand the challenges associated with developing new and innovative devices for the GI environment. This work along with major clinical needs in the field of medical diagnostics shaped the foundation of my research, which was developed and tested on the Magnetic Flexible Endoscope (MFE) platform (Figure 1.1) for colonoscopy. The MFE platform is composed of a soft-tether endoscopic capsule containing an Internal Permanent Magnet (IPM) actuated by employing a robotically manipulated External Permanent Magnet (EPM).

In fact, the limitations of the inherited control strategy [28, 29], implemented on the MFE platform by the previous group, motivated the research into new and more suitable control techniques to achieve better performance for each task. More specifically, my research was

divided in two main topics, the navigation of the magnetic endoscope inside the colon and the stabilization of the magnetic endoscope during interventional tasks, such as biopsy or polyp removal. The former was carried out by achieving the magnetic levitation of the endoscope, and the latter using a linear model-based control.

One limitation of inherited control techniques is the fact that the endoscope is in continuous contact with the colon wall. This may cause the endoscope to remain trapped into the colon folds and may hinder locomotion. Successful magnetic levitation of the endoscope would therefore enhance the navigation of the endoscope inside the patient's body by reducing contact with the environment. This is particularly important in the case of patients with chronic diseases of the colon whose colons are characterized by a fragile and delicate mucosa.

On-the-other-hand, the active stabilization of the endoscope during interventional tasks (i.e. biopsies, polyp removal or clip placement) would help to improve the accuracy of the task and to reduce the burden on the clinicians. To date, no examples of active endoscope stabilization for magnetically manipulated endoscopes have been found in literature.

1.3 Contributions

This section details the contributions of this work to the field of robotic endoscopy. The main contribution of the research presented in this dissertation is the development of advanced control strategies for manipulation of magnetically actuated medical robots. The research has been principally motivated by the main clinical need in the medical field of diagnostics.

The main research questions that formed the basis of the work presented in this thesis were:

- Would a suitable control approach enhance the navigation of the MFE inside the colon and improve the overall patient colonoscopy experience?
- The integration of diagnostic and interventional tasks within the MFE would allow the platform to be considered comparable to the standard colonoscopy. How could interventional routines be integrated in the MFE platform?
- Would the stabilization of the MFE enhance the accuracy during precision tasks such as biopsies or polyp removal?
- What are the next steps for improving the overall platform?

During my three years as a PhD. student, I worked to find an answer to these problems and contribute to their resolution.

In this thesis, Chapters 2, 4 and 5 correspond to the papers published during the three years of PhD. The papers used for these chapters are summarized in the following.

Literature review

The inspection of the GI tract is fundamental for the early detection and diagnosis of GI diseases, which are numerous and widespread. In the last decade, miniaturized robots for gastrointestinal inspection have been investigated with the aim of developing innovative, more sophisticated, and minimally invasive technologies to access this part of the body. Despite significant progress, the need for innovation is stronger than ever due to the combination of a growing disease prevalence and the harsh, difficult-to-access environment of the gut. To address limitations and develop innovative and more sophisticated technologies for diagnoses and therapy of the GI tract, researchers are pursuing novel designs and innovative strategies to enhance the physician's ability to treat GI diseases. Miniaturized devices with advanced locomotion techniques and sensing technologies have been at the forefront in achieving this. In order to develop new devices, capsule engineers need to understand the complex environment of the GI tract. The purpose of this chapter is therefore to provide a summary of the critical information regarding the anatomy, histology, physiology, mechanics, and chemistry of the gut as it pertains to medical device engineers. Providing a comprehensive primer of the GI tract can help engineers in this field to speed up the development of innovative technologies.

Relevant publications:

Barducci, L., Norton, J. C., Sarker, S., Mohammed, S., Jones, R., Valdastri, P., Terry, B. S. (2020). Fundamentals of the gut for capsule engineers. Progress in Biomedical Engineering, 2(4), 42002. https://doi.org/10.1088/2516-1091/abab4c

Improving magnetic endoscope navigation

A satisfying closed-loop control approach allows the clinician to navigate the endoscope inside the body, using only information from the camera, without knowing its pose. The main limitation of the inherited closed-loop control [28, 29], implemented by the previous group, is the continuous attraction between the two magnets, due to the lack of control along the gravity

direction. This may cause the endoscope to remain trapped in the anatomical environment and, thus, hinder the locomotion of the endoscope.

In this scenario, magnetic levitation of the endoscope would overcome the main limitation of the previous closed-loop control by adding the control of the 5^{th} DoF, the linear position along the gravity direction and an internal loop that aims at converging the actual force to the desired one, intended to enhance the stability of the control system. Magnetic levitation of the endoscope was achieved with two different control strategies, detailed in the following chapters. The performance of the magnetic levitation was compared with the previous inherited closed-loop control, in terms of contact with the colon wall and mean completion time to perform a colonoscopy. Different experimental environments, free space and training simulator colon phantom, were used to show the results.

Relevant publications:

Pittiglio, G., Barducci, L., Martin, J. W., Norton, J. C., Avizzano, C. A., Obstein, K. L., Valdastri, P., "Magnetic Levitation for Soft-Tethered Capsule Colonoscopy Actuated With a Single Permanent Magnet: A Dynamic Control Approach," in IEEE Robotics and Automation Letters, vol. 4, no. 2, pp. 1224-1231, April 2019, doi: 10.1109/LRA.2019.2894907.

Barducci, L., Pittiglio, G., Norton, J. C., Obstein, K.L., Valdastri, P., "Adaptive Dynamic Control for Magnetically Actuated Medical Robots," in IEEE Robotics and Automation Letters, vol. 4, no. 4, pp. 3633-3640, Oct. 2019, doi: 10.1109/LRA.2019.2928761.

Enhanced diagnostic and interventional tasks

To date, the control of magnetic endoscopes for colonoscopy has mainly been focused on navigation, with the aim of increasing the level of autonomy and reducing operator burden [30, 31]; however, interventional tasks such as biopsy, polyp removal, and clip placement are also extremely common in colonoscopy. Of these, the most performed is biopsy, in which an endoscopic instrument is introduced through the operative channel of the endoscope and passed into the colon, where a tissue sample is collected. Conventionally, during a biopsy routine the physician maintains stability of the endoscope's orientation while an assistant inserts the biopsy forceps. Maintaining the correct alignment of the endoscopic instrument to the target is therefore necessary to obtain the tissue sample. The ability to autonomously control the endoscope's orientation during the biopsy procedure would allow the physician to perform a biopsy without

the presence of another operator. This could potentially improve the technical burden of the procedure and the accuracy of the biopsy.

A model-based control, able to actively stabilize the endoscope's viewpoint at different inter-magnetic distances between IPM and EPM, allows for the closed-loop system to be optimized for each condition, achieving a general robust stability. Consequently, this permits the reduction of orientation error of the IPM by enhancing the overall procedure. The strategy used to stabilize the MFE was validated on a training simulator colon phantom and compared with the previous inherited closed-loop control.

Relevant publications:

Barducci, L., Scaglioni, B., Martin, J., Obstein, K. L., Valdastri, P. (2022). Active Stabilization of Interventional Tasks Utilizing a Magnetically Manipulated Endoscope. Frontiers in Robotics and AI, 9. https://doi.org/10.3389/frobt.2022.854081

Clinical study

After years of research on the MFE platform, the research group has been awarded funding for a pilot "clinical study". In this context, the platform must be revised and developed to meet the standards required by the notified body in order to obtain the Medicines and Healthcare products Regulatory Agency (MHRA) certification. This has led to a regulatory (Risk Analysis) and developmental process. This means embedding development of the platform in a quality control and assurance context and, thus, following codified development protocols. The quality management of the system includes testing at high level the entire platform and its main parts. The purpose of quality management is to guarantee that every time a process is performed, the same information, methods, skills and controls are used and applied in a consistent manner. If there are process issues or opportunities, this is then fed into the quality management system to ensure continuous improvement. In this context, my work in collaboration with the software team, mainly focused on developing and testing compliant medical code.

1.4 Thesis structure

The body of this thesis is organized into 6 chapters. Chapter 2 provides an in-depth literature review of the main properties of the GI tract, aiming to provide a comprehensive reference manual to engineers in the medical robotics field. Chapter 3 provides a complete description of

the MFE platform and its main components. The main technical contributions of this thesis are highlighted in Chapter 4 and 5, where new control techniques for the navigation and stabilization of the MFE are presented in detail. Chapter 6 provides a brief overview of the work done to transition the project into the first-in-human clinical trial. Chapter 7 then concludes by discussing the results and future directions of this work.

Chapter 2 - Fundamentals of the gut for capsule engineers

This chapter contains an in-depth literature review on the GI tract, providing the fundamental information regarding the anatomy, histology, physiology, mechanics, and chemistry as it pertains to engineers who wish to develop devices that operate within the GI region. The current state of endoscopy is introduced, as well as their main limitations that robotics aims to improve. The main aim of the review is to speed up the development of more effective and innovative mechatronic devices that operate within the GI tract.

Chapter 3 - The MFE: Magnetic Flexible Endoscope Platform

Herein, the MFE platform is introduced and described in detail, as well as the clinical motivations that led to the development of this platform. The localization algorithm for the magnetic endoscope is explained as well as the basics of the magnetic model used and the nomenclature adopted in this thesis.

Chapter 4 - Magnetic levitation for soft-tethered capsule colonoscopy

In this chapter, a successful levitation of the MFE is achieved, implementing two different control strategies. The levitation of the MFE is, here, introduced to overcome the main limitations of the pre-existing closed-loop control, such as the continuous attraction between the two magnets which prevents the endoscope from a smooth navigation of the colon. The experimental evaluation is done on bench-top and our methods are compared with the inherited control in terms of force applied on the gravity direction and, thus, contact of the endoscope with the environment as well as mean completion time to perform a colonoscopy.

Chapter 5 - Active stabilization for interventional tasks

Another important component of the colonoscopy is the ability to perform diagnostic and therapeutic tasks, such as biopsy and polyp removal. In fact, the possibility of performing interven-

tional tasks with magnetic endoscopes allows the MFE platform to be considered as a worthy replacement for the standard colonoscopy. In this chapter, a model-based linear controller is implemented in order to stabilize the endoscope in the presence of external disturbances, such as the insertion of the biopsy instrument through the endoscope working channel. This approach is again evaluated on bench-top and compared with the inherited closed-loop control.

Chapter 6 - Working towards clinical trials of the robotic colonoscopy platform

The next stage for the MFE platform is the first-in-human clinical trials. With this goal, the software team has worked on the quality management of the platform and on developing, testing and performing validation of software components. This is beneficial in obtaining the MHRA certification and achieving a better clinical trial outcome.

Chapter 7 - Conclusion and future directions

The findings of the work presented in this thesis are summarized and discussed in this chapter, along with limitations of the proposed solutions and possible future directions that could build upon this research.

Chapter 2

Fundamentals of the gut for capsule engineers

Chapter source: Fundamentals of the gut for capsule engineers, by Lavinia Barducci, Joseph C. Norton, Sunandita Sarker, Sayeed Mohammed, Ryan Jones, Pietro Valdastri, & Benjamin S Terry, Progress in Biomedical Engineering volume 2, (2020).

2.1 Abstract

The Gastrointestinal (GI) tract is a complex environment comprised of the mouth, esophagus, stomach, small and large intestines, rectum and anus, which all cooperate to form the complete working GI system. Access to the GI using endoscopy has been augmented over the past several decades by swallowable diagnostic electromechanical devices, such as pill cameras. Research continues today and into the foreseeable future on new and more capable miniature devices for the purposes of systemic drug delivery, therapy, tissue biopsy, microbiome sampling, and a host of other novel ground-breaking applications. The purpose of this review is to provide engineers in this field a comprehensive reference manual of the GI environment and its complex physical, biological, and chemical characteristics so they can more quickly understand the constraints and challenges associated with developing devices for the GI space. To accomplish this, the work reviews and summarizes a broad spectrum of literature covering the main anatomical and physiological properties of the GI tract that are pertinent to successful development and operation of an electromechanical device. Each organ in the GI is discussed in this context,

including the main mechanisms of digestion, chemical and mechanical processes that could impact devices, and GI motor behavior and resultant forces that may be experienced by objects as they move through the environment of the gut.

2.2 Introduction

The digestive system is made up of the GI tract, liver, pancreas and gallbladder. The GI tract is a large, hollow, tubular organ system that extends from the mouth to the anus. It is a complex environment that comprises the mouth, esophagus, stomach, small and large intestines. These organs have specific functions and they cooperate in order to form a complete working GI tract. The coordinated contractions of muscles, along with the release of hormones and enzymes facilitate the digestion of food, the absorption of nutrients, and the elimination of waste so that the body can carry out its functions of metabolism, growth, and repair [32].

The inspection of the GI tract is fundamental for the early detection and diagnosis of GI diseases, of which there are many. In the last decade, miniaturized robots for gastrointestinal inspection have been investigated with the aim of developing innovative, more sophisticated, and minimally invasive technologies to access this part of the body. Despite the progress achieved so far, the need for innovation is still present and stronger than ever due to the combination of a growing disease prevalence and the harsh, difficult-to-access environment of the gut.

According to the National Institutes of Health, more than 34 million Americans are suffering from diseases of the digestive system, 20 million of which have chronic disorders [33]. Digestive diseases encompass more than 40 acute, chronic, recurrent, or functional disorders. The most common digestive diseases are irritable Inflammatory Bowel Syndrome (IBS), Inflammatory Bowel Disease (IBD) (i.e. Crohn's Disease (CD) and Ulcerative Colitis (UC)), celiac disease, diverticulosis, and acid reflux. It is estimated that 8% of the U.S. population have chronic digestive diseases, 6% have acute episodes of digestive diseases, and 43% have intermittent digestive disorders. Only 43% are unaffected. As a group, digestive diseases account for 8%–9% of total U.S. mortality, of which 60% is due to malignant neoplasms and 40% due to non-malignant causes [34].

According to the International Agency for Research on Cancer [35], cancer is the leading cause of death in the 21st century. The statistics present some important data about the spreading of

cancer worldwide in 2018. Regarding colorectal cancer, the percentage of new cases was 6.1% and the percentage of deaths was 5.8%, while rectal cancer had a 3.9% incidence of new cases and 3.2% of deaths. Considering the stomach, the percentages were 5.7% and 8.2% of new cases and the number of deaths, respectively, while esophagus cancer counted 3.2% of new cases and 5.3% of deaths in 2018. The International Agency for Research on Cancer [35] also reports statistics about the estimated number of new cases (incidence rate, IR) and estimated number of deaths (mortality rate, MR) of each type of gastrointestinal cancer in different countries in 2018. These are reported in (2.1), where the estimated number has been rounded to the nearest one hundred for the sake of clarity.

Table 2.1: Incidence and mortality of gastrointestinal cancer in 2018 [35].

	North America		**Europe**		**Asia**		**Africa**	
	IR	**MR**	**IR**	**MR**	**IR**	**MR**	**IR**	**MR**
Colon	179 800	64 100	499 700	242 500	957 900	461 400	61 800	40 000
Stomach	29 300	13 400	133 300	102 200	769 700	584 400	31 100	28 700
Esophagus	22 700	18 200	53 000	45 100	444 600	397 700	28 500	27 700

Different procedures are used for examining the GI tract: capsule endoscopies are used to inspect the entire GI tract because of their small size, while other types of endoscopic procedures are used to inspect a particular organ. For example, gastroscopy is employed for the inspection of the esophagus and stomach, colonoscopy for the colon, sigmoidoscopy for the sigmoid colon and small bowel enteroscopy is used for the examination of the small intestine. The purposes of the devices are typically for both diagnosis and therapy, however, some lack therapeutic capabilities because of device size constraints. Despite the ubiquity of these procedures, they can be stressful and painful for the patient [25, 32] due largely to the construction of the endoscopes, which consist of semi-rigid tubes that are pushed and twisted through the body of the patient by the physician, causing discomfort as the instrument deforms the sensitive GI tract.

According to the Center for Disease Control and Prevention [36], only 66% of Americans comply with screening guidelines, and therefore, an estimated 23 million people in the United States avoid these procedures. This lack of intervention increases the risk of developing a cancer [10]. Introducing a less–invasive procedure could increase patient compliance to the endoscopic procedure by reducing procedural discomfort (and the associated anxiety), risk of adverse events, and the potential need for sedation [11, 37]. This has motivated many to develop new technologies to replace the standard flexible endoscope [12].

To develop new and more sophisticated devices, capsule engineers need to understand this complex environment. Therefore, the purpose of this paper is to provide a summary of the critical information regarding the anatomy, histology, physiology, mechanics, and chemistry of the gut as it pertains to medical device engineers. Providing a comprehensive primer of the GI tract can help engineers in this field to speed the development of innovative technologies.

The paper will describe the characteristics of the esophagus, stomach, small and large intestines — the regions of primary interest to engineers that develop Capsule Endoscope (CE) and similar devices. Given that capsules are typically designed to travel the GI tract, the liver, pancreas and gallbladder are not the main focus of our research but are described briefly since their enzymatic secretions help with the digestion of the food. Although, focus is placed on providing a comprehensive description of the healthy GI tract, the most common ways disease impacts its properties and function is also discussed briefly.

The paper is organized as follows. In section 2.3 we briefly summarize the current non-invasive technologies and we discuss their main limitations. In sections 2.4 and 2.5, we first provide a general description of the anatomy and histology of the GI tract. In sections 2.6 and 2.7 respectively, we present the chemical and mechanical properties of the GI tract, and in section 2.8 we investigate the motor behavior of the gut. In section 2.9 we summarize all the forces that act on an untethered device in order to understand the capsule dynamics within the GI tract. Section 2.10 considers the possible physiological alterations to the GI tract from the most common and severe digestive diseases. Finally, in section 2.11 we summarize the work, and we briefly discuss open challenges about medical robotic devices; more detailed discussions related to each topic of the paper are included throughout the article.

2.3 Current non-invasive endoscopic technologies

Conventional flexible endoscopy (e.g. colonoscopy) has been widely used to inspect the entire GI tract. However, despite the widespread adoption of endoscopes, issues around their invasiveness lead to limitation in their ability to diagnose and treat GI disease. Therefore, the demand for new, less invasive and more sophisticated procedures has increased. In the last decades, completely minimally invasive methods have become commercially available for diagnosing the GI tract [38] and researchers have studied appealing non-invasive alternatives to traditional diagnostic techniques. The new technologies are briefly discussed in the following, highlighting

the major advantage and disadvantages of each technique.

Virtual endoscopy is a technique based on computed tomography (CT) or on magnetic resonance imaging, and is used to inspect the GI tract [25, 39, 40]. Despite it being completely noninvasive and almost comparable to standard endoscopy in terms of diagnostic yield, its main drawbacks are an inability to biopsy, impossibility to deliver in-situ therapy and limited accuracy, particularly with small or very flat lesions.

Similarly, in the last 20 years, swallowable CEs have been developed and commercialized to facilitate minimally invasive exploration of hard–to–reach regions of the GI tract. To date, the most prevalent clinically used CEs worldwide are reported in table 2.2 [13, 25, 42, 43].

Despite encouraging results obtained by current CE technologies, their main limitation lies in the fact that their sensitivity (the proportion of positive cases correctly identified) is not yet comparable to the sensitivity of the standard endoscopes. For example, the sensitivity of the PillCam, the most advanced capsule developed, is still less than 90%, while standard endoscopes can reach in excess of 95% sensitivity [12, 44]. Other important limitations are [12, 13]:

- Passive locomotion: the physician is not able to control the pose of the capsule (or orientation of the camera) which leads to inadequate inspection of the organ in some cases.
- Minor interventions (e.g. Biopsy collection) are the main advantage of standard endoscopes and are not currently possible with commercial CEs. This is largely due to a lack of device position control, limited on-board space (or payload), and the absence of a stable platform.
- No means of insufflation: the inability to distend collapsed tissue may lead to reduced visibility, particularly in the cavernous environments of the stomach and colon.

Several solutions have been developed for enabling active locomotion capsules and thus overcome the main limitations of passive locomotion. Fundamentally, two major solutions have been exploited to address the active locomotion problem: onboard locomotion (generally this is referred as a mechanical approach) and an external locomotion technique (whereby forces and torques are transmitted to the capsule from outside the body, generally via magnetic fields) [12, 41, 45, 46].

In the last decades, a new category of flexible endoscopes has been explored by researchers.

Table 2.2: GI capsules in clinical use today [12, 41–43].

	PillCam ESO3	PillCam COLON2	Endo Capsule	Capso Cam	Miro Cam	OMOM	Navi Cam
Purpose	Esophageal imaging	Colon imaging	Small bowel imaging	Small bowel imaging	Small bowel imaging and navigation	Small bowel imaging	Stomach imaging and navigation
Dimension (mm)	26.0×11.0	31.5×11.6	26.0×11.0	31.0×11.3	24.0×11.0	27.9×13.0	28.0×12.0
Weight (g)	3.4	2.9	3.8	4.0	3.4	6.0	5.0
Frame rate	Adaptive Frame Rate (AFR): 2–6 images per second.	Adaptive Frame Rate (AFR): 2–6 images per second.	2 fps	4 high resolution camera: maximum of 20 fps (5 fps per camera)	3 fps	0.5-2 fps	2 fps
Angle of view	160 deg	160 deg	160 deg	360 deg	170 deg	140 deg	140 deg
Illumination	2×6 white LEDs	2×6 white LEDs	6 white LEDs	LEDs	6 white LEDs	6 white LEDs	LED
Recording time	30 min	10 h	9 h	15 h	11 h	7-9 h	8 h
Regulatory approval	Yes	Yes	Yes	No	Yes	Yes	Yes

These advanced flexible endoscopes, or soft-tethered capsules, are designed to preserve the major functionalities of conventional endoscopy that are familiar to physicians. At the same time, the flexibility of the endoscope body permits it to conform to the shape of the bowel, reducing tissue stretching and the associated discomfort for the patient [47, 48].

Advanced flexible endoscopes have the advantage of overcoming the main limitations related to the CEs [49–51]. The advantage of an actuation mechanism, such as the magnetic field, is the ability to pull and steer the endoscope inside the body and so completely inspect the organ. Moreover, the tether (with cables and lumen) allows the physician to use the endoscope both as a diagnostic or therapeutic instrument, and with all the typical auxiliary functions such as insufflation, irrigation and suction. However, the presence of the tether (although soft and flexible) creates friction in the environment and makes locomotion challenging [25]. Other research has addressed the problem of drag on the soft tether by modifying the locomotion strategy [52].

Aside from standard diagnostic routine, capsule robots are being used as a platform for versatile applications such as drug delivery, biosensing, and active diagnostics and intervention [53]. Researchers have measured pH, core body temperature, oxygenation, electric conductivity and, also, blood inside the intestine via capsule robots. These have extended the boundary towards intervention and therapeutic manipulation [54]. Clip deployment for stopping bleeding, systemic and topical drug delivery, biopsy tissue collection and micro-ultrasound imaging are some other applications being investigate. Even though interventional capsules are mostly at the proof–of–concept stage of development, in-vivo animal studies, and benchtop experiment results are encouraging [24, 55–57].

Despite the advance in current technologies the need for novel designs and innovative strategies to enhance the physician's ability to diagnose and treat GI diseases is still present. Miniaturized, capsule-like devices with advanced locomotion techniques and sensing technologies have been at the forefront in achieving this. For this reason, an adequate knowledge of the entire GI tract is mandatory for all the engineers in the medical and endoscopic field.

2.4 Anatomy and physiology of the GI

The human GI tract is a series of multilayered, tubular organs which extend from the oral cavity through the esophagus, stomach, small and large intestines and terminating at the anus (figure 2.1). The GI tract has a total average length of 795 ± 128 cm, it decreases with age and is significantly longer in men [58]. The GI tract is one of the most dynamic organ systems [59]; muscular contractions, along with the release of hormones and enzymes, enable the digestion process [60, 61]. In this section, the anatomy of the GI tract will be discussed, focusing on the esophagus, stomach, small and large intestine and the mesentery. The liver, gallbladder and pancreas, are not the focus of this work but will be discussed briefly for the sake of clarity.

2.4.1 Esophagus

The esophagus is an 18–25 cm long muscular tube that connects the oral cavity to the stomach [61–63]. It is a dynamic tube which serves to propel food, via active peristaltic contractions, toward the stomach for continued digestion and absorption of nutrients. When empty, the esophagus is a collapsed lumen, but it can distend to approximately 2–3 cm to propel a food bolus [63, 64].

In general, the ease of passage of a body through the esophagus and into the stomach depends on the length and diameter of the ingested object. Bodies longer than 60 mm and with a diameter more than 25 mm make the passage difficult and objects can become lodged; in these cases an esophagogastroscopy is necessary [65–67]. However, the current swallowable capsules approved by the FDA present smaller values for diameter and length and give a more ideal target size. These values are presented in table 2.2.

The passage of food through the esophagus is regulated by two principal high–pressure valves: the upper and the lower sphincter. These two valves are located at the beginning and at the end of the esophagus, but there is not a clear anatomic demarcation that defines the two zones [64]. The upper esophageal sphincter controls the movement of food from the pharynx into the esophagus, while the lower esophageal sphincter (also called gastroesophageal or cardiac sphincter) lets food pass into the stomach; the latter can also contract to prevent stomach acids from backing up into the esophagus [64].

The normal esophagus has a wall thickness of 4.7 mm (range 4.44–4.95 mm) during contrac-

tion and 2.11 mm (range 2.00–2.23 mm) when the esophagus is dilated. The thickness of the esophageal wall depends also on the sex and age of the patient [68, 69].

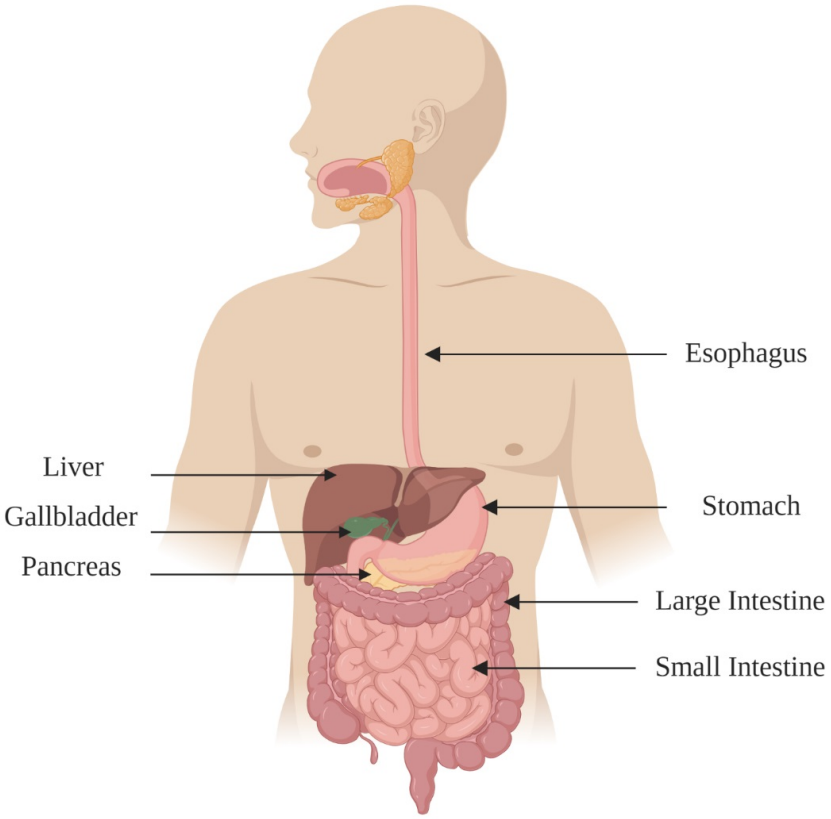

Figure 2.1: Anatomy of the digestive system, showing all organs.

2.4.2 Stomach

The stomach is a dilated and J-shaped organ that rests on the left of the central region of the abdomen at the level of the first lumbar vertebra [60]. The main functions of the stomach are the temporary storage, mixing, breakdown, and digestion of food [70].

As shown in figure 2.2, the stomach has two openings (esophageal and the duodenal) and five major regions, including: the cardia, fundus, body, antrum and the pylorus [63]. The cardia is the point where the esophagus connects to the stomach. The fundus is dome shaped and locates inferior to the diaphragm, above and to the left of the cardia. Below the fundus is the 'body', the main part of the stomach. The pylorus is a funnel-shaped valve which connects the stomach to the duodenum [70]. The pylorus has two parts: the pyloric antrum, which is connected to the body of the stomach, and the pyloric canal, which is connected to the duodenum. The smooth muscle pyloric sphincter is located at this latter point of connection and controls stomach emptying. The pyloric diameter is controlled by the contractions of the

sphincter and this determines the flow resistance [71].

Each region of the stomach has a different function: the fundus can relax to accept large volumes of collected digestive gases; the gastric chief cell in the stomach secretes pepsinogen and hydrochloric acid, produced by gastric parietal cells, to break–down and mix the food and liquid; the pylorus is responsible for mucus, protein–digesting enzyme (pepsin) secretion, and handles the emptying of the stomach through the duodenum [70].

Stomach emptying is an essential factor that capsule engineers should consider. Although the stomach volume is only 0.8 l when empty, it can expand up to 1.5–2 l for a typical male and up to 0.9–1.5 l for women and children. The emptying rate is affected by meal composition and consistency [72], body position [73], smoking [74] and gender [75]. On average, women have a slower gastric emptying compared to men (74 min vs. 63 min) and smokers have a significantly faster gastric emptying compared to non–smokers (56 min vs. 67 min). Age, body mass and alcohol consumption habits are not known to affect gastric emptying times [76].

The mean thickness of the gastric wall was measured as 4 mm when distended and 5–10 mm during fasting [77]. In studies done by Huh et al [78] endoscopic ultrasound was used to acquire in-vivo data on wall thickness of the stomach when it was waterfilled (i.e. distended). The measurements were taken in a group of ten and five measurements in different locations were obtained resulting in a mean thickness of 3.92 ± 0.16 mm.

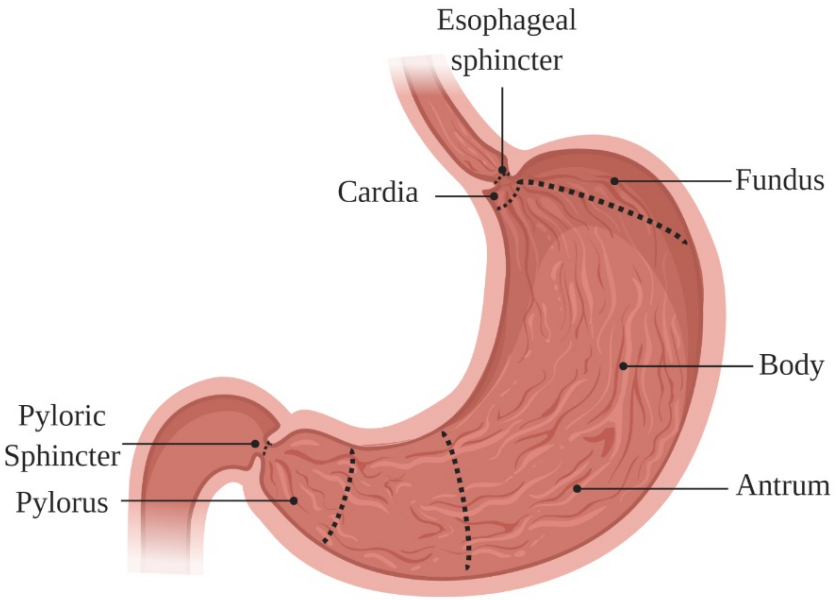

Figure 2.2: The functional regions of the stomach.

2.4.3 Small intestine

The small intestine (or small bowel) is a crucial component of the digestive system and is responsible for the absorption of important nutrients [63]. Here, most of the chemical and mechanical digestion is carried out [79]. It is a long, approximately 6 m, continuous, and highly tortuous tube running from the pylorus of the stomach to the ileocecal valve where it meets the large intestine. There are three main sections to the small intestine: duodenum, jejunum and ileum [63]. These sections, described below, are shown in figure 2.3.

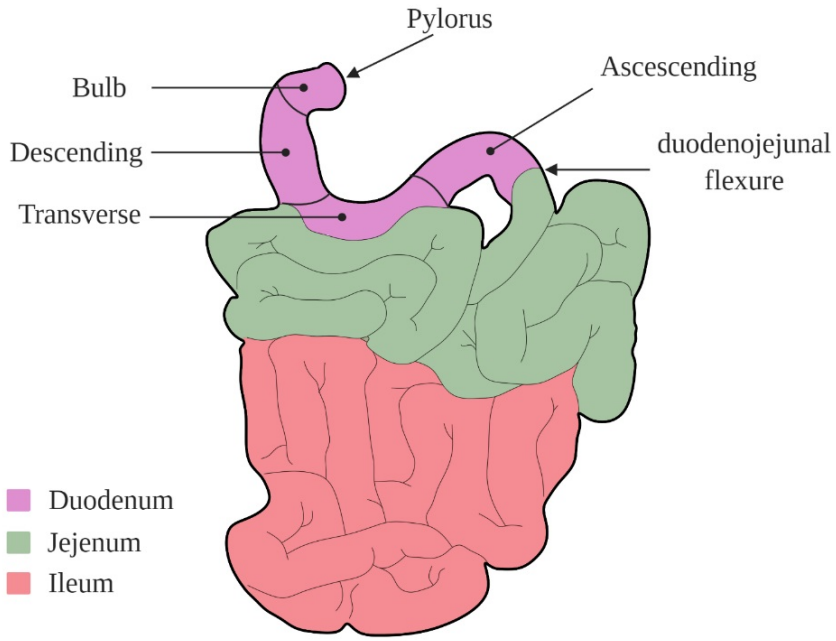

Figure 2.3: Small intestine.

The duodenum is the first section of the small intestine and forms a 'C' shape around the head of the pancreas. Its main function is to neutralize the acidic gastric contents (called 'chyme') and to initiate further digestion [80]. Brunner's glands in the submucosa secrete an alkaline mucus which neutralizes the chyme and protects the surface of the duodenum. It is about 25 cm in length in adults, beginning at the pylorus and ending at the ligament of Treitz, which is the junction between the duodenum and jejunum (duodenojejunal flexure) [80, 81] (figure 2.3). The duodenum is largely retroperitoneal and has an anatomic relationship with the pancreas. It has four sections: bulb, descending, transverse, and ascending. The bulb section begins at the pylorus, which is approximately 5 cm in length for adults and demarcated by the pre-pyloric vein. The descending section is retroperitoneal and is approximately 10 cm in length. The transverse section is also retroperitoneal and is bordered by the pancreas superiorly and the hepatic flexure of the colon anteriorly. The fourth portion of the duodenum courses in a cephalad direction

to the left of the aorta and inferior to the neck of the pancreas. The duodenum contains a slender band of skeletal muscle and a fibromuscular band of smooth muscle in the horizontal and ascending parts. These can contract to widen the angle of the duodenojejunal flexure and allow movement of intestinal contents [81].

The jejunum and ileum lie within the peritoneal cavity and are the most tortuous parts of the small intestine. Together, they are approximately 4–6 m long comprising approximately 40% jejunum and 60% ileum [80] with no clear junction between the two sections. Generally, the jejunum has a thicker mucosal lining (i.e. thicker wall), larger diameters, redder color, and less fatty mesentery than the ileum. Moreover, the mesentery of the jejunum is attached to the left of the aorta while the mesentery of the ileum is attached to the right [82]. The mucosa of these sections is highly folded. These folds, called plicae circulares, slow the passage of the partly digested food and increase the surface area (by 1.6 times) to aid absorption of nutrients [62]. The majority of plicae extends transversely around the small intestine for about 50%–65% of its circumference while some of these form complete circles and others are spiral. The largest folds are about 1 cm in depth at their broadest part and usually the large and small folds alternate with each other [82].

Table 2.3: Mean and standard deviation values for the small intestine parameters (diameter, wall thickness, fold number per 2.5 cm, fold thickness) [62, 83].

	Diameter (mm)	Wall thickness (mm)	Fold number per 2.5 cm	Fold thickness (mm)	Interfold distance (mm)
Duodenum	24.8 ± 4.5	1.5 ± 0.6	4.5 ± 0.7	2.1 ± 0.6	4.7 ± 1.54
Jejunum	24.5 ± 4.2	1.5 ± 0.5	4.6 ± 0.8	2.2 ± 0.7	4.59 ± 3.56
Proximal ileum	19.5 ± 3.6	1.6 ± 0.4	1.8 ± 0.6	1.9 ± 0.5	16.8 ± 6.75
Distal ileum	18.9 ± 4.2	1.4 ± 0.5	1.6 ± 0.5	1.8 ± 0.5	18.5 ± 7.18
Terminal ileum	18.7 ± 3.6	1.5 ± 0.4	1.5 ± 0.6	1.8 ± 0.4	17.91 ± 7.86

The total length of the small intestine varies with age [84]. Mean length at 1 year is 3.8 m, at 5 years is 4.5 m, at 10 years is 5 m, and at 20 years is 5.75 m [62, 84, 85]. It becomes longer when the bowel is empty and after death; thus, use of cadaveric tissue for capsule development should consider this fact. It is approximately 15 mm in diameter after 35 weeks of gestational age [86] and 25 mm in adults [62, 83].

The mean values of small intestine parameters are outlined in table 2.3 [83]. There is no statistical difference in these bowel parameters over an age range of 17–73 or between men and women, while some pathological effects can cause changes in these parameters [83].

As shown in table 2.3, the duodenum and jejunum have similar bowel diameter, wall thickness, fold number, and fold thickness. The interfold distance gradually decreases in size to its smallest measurements in the terminal ileum. The bowel diameter, wall thickness, interfold distance and fold thickness of the proximal ileum, distal ileum and terminal ileum are similar. The parameters used in table 2.3 are illustrated in figure 2.4.

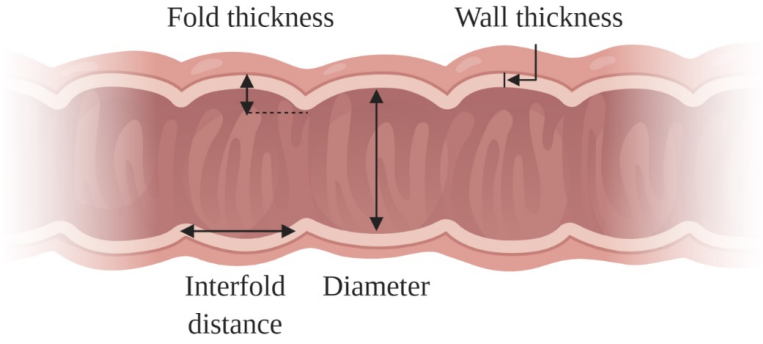

Figure 2.4: Main parameters of small intestine.

2.4.4 Large intestine

The large intestine (colon or large bowel) is the last part of the GI tract and, like the small intestine, is tubular and tortuous in shape. It is shorter at approximately 1.5 m, has more pronounced folds and a larger diameter. By the time digestive products reach the large intestine, almost all the nutritionally useful products have been removed; therefore, it does not play a major role in absorption of nutrients. Instead, the main purpose of the large intestine is the absorption of water (approximately 1.5 l of water arrive in the colon each day), Na+ and other minerals, and the collection and excretion of waste (stool) via the anus [63, 87].

The large intestine has six sections, as shown in figure 2.5: the cecum, the ascending colon, the transverse colon, the descending colon, the sigmoid colon, and the rectum. The first and middle parts of the colon are called the proximal colon. This includes the cecum, the ascending colon, and the transverse colon. The last part of the colon is called the distal colon and includes the descending colon, the sigmoid colon, rectum and anus. The ascending colon, descending colon, and rectum are retroperitoneal and fixed in location while the other two sections are intraperitoneal and therefore mobile [63, 87].

Eickhoff et al [88] used a CT colonography in order to obtain more information about the number of colonic flexures (defined as an acute angle $< 90\,\text{deg}$), and degree of tortuosity (judged on a 10–point visual analogue scale (VAS)). They found that the average number of flexures in

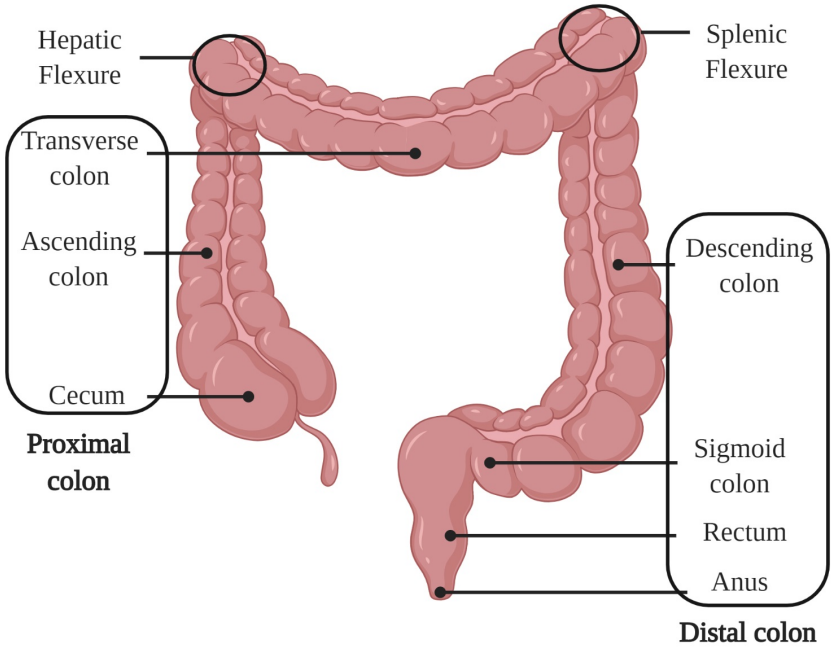

Figure 2.5: Large intestine.

a colon is 9.6 ± 2.4, and the VAS was found to be 3.7 ± 1.9. Cases with a major number of flexures and an increased degree of tortuosity are difficult to access and increase the chance of incomplete colonoscopy. Moreover, Alazmani et al [89] demonstrated that the tortuosity of the colon when the patient is in supine position is higher than in the prone position.

Table 2.4 reports the diameter of the large intestine described by Sadahiro et al [90], focusing on the difference between male and female. The diameters of the descending colon, sigmoid colon, and rectum are larger in males than in females.

Table 2.4: Diameter (cm) of distended large intestine [62, 90].

	Male	Female
Cecum	4.7 ± 0.9	4.8 ± 0.8
Ascendant colon	4.8 ± 1.2	5.0 ± 2.0
Transverse colon	4.2 ± 1.2	4.2 ± 0.7
Descendant colon	3.4 ± 1.2	3.2 ± 0.6
Colon sigmoid	3.4 ± 0.6	3.2 ± 0.6
Rectum	4.0 ± 1.0	3.5 ± 1.0

Table 2.5: Comparison of the colon diameter (cm) in supine and prone positions [89].

	Supine	prone
Rectum	3.6 ± 0.8	3.7 ± 0.7
Sigmoid	2.6 ± 0.4	2.6 ± 0.3
Descending colon	3.3 ± 0.6	3.2 ± 0.5
Transverse colon	3.7 ± 0.4	3.6 ± 0.5
Ascending colon	4.5 ± 0.7	4.3 ± 0.7
Cecum	4.4 ± 0.7	3.8 ± 0.6
Proximal colon	4.2 ± 0.4	3.9 ± 0.5
Distal colon	3.1 ± 0.5	3.1 ± 0.4
Total colon	4.7 ± 0.5	3.5 ± 0.4

Table 2.6: Comparison of the colon length (cm) in supine and prone positions [62, 89].

	Supine	prone
Rectum	23.4 ± 6.7	23.1 ± 3.9
Sigmoid	50.6 ± 13.9	49.9 ± 11.7
Descending colon	24.2 ± 7.8	26.0 ± 7.8
Transverse colon	57.2 ± 9.3	57.3 ± 10.9
Ascending colon	21.7 ± 4.2	19.7 ± 4.0
Cecum	$0.7.8 \pm 2.9$	6.9 ± 2.3
Proximal colon	86.6 ± 9.7	84.0 ± 10.2
Distal colon	98.3 ± 14.7	99.0 ± 11.8
Total colon	185.0 ± 18.3	183.0 ± 16.9

Table 2.7: Mean and standard deviation values of the length (cm) of the intestine [17, 21].

	Men			Women		
	Avg±std	Min	Max	Avg±std	Min	Max
Duodenum (1)	27.8 ± 6.8	17	56	25.2 ± 5.4	17	48
Jejunum-ileum (2)	643.9 ± 110.8	365	1000	573.8 ± 97.1	280	840
Small Intestine (1+2)	670.7 ± 113.1	390	1030	599.2 ± 98.2	298	860
Right Colon (3)	74.1 ± 17.4	40	146	71.9 ± 16.5	40	125
Left Colon (4)	94.2 ± 27.2	33	220	82.9 ± 20.1	34	123
Colon (3+4)	166 ± 36.2	80	313	155 ± 28.6	80	214
Whole Intestine (1+2+3+4)	836.7 ± 132.1	550	1316	754.2 ± 111	378	1013

Tables 2.5 and 2.6 report the diameter and length of the large intestine, considering the supine and prone position of the patient. The research by Alazmani et al [89] demonstrates that the diameter is governed largely by intra-abdominal compression and pelvic motion. Therefore, changing the position of the patient from prone to supine affects the position of the internal organs, and thus, the compression of the colon [89].

The mean values of the length of the entire intestine are summarized in table 2.7. The study by Hounnou et al [58] shows the length of the whole intestine is longer in men than women and the length decreases with age, and increases with weight while it does not vary with height.

Regarding the thickness of the colon wall, the studies conducted by Wiesner et al [91] report

a correlation between wall thickness and colonic distention. A normal wall thickness is ranged between 0.2 and 2.5 mm if the colon is distended and up to 6 mm if the colon is contracted.

2.4.5 Liver, pancreas and gall bladder

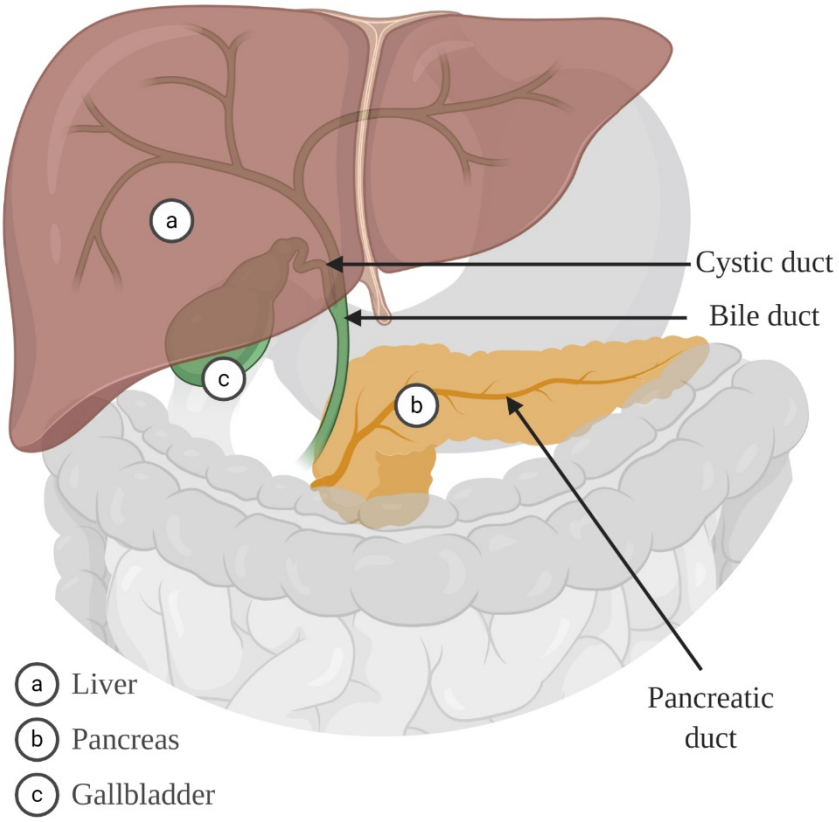

Figure 2.6: Liver, pancreas and gall bladder.

One of the primary functions of the liver, pancreas, and gall bladder is to assist the GI tract in breaking down food into its component nutrients by secreting enzymes. These organs are illustrated in figure 2.6.

The liver is situated in the right upper quadrant of the abdomen and is divided into two primary lobes: a large right lobe and a smaller left lobe. The liver has an important role in digestion; it produces bile, a thick fluid which contains enzymes that help to dissolve fat in the intestines, and metabolizes nutrients that are absorbed by the intestines [92].

The gall bladder is a hollow, pear shaped, 8–10 cm long organ that is posterior to the liver. It is composed of three sections: fundus, body, and neck. Its main function is storage of bile which is then released via the cystic duct, a 1–2 cm long canal, into the biliary duct system linked to the duodenum [93].

The pancreas is a lobular organ that lies posterior to the stomach. It secretes fluid rich in carbohydrates and inactive enzymes which become active once they reach the duodenum. The hormone secretion is triggered by the duodenum in the presence of chyme. The fluids secreted by the pancreas are then released into the duodenum via the pancreatic duct. The particular enzymes produced by the pancreas are discussed in section 2.5 [94].

2.4.6 Mesentery

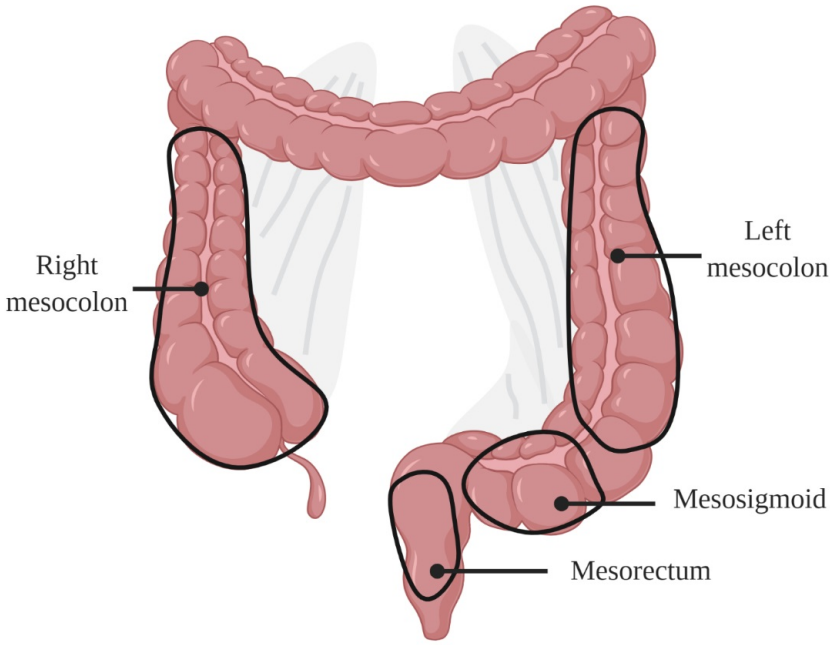

Figure 2.7: Colon regions where the mesentery is attached to.

The mesentery is a continuous set of ruffled and folded tissues that extends from the base of the stomach down to the rectum. It suspends the intestines from the abdominal wall in multiple regions [95]. Its main functions are to fix all abdominal digestive organs, connect them to the other systems and to store fat. It also helps the lymphatic system to transport lymph (fluid containing white blood cells) throughout the body [96].

Knowing how the mesentery is organized and attached to the abdominal wall is necessary in order to understand how it may impact the mechanical properties of the bowel and to quantify the sensitivity of each region of the GI tract. In the study of White et al [97] the failure stress values for the mesentery in porcine models was characterized.

Most of the small intestine is not attached to the abdominal wall and so is mobile; however, the large intestine is more fixed (where the anchorage system is deficient, the organ is mobile

and prone to twisting around the attached region of the mesentery). The right mesocolon is the continuation of the small intestinal mesentery. The transverse mesocolon starts at the hepatic flexure and it continues as the left mesocolon at the splenic flexure. The right and left mesocolon are similar and both are attached to the posterior abdominal wall. The mesosigmoid comprises two regions: the medial region is attached to the posterial abdominal wall while the lateral region is mobile. The mesorectum terminates proximal to the pelvic floor [96]. The main regions of the large intestine where the mesentery is attached to are shown in figure 2.7.

2.5 Histology of the GI

Histology is the study of the microanatomy of tissues. Knowing the composition of tissue is necessary in order to understand how its characteristics can affect the function of a device (e.g. the surface texture) and how specific cells (or regions) can be targeted for drug delivery. In this section, the histological properties of the tissues of the GI tract will be summarized. The most common layers of a digestive tissue are shown graphically in figure 2.8; however, subtle differences between organs are elaborated on in subsequent paragraphs.

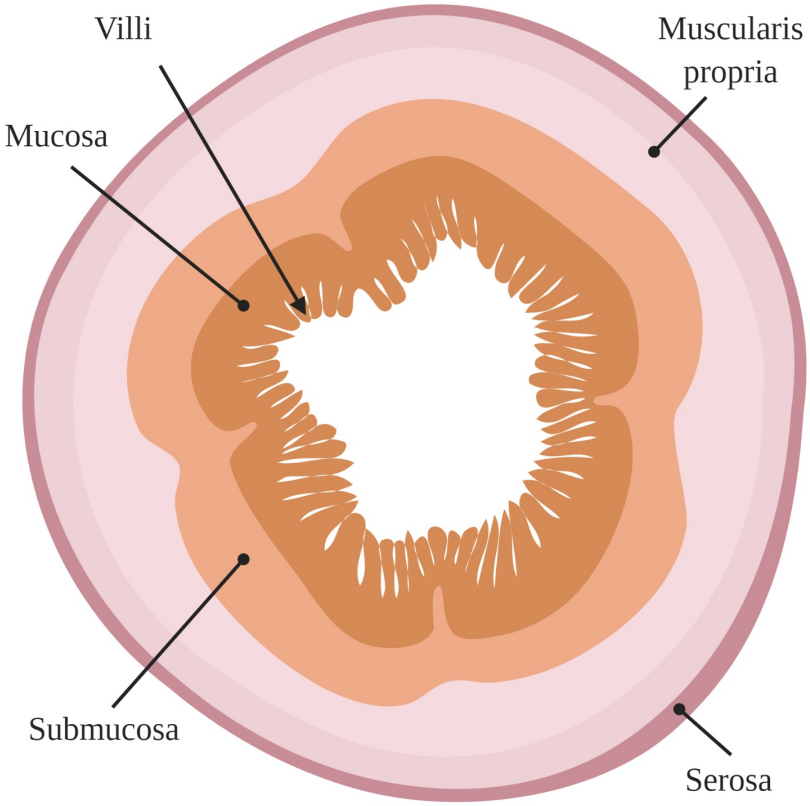

Figure 2.8: The tissue layers of the GI tract.

2.5.1 Esophagus

The wall of the esophagus is composed of four layers: mucosa, submucosa, muscularis propria, and adventitia. With respect to the other organs of the GI tract, the esophagus is the only one that does not have a serosa layer. The missing serosa layer allows esophageal cancer to spread easily and for this reason the surgical treatment is more challenging. Without a serosa layer, possible luminal disruptions are also more difficult to repair.

The mucosa is thick and red at the beginning and paler at the end of the esophagus. Longitudinal folds are present in the mucosa but they disappear when the esophagus is distended. The mucosa consists of three sublayers: mucous membrane, lamina propria and muscularis mucosa. The submucosa is made up of connective tissue, cells such as lymphocytes and plasma, and mucous glands. The secretion of these glands is important for the clearance of the esophagus and for tissue resistance to acid. The muscularis propria, which is responsible for motor function, is composed of striated (skeletal) muscle in the upper part and of smooth muscle in the lower part of the esophagus. The middle area, called the transition zone, is a mixture of both muscles. The adventitia is the external fibrous layer and connects the esophagus with the surrounding environment. Therefore, it is composed of connective tissue, small vessels, lymphatic channels, and nerve fibers [64].

2.5.2 Stomach

The wall of the stomach consists of four layers: mucosa, submucosa, muscularis propria (or muscularis externa), and serosa [8]. The mucosa is relatively thick and contains numerous gastric glands and pits. The mucosa of the stomach has a mean thickness of 1.26 ± 0.07 mm and accounts for about $32\% \pm 7\%$ of the total thickness of the stomach [78]. It has a prominent layer of smooth muscle called muscularis mucosa, which helps to expel the contents of the gastric glands. The mean thickness of the muscularis mucosa is 0.17 ± 0.09 mm [98]. The submucosa, made up of connective tissue and lymph vessels, separates the mucosa from the muscularis externa. The muscularis externa consists of three layers of smooth muscle: inner oblique layer, middle circular layer, and external longitudinal layer. The three layers are not always visible but have different functions: the inner oblique layer helps to mechanically break down food; the middle circular layer of the muscularis is thick and forms the pyloric sphincter; and the external longitudinal layer is responsible for moving the bolus toward the pylorus of the stomach [98].

The serosa is the outermost layer that covers all the stomach wall [8].

2.5.3 Small intestine

The small intestine also has four tissue layers: mucosa, submucosa, muscularis propria, and serosa, as shown in figure 2.8. The mucosa secretes digestive enzymes and hormones, and has many protrusions called villi. These dramatically increase the surface area of the small intestine (by $60 - 120$ times) helping the absorption of the digested food [62]. This layer is the thickest and can make up 35%–40% of the overall wall of the small intestine. The submucosa is the layer of dense, irregular connective tissue or loose connective tissue and contains mucous glands, blood vessels, lymph vessels, and nerves. It supports the mucosa and joins the mucosa to the underlying smooth muscle. The muscularis propria is a region of muscle nearby the submucosa membrane. It usually has two distinct layers of smooth muscle (circular and longitudinal) and is responsible for peristaltic movement. The serosa is the outermost layer of the intestine: it is a smooth membrane consisting of a thin layer of connective tissue and a thin layer of cells that secrete serous fluid [8].

The three main sections of small intestine are similar at a microscopic level. Therefore, it can be assumed that the previously mentioned sections of the small intestine have layers of the same thickness. The mucosa and the submucosa have a thickness of 0.4 ± 0.1 mm while the thickness of the muscularis propria is 0.4 ± 0.2 mm [99]. The three sections have slightly different functions. For example, unlike in the jejunum and ileum, the submucosa in the duodenum has Brunner's glands whose main function is to produce a mucus–rich, alkaline secretion to neutralize the acidic content of chyme introduced from the stomach and to provide an alkaline condition for optimal intestinal enzyme activity for enabling absorption. On–the–other–hand, the ileum has Peyer's patches in the mucosa whose function is the immune surveillance system of the intestinal lumen [8].

2.5.4 Large intestine

The histology of the large intestine is similar to that of the small intestine. However, since the function of the large intestine is to absorb water there is no plicae circulares or villi. Therefore, compared with the small intestine, it is more uniform and flatter on the microscopic scale [8, 63]. The mean thickness of the large intestine wall is 1080 ± 239 μm in which the mean thickness of the mucosa is 499 ± 104 μm, the thickness of the muscularis mucosa is 62 ± 32 μm, and the

submucosa is 519 ± 234 μm [98, 100]. The mucosa is composed by a thin layer of epithelial cells (epithelium), connective tissue (lamina propria), and muscle (muscularis mucosa). The submucosa surrounds the mucosa, and it is made up of mucous glands, blood vessels, lymph vessels, and nerves. The muscularis propria is a layer of muscle that surrounds the wall of the colon and rectum. The serosa is the outer layer of the colon that it is not found on most of the rectum [8].

2.5.5 Mucus

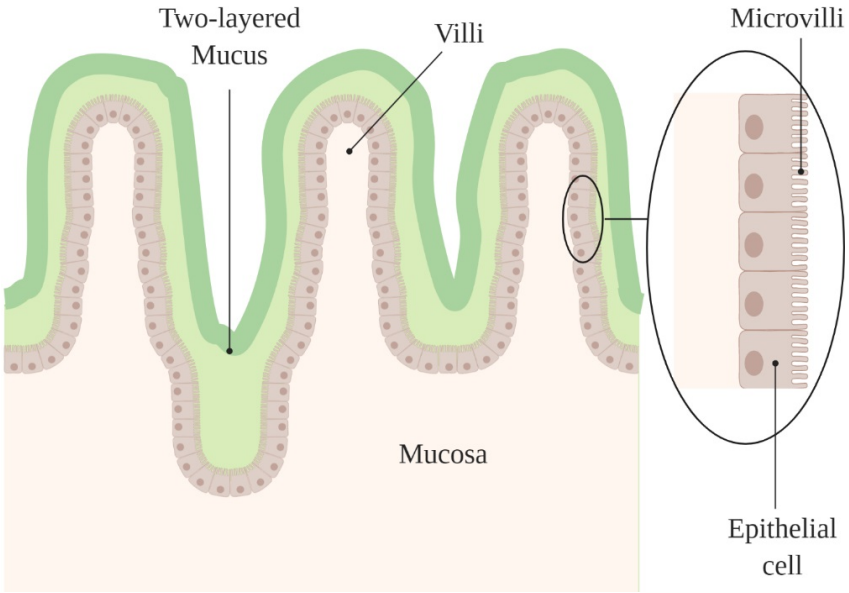

Figure 2.9: Mucus.

Mucus is an essential factor to consider in device development, having a direct impact on the navigation of a device inside the GI tract and its interaction with the tissue for diagnosis and treatment (e.g. drug delivery). Mucus is present on all surfaces of the GI tract and creates a physical barrier between the epithelium and the object in contact with it. For navigation, this can result in a slippage plane that facilitates the easy passage of the object through the GI tract, protecting the tissue from mechanical wear. Alternatively, it can be utilized for the opposite—leveraging muco-adhesion to gain traction for locomotion or anchoring. For diagnosis and treatment, this layer can be a source of information on gut health, or a physical barrier through which the tool, sensor or drug must penetrate.

Mucus (figure 2.9) is a complex biological material and its main functions are the lubrication of the tissue in order to transport the chyme from the esophagus to the colon [101], and the creation of a barrier to protect the surfaces of the GI tract and control the bacterial interaction

with the immune system [101, 102]. The mucus is a semipermeable barrier that enables the exchange of nutrients, water, gases, and hormones, but at the same time, it is impermeable to most bacteria and pathogens [103]. The mucus has an important role in drug delivery since it behaves as a barrier to some molecules and thus, drugs. Its viscoelasticity and pH properties can impact the delivery and absorption of drugs [104–106].

The composition of the mucus varies markedly along the GI tract. The mucus is normally composed of water, and so, it becomes a viscous structure when dehydrated [102]. The mucus is composed of mucins, a protein that gives gel–like properties to the mucus. In the mouth, the salivary glands produce MUC5B and MUC7, which lubricate the food in order to pass through the esophagus. The stomach and colon have a two–layered system, and the major component of the colon mucus is the MUC2 mucin while the MUC5AC mucin is the major component of the stomach mucus. Both are produced by the goblet cells [102]. The small intestine has, in contrast to the stomach and colon, only one type of surface mucus, composed of MUC2 [107].

The two–layered structure of mucus in the colon is noteworthy [102]: the outer layer is permeable, and therefore, is the typical habitat for bacteria; however, the bacteria in the colon do not have any direct contact with the epithelial cells since the inner mucus layer is impermeable. The inner mucus layer is continuously secreted from the goblet cells. The inner layer of both the colonic and stomach mucus is attached to the epithelial cells and is not easily removed, while the outer layer easily sloughs off. The outer layer of the colon is easier to remove compared to the outer layer of the stomach. The mucus of the small intestine does not normally adhere to the epithelial cells and it is easier to remove [102]. The mucus in the small intestine covers the overall space between the villi, and since it is not anchored to the epithelial cells, it moves with the peristaltic waves. However, new mucus is constantly produced from the goblet cells. Here, the mucus is also formed by antibacterial proteins whose function is to limit the number of intact bacteria that can reach the epithelium [102].

In humans the thickness of the colonic inner layer is about 200–300 μm [102]. The spontaneous mucus growth is 240 ± 60 $\mu m h^{-1}$ and the final mucus thickness is 480 ± 70 μm in the colon [108]. The mucus of the stomach has a mean value of 180 μm with a range of 50–450 μm. The thickness depends mainly on digestive activity in the small intestine [103].

The viscoelasticity of the mucus depends on the level of hydration and on mucin concentration [103]. The slope of viscosity versus the shear rate for mucus is usually within the range of -1

to −0.5, with an average of −0.85. The viscosity of healthy gastric mucus is about 0.085 Pa s at a shear rate of 1.15 s^{-1}, but this value can increase significantly during duodenal ulceration [101].

2.6 Chemical makeup of the contents of each region

The chemical properties of the GI tract, such as the pH, the enzymatic composition and the metabolic activity, are crucial for determining appropriate materials for the design of the device, selecting sensors and for choosing a location inside the gut for targeted drug delivery.

2.6.1 pH

The pH has a crucial role in the digestive tract, helping to create a favorable environment for the breakdown of food and controlling bacteria metabolism. The pH along a healthy gut is presented in table 2.8 [109–111]. The saliva has a near neutral pH, but the oral cavity pH may be modified by food. Secretion of different enzymes and chemicals controls the overall pH profile of the gut. Regarding the esophagus, the normal value of pH is between 6.0 and 7.0 but it can drop down to 4.0 in the presence of gastroesophageal reflux [112, 113].

Table 2.8: The pH values at different locations of the human gut.

Location	pH (mean ± SD)
Stomach [109]	2.9 ± 1.97
Duodenum [110]	6.6 ± 0.5
Jejunum [109]	7.1 ± 0.6
Ileum [110]	7.5 ± 0.4
Large intestine [110]	6.6 ± 0.7

2.6.2 Chemicals and enzymes

Digestion is a complex process and consists of both mechanical and chemical mechanisms. The former is relatively simple and involves physical breakdown of food through muscular contractions. The latter is a more complex mechanism that reduces food into its chemical components which are then absorbed. In healthy individuals a substantial amount of fluid and ions, about 7 l, is secreted and reabsorbed daily by the GI tract.

Chemical digestion begins first in the mouth by means of the salivary enzyme amylase which breaks down starches into glucose. The esophagus does not produce digestive enzymes but does produce mucus for lubrication and protection as food travels to the stomach [114].

The cells in the lining of the stomach wall secrete hydrochloric acid (HCl), potassium chloride (KCl), and sodium chloride (NaCl). Combined, these are known as gastric acid. Bicarbonate, a base, is located to buffer the gastric fluid and mucus, a viscous fluid, protects the stomach wall. The gastric chief cells in the stomach release pepsinogen and gastric lipase that help to digest protein and lipid, respectively. Also, amylase, produced in the oral cavity and transferred to the stomach with food, helps to continue the digestion of starch. A healthy adult human secretes about 1.5 l of gastric fluids per day [114].

The intestinal gland, placed between the villi of the small intestine, secretes a solution almost similar to interstitial fluid. The villi contain goblet cells that produce mucus. Intestinal epithelium produces various enzymes (i.e. enterokinase, disaccharidases, and peptidases). Daily volume of total intestinal secretion is about 1.8 l. These enzymes are mostly secluded within the cells and do not contribute to luminal flow. The exocrine enzymes produced in the pancreas, along with sodium bicarbonate, are propelled into the duodenum.

The pancreatic enzymes consist of amylase, lipase, colipase and phospholipase, cholesterol esterase, trypsinogen, chymotrypsinogen, and carboxypolypeptidase. A total of 1.0–1.5 l of fluid are secreted each day. Also, about 1.5 l of bile are secreted every day in the liver and the excess is stored in the gall bladder. Bile flows to the small intestine in the presence of fats in the duodenum. Bile contains water, bile salts, bile pigments, cholesterol, inorganic salts, fatty acids, fat, and lecithin [114].

The large intestine secretes about 0.2 l of fluid per day, mostly in form of mucus, as the primary function is the absorption. It can absorbs a large amount of water, electrolytes and minerals secreted from other regions, but no chemical digestion is carried on in the large intestine [115].

A summary of the key enzymes and chemicals are presented in table 2.9.

Table 2.9: Summary of enzymes and chemical composition at different locations of the human gut [115].

Location	Daily volume (cc)	Enzymes	Fluids and ions
Stomach	1500	Pepsinogen Gastric Lipase	Hydrochloric acid Potassium chloride Sodium chloride Mucus
Small intestine	1800	Enterokinase Disaccharidases Peptidases	Mucus Intestinal fluid
Large intestine	200	-	Mucus
Pancreas	1500	Amylase Lipase, Nucleases Cholesterol esterase Tripsinogen Chymotripsinogen Carboxypolypeptidase	Sodium bicarbonate
Liver	1500	Lactate dehydrogenase aspartate and alanine aminotransferases	Bile

2.6.3 Gut microbiota and metabolites

Gut microbiota play a major role in human physiology by producing vitamins, facilitating digestion, modulating the mucosal immune system and contributing to host defense against pathogens [116, 117]. A healthy human gut hosts trillions of microbes which are essential for maintaining immune and metabolic homeostasis and protecting against pathogens [118].

The esophagus is an environment that contains a consistent quantity of microbiota. The major component of the microbiota in a healthy esophagus is Streptococcus [119]. The human stomach has acidic conditions and other antimicrobial factors and has been viewed as an inhospitable environment for microorganisms. However, a diverse community, as large as 128 phylotypes among eight bacterial phyla, have been detected in the human stomach, such as Proteobacteria, Firmicutes, Actinobacteria, Bacteroidetes, and Fusobacteria phyla [120]. The small intestine microbiota contains a facultative and strict anaerobes mainly consisting of Streptococcus sp., Escherichia coli, Clostridium sp., and high G + C organisms [121]. These microbes have developed different survival strategies to survive the harsh environment of the small intestine. A total of 395 bacterial phylotypes are identified in large intestinal mucosal and fecal samples, consisting mainly of Firmicutes and Bacteroidetes phyla [122, 123]. Only a few sequences associated with the Proteobacteria, Actinobacteria, Fusobacteria, and Verrucomicrobia phyla were found due to the strict anaerobic mucosal regions [123].

The GI tract is not only a food digesting and absorbing system; it is also an endocrine organ which secretes hormones in control of various metabolic processes and a lymphoid organ which modulates the microbial control of host metabolism. Dietary substrates metabolized by the gut microbiota comprise carbohydrates, amino acids, fatty acids, and phytochemicals. Some outputs of the microbiota metabolism are acetate, propionate, butyrate derived from carbohydrates, valerate, and caproate derived from amino acid [124].

2.7 Passive mechanical properties

The mechanical properties generally describe the ability of a tissue to resist deformation. However, the stress–strain behavior is complex and understanding the hyperelastic nature of the tissue is essential for the study of the locomotion of a device and the mechanical interaction with the tissue. This can inform both the real–time control of the device and modelling during

the early, conceptualization stage. In this section, the passive mechanical properties of the hollow organs of the GI tract are summarized.

2.7.1 Stress–strain behavior

The multi–layer structure of the GI tissue results in a complex stress–strain behavior that not only varies with strain rate, but also depending on the region of the GI tract and direction of stress applied. This is due largely to the fact that each layer of the GI tract has distinct mechanical properties which allow different tissue to bear different deformation and stress [125].

The mucosa is loosely adherent to the underlying structures in most areas and cannot withstand large stress. The submucosa has a mobile lattice of collagen fiber bundles with two layers of muscle lining: circular and longitudinal. This allows the submucosa to resist significant mechanical stress, but for a short duration. The serosa is typically the thinnest layer of the wall and hence contributes the least to the overall tissue wall strength [126]. In summary, the mechanical strength of the bowel wall is determined largely by the submucosa and muscular layers while the serosa and mucosa have no significant strength [127]. In table 2.10, the values of maximal stress and destructive strain are provided for longitudinal and circumferential specimens of different locations of the gut. Herein, the values of longitudinal and circumferential testing of surgically removed stomach specimens are practically identical. On–the–other–hand, stress and strain characteristics for small and large intestines, and the esophagus, vary significantly depending on direction of the load (i.e. are anisotropic) [125].

Table 2.10: Maximal stress and destructive strain for different locations of the gut.

Location	Maximum ultimate stress (MPa)	Ultimate strain (%)
Esophagus (cervical part) [128]	2.19 ± 0.06 (Longitudinal)	70.0 ± 7
	1.41 ± 0.05 (Circumferential)	82.5 ± 9
Stomach [125]	0.67 ± 0.19 (Longitudinal)	93.3 ± 18.57
	1.41 ± 0.05 (Circumferential)	103.12 ± 20.23
Small intestine [125]	0.548 ± 0.329 (Longitudinal)	85.76 ± 18.6
	0.92 ± 0.48 (Circumferential)	84.02 ± 19.73
Large intestine [125]	1.188 ± 0.302 (Longitudinal)	40.94 ± 12.5
	0.645 ± 0.165 (Circumferential)	87.85 ± 27.0

2.7.2 Viscoelasticity properties

A time–dependent mechanical test, performed on a excised porcine esophagus, showed that the esophagus has quasi–linear viscoelastic properties [129]. Results showed that the stress relaxed by 20%–30% of the peak within the first 10 s and stabilized at $\sim 50\%$ of the peak after 300 s.

In a study of porcine stomach, it was shown that a higher stress relaxation rate appeared in the first 100 s, and it was about 70% of the total [130]. An in–vitro porcine study found that small intestine tissue relaxes a lot faster than stomach or esophagus. With an increased shear strain from 50% to 200%, all stress curves decrease exponentially from their highest points to some steady states at $\sim 20\%$ within 2 s [131].

2.8 Motor behavior of the GI

The muscle contractions due to peristaltic movement are described in this section. These movements impact the navigation of the device inside the GI tract and must be taken into consideration during design. This includes the study of appropriate materials, device dimensions, device shape, and effective control strategies that ensure the device is able to cope with the movement of the organs while navigating the GI tract.

2.8.1 Peristalsis and the migrating motor complex

Peristalsis in the GI tract comprises a series of propagating muscular contractions which help with the digestion and transportation of food. Each part of the GI tract has a distinct type of motility and these are described in the following.

The stomach can be divided into two functional regions: gastric reservoir and gastric pump. The primary function of the gastric reservoir is to aid in digestion of the food [132]. The reservoir stores the food and then this is processed through a series of acids and enzymes secreted from the gastric wall. The secretions act as a non–immunological defense against invading pathogens, and food is processed for a complex diet. The primary function of the gastric pump, which is anatomically provided by the antrum and the pylorus, is gastrointestinal motility, or rather the transmission of the food through the intestine [132].

The food bolus is transferred to the distal part of the stomach with the help of tonic contractions as shown in figure 2.10. Tonic contractions are sustained contractions lasting from several minutes to several hours. In the distal part of the stomach, peristaltic waves—muscular contractions initiated by spontaneous electrical waves—are generated in order to move chime. These are generated from a particular type of cell called interstitial cells of Cajal (ICC) [133, 134]. These cells generate a potential within their membranes called the electrical pacesetter potential [135]. This potential drives the electrical events within the smooth muscle of the

stomach and also determines the frequency and velocity of the slow waves in the distal part of the stomach [136]. In Cheng's study [137], a laparoscopic device had been used to record these values and found that, for humans, the frequency of the waves is $2.83 \pm 0.35\ min^{-1}$ and the propagation velocity is 3.0–8.0 $mm\ s^{-1}$.

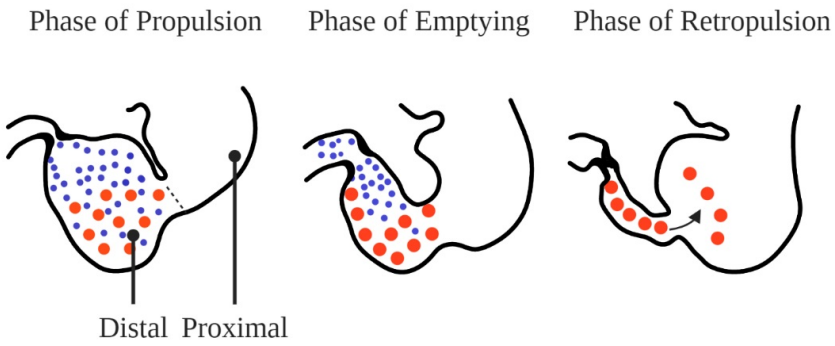

Figure 2.10: Different phases of gastric digestion.

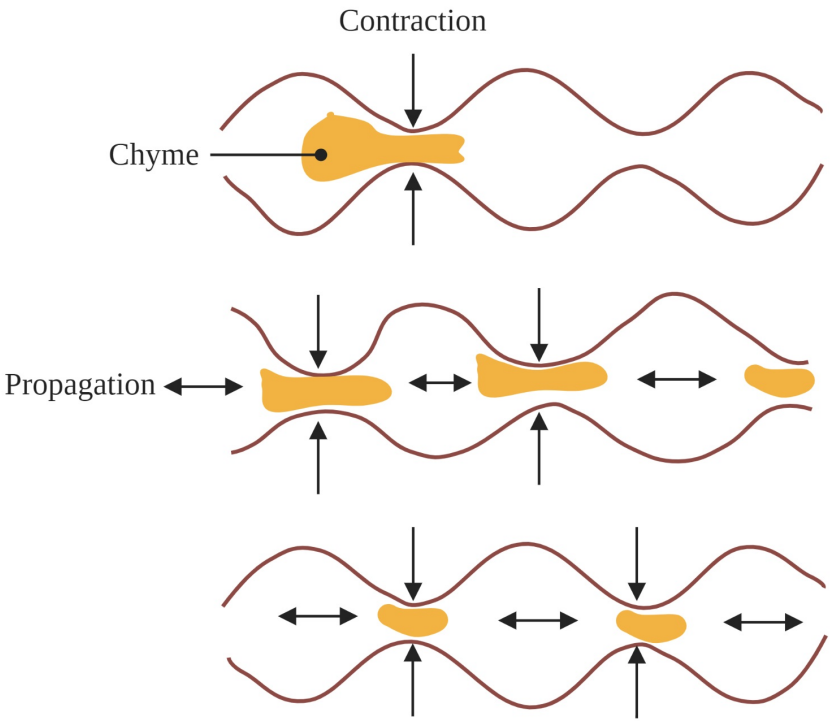

Figure 2.11: Segmentation motility inside small intestine.

Like the stomach, the intestines also have an ICC network between the tissue layers. The ICC produces electrical pacesetter potential which generates slow waves inside the intestine. Additionally, there are two types of motility in the intestines—segmentation and peristalsis. Segmentation is a mixing type of motility. The chyme moves back and forth through successive relaxation and contraction cycles of the stomach, as shown in figure 2.11. In this type of movement, the inner muscle mass aids in the contraction and in the constricting of the food

bolus. In the distal part of the duodenum, the frequency of segmentation is approximately 12 contractions min^{-1}, and for the ileum it is 3–4 contractions min^{-1} [138, 139].

Peristalsis moves the chyme from one segment of the lumen to the forward segment, as shown in figure 2.12; it is called progressive movement. In order to generate this type of movement there is a sequential contraction and relaxation just like the segmentation motility; however, here the outer muscle layer contracts and shortens, while the inner layer relaxes and widens. The motion waves are generated along the entire length of the GI—from the mouth to the anus. There are two types of peristaltic waves: the basic peristalsis that moves only 10 cm along the small intestine at each contraction of the intestine and the 'peristaltic rushes' that occur occasionally and move along the entire bowel with a high amplitude. The average velocity of basic peristalsis is around 1–2 $cm\ min^{-1}$ [46] and the peristaltic rushes are around 2 $cm\ s^{-1}$ [140].

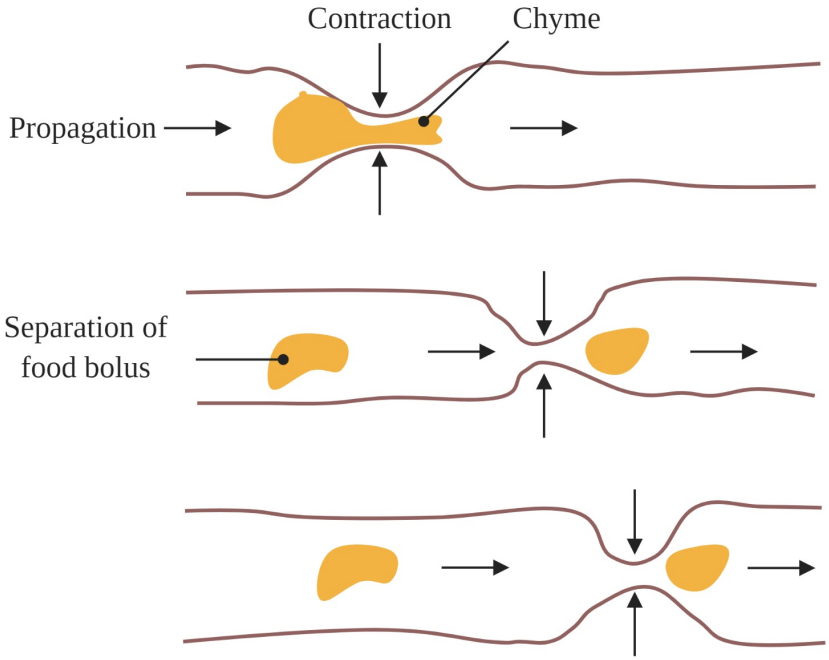

Figure 2.12: Peristalsis movement along the lumen.

The chyme, after passing the ileocecal valve, reaches the large intestine. Here the motility action is not as active as the stomach or small intestine. Colonic motility consists of three types of contractions: the rhythmic phasic contractions (RPCs), the giant migrating contractions (GMCs) and the tonic contractions. The first causes slow net distal propulsion, the second occurs infrequently but produces mass movements, and the third aids RPCs in their motor function [141]. According to Sarna et.al [141], the average frequency of GMCs is around 6–10

per day and each contraction lasts, on average, for 20 s. The propagation velocity at the distal part of the colon is about 1 $cm\ s^{-1}$.

In a study by Rao et al [142] the number of peristaltic contractions occurring in healthy humans during 24 h was considered. The frequency of contractions increased after waking and a meal, while it decreased in the colon during sleep, when motor activity is reduced [142].

Table 2.11: Frequency and propagation velocity of different motilities in the human GI tract.

Region	Motility pattern	Frequency	velocity
Stomach [137, 143]	Tonic Contraction	$2.83 \pm 0.35\ min^{-1}$	3.0–8.0 $mm\ s^{-1}$
Small intestine	Segmentation in Duodenum [139]	12 min^{-1}	12 $cm\ min^{-1}$
	Segmentation in Ileum [139]	8 min^{-1}	-
	Segmentation in Jejenum [140]	-	6 $cm\ min^{-1}$
	Peristalsis [46]	-	1-2 $cm\ min^{-1}$
	Rush peristalsis [140]		1.4-2.8 $cm\ s^{-1}$
Colon [141, 142, 144]	Strong peristaltic movement	6-10 d^{-1}	$1cm\ s^{-1}$

The frequency and the velocity of propagation in different sections of the GI tract are summarized in table 2.11.

2.8.2 Transit time through the various regions

Transit time is the time that it takes food to travel from the mouth through the digestive system to the anus. This can vary greatly between individuals and depends also on the composition of the meal.

Fryne et al [145] measured the transit time through various regions of the GI using a magnetic tracking system. The observed gastric time was 35.5 min (range 4–73 min) and the transit time for the small intestine was 261 min (range 241–402 min). They also measured the motility data of the small intestine due to peristalsis. The propagation velocity was reported as 2.2 $cm\ min^{-1}$ during post-prandial state and 2.3 $cm\ min^{-1}$ during fasting phase. In addition, they measured the contraction frequency of the stomach and intestine. The measured value for the stomach was $2.85 \pm 0.29\ min^{-1}$ and for the intestine was $9.90 \pm 0.14\ min^{-1}$ post-prandial and $10.53 \pm 0.29\ min^{-1}$ during fasting. In a study by Degen and Phillips [146] it was demonstrated that there is not a substantial difference between the transit time in men and women. The gastrointestinal emptying time, measured with different techniques, is shown in table 2.12.

Table 2.12: The gastric and intestinal emptying time.

Author	Device	Gastric (min)	Intestinal (min)
Fryne et al [145]	Pillcam	57.5	275
	MTS-1	56	255
	Magnetic Pill	35.5	260.5
Maurer et al [147]	Radiolabeled meal	-	231
Miller et al [148]	Lactulose Breath test	-	234
Camilleri et al [149]	Resin pellets	164	168

Most of the devices that have recorded data for transit time have been used in fasting states. In real–life scenarios, the diet has to be taken into consideration. Krevsky et al [150] used a different approach to measure the transit times through different sections of the GI tract. Human volunteers ingested food containing indium pellets and the transit times through various sections of small bowel were determined by measuring the radioactive signal. The data showed that the transit time to fully empty the stomach was 120–180 *min* and for emptying 50% of the small intestine was 150–180 *min*. The transit time through the colon was about 300–360 *min*. Cummings et al [151] performed a study in which 12 human subjects were fed, after each meal, with radio–opaque pellets for several weeks of controlled diet and measured the transit time. There were three different types of diet: Ad libitum diet (i.e. free–feeding or feeding on demand), standard diet, and high fiber diet. The mean transit time for each diet of the 12 individuals is shown in table 2.13.

Table 2.13: Mean transit time (days) calculated from marker size [151].

Ad libitum diet (studies 1–6)		Standard diet (studies 7–12)		High fiber diet (studies 7–11)	
Mean	Range	Mean	Range	Mean	Range
2.1	0.7-3.1	2.8	1.9-3.6	2.3	2.0-2.7
3.1	2.3-4.0	2.1	1.3-2.6	1.8	1.5-2.3
2.1	1.4-2.7	2.1	1.2-2.6	1.6	1.3-2.0
2.1	1.2-2.6	2.9	2.1-3.7	1.7	1.3-2.1
2.2	1.3-3.5	2.5	1.9-3.3	1.0	0.7-1.6
2.4	1.7-3.2	3.5	2.5-4.8		

2.8.3 Post-prandial and fasting states and their effect on motor behavior

The peristaltic motion still pertains during fasting, but it is different in action and timing than during the post-prandial state. The movement is propulsive—originating from the pylorus up to the ileum—and is called the migratory motor complex (MMC) [152]. It is a kind of 'housekeeping' movement in which the MMC sweeps away any leftover food inside the lumen. This is a critical activity as a stagnant bolus can cause bacterial growth inside the lumen. The MMC is generated by a hormone called 'motilin' which is secreted during the fasting state.

This state lasts over a period of 90–120 min [152]. During fasting, the MMC occurs in repeated cycles. This cyclic pattern, as shown in figure 2.13, is divided into three phases. Phase I is the motor quiescent period lasting 40%–60% of the cycle length and when slow waves are rarely associated with spikes. Phase II presents irregular contractions in the small intestine and lasts 20%–30% of the cycle length. Phase III is the MMC characterized by spikes and contractions and lasts for 5–10 *min* [153].

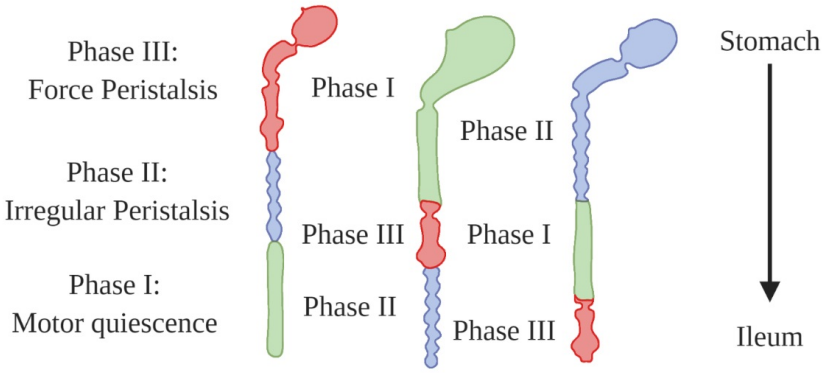

Figure 2.13: The three phases of interdigestive motility pattern.

During the fasting and post-prandial states, the proximal and distal colon experience two different motor activities, namely: 'tonic' and 'phasic'. The former consists of long contractions lasting for several minutes up to hours; the latter comprises brief periods of relaxation and contraction. During fasting, the motility is similar between the proximal and distal colon. On the contrary, during the post-prandial, the distal colon experiences an increase in the phasic motor activity. In addition, the tonic activity, due to the meal, causes immediate tonic contraction in the proximal and distal colon [154].

2.9 Forces on objects moving through the GI

The motion of a device through the GI tract is strictly related to all the forces acting on it in the environment, of which there are many. The forces are highly variable and often too complex to predict. Although they are derived from a variety of sources, they can be interdependent. These are separated here into passive forces—those that are not generated as a result of the movement of the object (e.g. muscular contractions in the bowel wall) and active forces—those that are (e.g. friction). These are summarized in figure 2.14.

The aim of this chapter is to summarize all these forces applied to the object and provide the

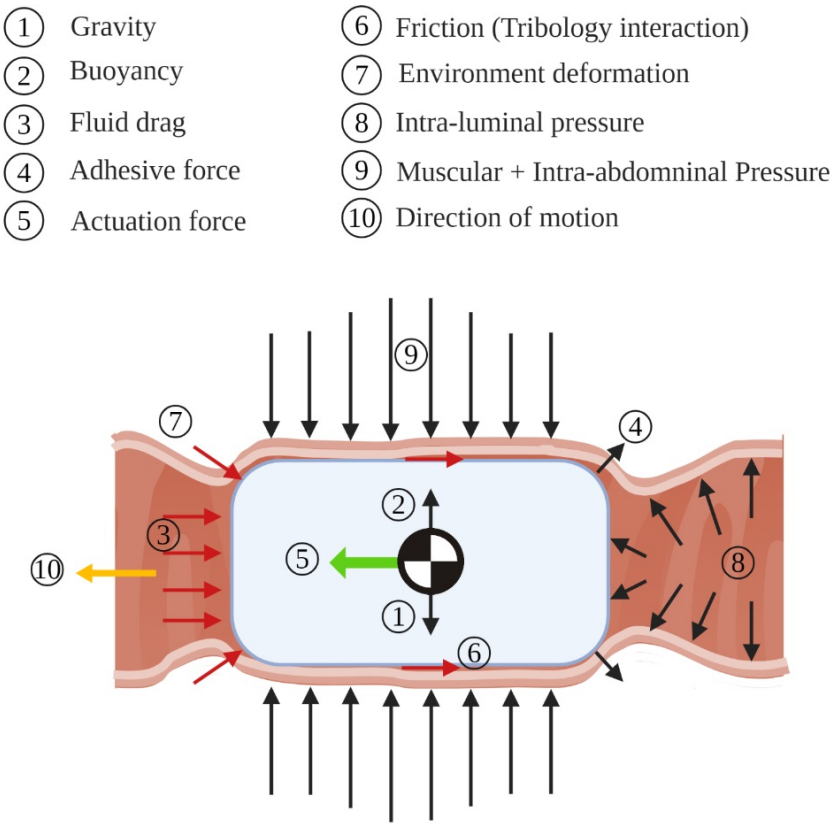

Figure 2.14: The forces acting on an object moving through the GI tract.

key factors affecting their magnitude. While it is challenging to predict them all accurately, it is useful to have a broad understanding of them during the mechatronic design of a device for this environment.

2.9.1 Passive forces

The passive forces acting on an object are shown with black arrows in figure 2.14. They include gravity, buoyancy, muscular contractions generated by the GI, abdominal pressure, intraluminal pressure, and mucosal adhesion.

Gravity and buoyancy

The most constant and simple forces to define are gravitational force and buoyancy. The magnitude of gravitational force is proportional to the mass of the object, and the direction is always downward in the world frame. Buoyancy opposes gravity and is calculated as $F_b = \rho V g$, where V is the volume of the object and ρ is the density of the fluid surrounding it, which varies slightly along the GI region. In general, the fluid can be assumed to be a Newtonian fluid with a density of 1 $kg\ l^{-1}$ [155].

Since the directions of gravity and buoyancy are always along the vertical axis, how they impact the object's dynamics depends on the orientation of the object and the surrounding environment. For example, if the lumen and object are horizontal, they can align with and impact object–tissue contact forces; if the lumen and object are vertical, they align with and can impact propulsive force for locomotion.

Abdominal pressure

The GI tract runs through the core of the body and as such, passes by other organs and soft tissues, all having mass and some of which are moving. The abdominal pressure exerted on an object is the summation of the mass of tissue above the object (assuming bones are self–supporting) and the forces generated by muscular contractions in the environment. The former could be approximated by knowing the volume and density of the tissue above the object. Densities of soft tissues range from 0.95 to 1.05 $g\ cm^{-3}$ [156], and volumes can be approximated by medical imaging and device localization. The latter include sources such as the beating heart, contracting diaphragm and skeletal muscle movements. This component is challenging to quantify, as it is dependent on the individual's physiology, level of activity during the procedure, the orientation of the body, and the pose of the object within the body.

A simpler approximation can be made by considering the abdomen as a whole and measuring the intra-abdominal pressure (IAP) — a clinical parameter that is typically measured by monitoring the pressure in the bladder. In a healthy adult, the pressure ranges from 5 to 7 $mmHg$ but can vary considerably, particularly in ill and obese patients, where values can be $> 25\ mmHg$. Body posture can also have a significant impact on IAP, especially if the individual is lying prone or if the individual is inclined (or standing) [157–159]. Muscular contractions can greatly alter IAP, with one study showing that during coughing and forced expiring, values of 46 and 36 $mmHg$ respectively can be seen [160].

GI muscular contractions

GI muscular contractions are described in chapter 6 and are mostly prominent in the small intestine. They are primarily generated by the myenteron (muscular layer of the intestine), which creates pendular movements, segmental contractions, peristalsis, and gradual reflexes [161, 162]. To estimate their effects on the object dynamics, it is necessary to understand the magnitude, shape, and frequency of the contact force [163]. A general theoretical model of a

solid bolus transported by peristalsis was formulated by Bertuzzi [163]. Miftahof et al described bolus transport models specific to the GI tract to predict contact forces [161, 164, 165].

Intraluminal pressure

Gases and liquids in the GI tract can become pressurized and exert forces on the surrounding tissue and object. These can be artificially generated (e.g. insufflation from an endoscope) or naturally generated (e.g. as a result of chemical processes in the gut). The primary impact of intraluminal pressure is a reduction in contact pressure on the object as it counteracts the other surrounding contact pressures, including those mentioned above. This is an important factor to consider as the net contact pressure greatly impacts the degree of object–tissue contact, tissue deformation, and therefore, both adhesion and the active forces on the object.

Summary—Net contact pressure

This subsection gives an indication of the expected contact pressures experienced by a capsule in the small intestine—the region with the highest expected contact pressure due to its muscular contractions and small lumen diameter. In other words, this gives a practical example of the summation of pressures described in previous section. A device called the migrating motor complex force sensor was used to measure the force per centimeter of length exerted by the small bowel on a capsule–like object [166–169]. The contact force depends on the position of the body, and the distal small bowel exerts 92% more contact force against the capsule than the proximal small bowel, with the primary reason being that the distal small bowel has a smaller diameter than the proximal small bowel [167]. In table 2.14 the mean values of the contact force measured with different techniques in different works are summarized.

Table 2.14: The contact force on capsule.

Author	Length of capsule	Contact force
Calio et al [170]	33 mm	0.25 $N\ cm^{-1}$
Terry et al [167]	35 mm	0.9–2.9 $N\ cm^{-1}$
Miftahof et al [164]	35 mm	0.15–1.9 $N\ cm^{-1}$

Adhesion

Mucus, described in section 2.5.5, lines the inner surface of the GI and is continually secreted by goblet cells [102]. The glycoprotein molecules in the mucus have an ability to adhere to solids because of their hydrophilic and viscoelastic properties. Mucosal adhesivity is the interfacial

ability to bond with a solid surface. It is measured by the energy required to separate the two adhered surfaces and can be affected by several factors, such as hydration, mucus surface tension, wettability, temperature, and dwell time (the amount of time the mucosa is in contact with the solid surface prior to separation) [171]. Mucosa adhesivity can be useful in device design; for example, it can be a solution to increase static friction to avoid migration of the capsule inside the GI tract.

The inherent adhesivity between a capsule and mucosa was investigated by changing the factors of adhesive modality (peel and tack), material (polycarbonate, micropatterned polydimethylsiloxane, stainless steel, and mucosa), and bowel region (proximal, middle, and distal). The results show the mean tack strength of the mucosa to engineering materials was 0.198 ± 0.070 $mJ\ cm^{-2}$. The mean peel strength was 0.055 ± 0.016 $mJ\ cm^{-2}$ [172]. As the results suggest, the adhesive tack strength between the mucosa and other material is larger than the peel strength.

Mucus thickness has some influence on mucoadhesion performance which is an important factor to consider given the varying thickness throughout the GI tract. Varum et al [173]. performed experiments on pigs, which is the closest model to human mucosa, in order to evaluate the mucoadhesion. The experimental results showed the mean detachment forces are dependent on mucus thickness: 0.084 ± 0.025 N for the stomach, 0.0575 ± 0.0125 N for the small intestine and 0.066 ± 0.009 N for the colon [173].

Other tests were conducted by Kern et al [174] to find a nonlinear empirical model to describe the adhesion that includes the load (F_{load}), dwell time (T_{dwell}), and separation rate (v_{sep}). The main important parameters taken into consideration are the maximum stress (σ_{max}), defined as the ratio of the maximum measured force and the total capsule contact area achieved during the adhesion response, the total vertical probe displacement (δ_{total}) during the adhesion response, and total effective adhesion energy (E_{eff}), defined as the total area under the force displacement curve. The empirical equations are reported in table 2.15. As the table shows, F_{load} is a significant factor only for σ_{max} and E_{eff} while T_{dwell} has no observed effect. Moreover, it has been noticed that as F_{load} increases σ_{max} and E_{eff} decrease.

Table 2.15: Adhesion model [174].

Critical design parameter	Model equation
Maximum stress	$\sigma_{max} = 972.491 v_{sep}^{0.31} - 7.711 F_{load}^2 - 9.577 F_{load} v_{sep}$
Total displacement	$\delta_{total} = 0.791 v_{sep}^3$
Effective adhesion energy	$E_{eff} = (0.155 v_{sep} - 0.010 F_{load} v_{sep})^0.583$

Numerous studies have exploited mucoadhesion further by developing mucoadhesives to chemically bond to the mucosa to improve traction and/or adhesion. This can result in significantly higher adhesive forces while, in some cases, maintaining the ability to repeatedly reattach to the mucosa [175–178].

2.9.2 Active forces

The active forces on an object as it moves through the GI are shown with red arrows in figure 2.14 and encompass the tribology of the contact, the drag of the object moving through a fluid, and tissue deformation during object motion. They depend largely on the properties of the GI tract and the object, as well as the properties of the surrounding tissue and fluid. These forces are applicable to all devices, including those with contact–based actuation, where the device must maximize traction against the tissue; passive locomotion, where the device must minimize frictional resistance to facilitate smooth passage through the lumen; and anchoring requirements, where the device must secure itself, through high friction or adhesion, to the lumen.

Tribology

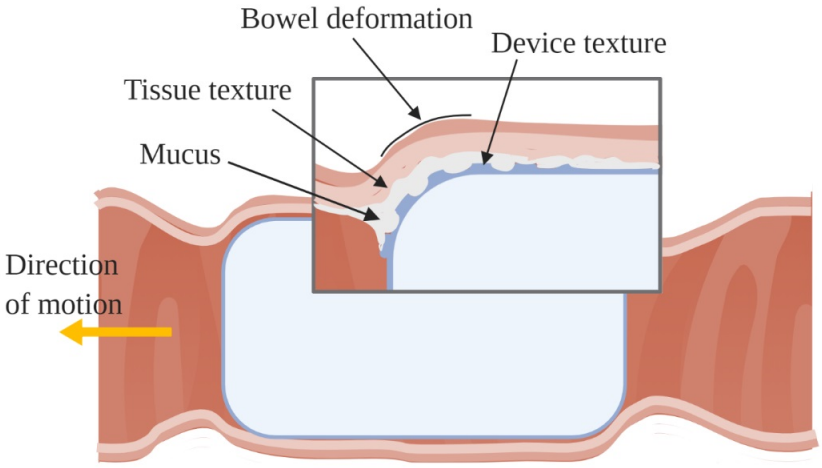

Figure 2.15: Factors affecting the tribology of an object moving through the GI tract.

Figure 2.15 aims to summarize the primary factors affecting the tribology of an object moving through the GI tract, including the size and shape of the object, its velocity, the properties of the mucus, the properties of the tissue, the contact force, the texture of the object, and the texture of the tissue. This is a complex interaction, with the mucosa and underlying tissue being viscoelastic, inhomogeneous, and nonlinearly deformable (chapter 2.6). Additionally, the con-

tact pressures—described in the previous section—vary considerably, as does the macro—and micro-scale morphology of the tissue. The tissue also continually excretes a non-Newtonian mucus (section 2.5.5) which, depending on the velocity and scale of the device, can either increase or decrease total frictional resistance.

Understandably, it is complicated to create an all–encompassing and accurate model that considers all the factors mentioned above. However, an understanding of the tribological properties is useful to design functional surfaces and appropriate control techniques for this unique environment. Sliker et al developed a model to predict the resistance force on a capsule which was validated by performing drag force experiments [179]. Kim et al developed an analytical model based on a hoop stress analysis, and compared it to finite element model results [180]. A similar model was developed by Woo et al [181], using a hoop stress analysis and tensile properties reported by Baek et al [182], but including an empirical model for a propulsion force due to electrical stimulus of the bowel.

Perhaps the most intuitive is a study by Zhang et al, where a velocity–dependent model is presented [183]. In this scenario, the total friction acting on a capsule can be written as a summation of the environmental resistance, Coulomb friction, and viscous resistance (or drag) [182, 183]

$$F = F_e + F_v + F_c \tag{2.1}$$

where Fe is the environmental resistance, F_v is the viscous resistance and F_c is the Coulomb friction. The environmental resistance F_e is the amount of force required to deform the tissue in contact with the object and is related to an elastic restoring force as

$$F_e = PS \sin\theta \tag{2.2}$$

where θ is the slant angle of the object-tissue contact patch, P is contact pressure and S is the contact area. Tissue is viscoelastic, and so P increases with an increasing shear rate. This is shown to be the dominant component of resistance during an object's interaction with the GI tissue and has other names, including 'edge effects' [184]. The viscous friction or drag is related to the rheological properties of the fluid in the contact patch and can be expressed as

$$F_v = \delta v \tag{2.3}$$

where the apparent viscosity coefficient, $\delta = 11.24(\frac{v}{d})^{-0.7552} + 0.1148$, d is the mean value of intestinal mucus thickness and v is relative velocity [183]. In other words, this is the resistance of the mucus during shear and is velocity dependent. While static, resistance comes from the adhesive bonds and, during shear, from the viscosity of the fluid [185, 186]. The Coulomb friction is decided by

$$F_c = \mu PS \cos\theta \tag{2.4}$$

where μ is the coulomb friction coefficient and the normal force has been replaced by $PS\cos\theta$ to account for the hoop stress. The friction coefficient is influenced by the texture of the capsule and intestinal surface.

Equations 2.1 - 2.3 are all velocity dependent, and other literature supports this, while also showing a total resistance dependency with object diameter, length [180, 181, 187, 188], and normal force [189, 190]. The key factors affecting the friction are the capsule dimensions, surface geometry and the speed, while the effect of the weight is trivial. Ignoring the factor of weight, the diameter affects the friction more than the length [191]. Wang et al [191] describe how resistance changes with capsule size and velocity as

$$F(v) = Kv^{\frac{1}{n}} + C \tag{2.5}$$

where K and $C > 0$ are related to the R and L, radius and length of the capsule, respectively.

Fluid drag

While there may not always be high volumes of fluid in the GI tract, it is important to consider any impact of drag as an object moves through a fluid–filled environment. In these cases, the drag opposes motion and is equal to

$$F_D = \frac{1}{2}\rho v^2 C_D A \tag{2.6}$$

where ρ is the density of the fluid, v is the velocity of the object, C_D is the drag coefficient, and A is the contact area of the front face of the object.

2.10 The impact of disease on GI physiology

Throughout this work we have described all the properties and characteristics of the GI tract in its healthy state, which can be considered as the generic and most common condition. However, having some knowledge of the possible GI alterations in the presence of digestive diseases is useful, and in–depth investigation can be done as required for the application. Therefore, here, we discuss the most common changes that can be seen from cancers and other diseases, including IBS, IBD and celiac disease. IBD includes UC and CD, both characterized by chronic inflammation of the gut [192]. Although UC and CD are grouped under IBD, they have different characteristics. UC is an inflammation condition of the mucosa of the large intestine and is related to the presence of bacteria in the colon, which produce colitis. However, CD usually occurs in the ileocaecal region [193]. Both present an irregular mucosal surface and transmucosal inflammation [193, 194]. Here we consider how these diseases impact GI transit time, pH, microbiota and wall thickness [192].

Regarding the GI transit time, Bai et al [192] report that there is no significant difference in gastric emptying time and small intestine transit time between healthy subjects and IBS patients. However, they report that the IBS patients have a longer colonic transit time. Regarding UC and CD patients, Bai et al report a slightly longer orocecal (mouth—cecum) transit time [192, 195]. On–the–other–hand, celiac patients show a longer orocecal transit time but no alteration in small intestine transit time [195].

Gastric and small intestine pH profiles in patients with IBD are similar to those in healthy samples, while the pH of the CD colon is much lower (5.3 ± 0.3 in the right colon and 5.3 ± 0.7 in the left colon) [196]. Regarding celiac disease, a higher pH in the small bowel and unaltered pH value in the stomach have been reported by Effinger et al [195]. Digestive diseases could also mutate and reduce the intestinal concentration of bile salts, which affect the luminal pH and, thus, the digestion of food (i.e. transit time) [192].

There is a strong correlation between gut microbiota, IBD, IBS and digestive diseases in general. IBD has been shown to lead to a decrease of bacteria with anti–inflammatory capacities

(Proteobacteria) and an increase of bacteria with inflammatory capacities (Faecalibacterium, Helicobacter species) [117, 195]. Regarding celiac patients, the microbiota was found to be rich in potentially pathogenic bacteria and poor in species such as Lactobacilli and Bifidobacteria [195]. Regarding colorectal cancer, a study by Tojo et al [197] shows that the alteration of composition and function of the microbiota is correlated to the presence of colorectal cancer as well as IBD or IBS. Sample of colorectal tumor have shown many bacterial such as Bacteroides vulgatus, E. coli and Enterococcus faecalis [197]. Other microbial systems have been reported in association with gastroesophageal reflux (Veillonella, Prevotella, Haemophilus, Neisseria, Campylobacter, and Fusobacterium) and adenocarcinoma in the esophagus (Campylobacter) [119]. Moreover, gut microbiota alterations may contribute to pancreatic diseases including pancreatitis, chronic pancreatitis, and pancreatic cancer [116].

Wall thickness is a common indication of disease as it is proportional to the resulting inflammation. With UC the small intestine is characteristically thickened and presents with ulceration of the mucosa [193], while the colon wall can thicken up to 8 mm in the presence of CD [194]. With regard to GI cancers, it has been proven that wall thickness is a good approach to evaluate and target the presence of a tumor. For example, in the esophagus a thickness above 5 mm is considered abnormal [198]. Similarly, Suk et al [77] classify gastric diseases with respect to wall thickness. In particular, diseases have been classified as normal or benign disease (BD), early gastric cancer (EGC), and advanced gastric cancer (AGC). BD presents a thickness of the gastric wall of 4.9 ± 1.6 mm, the EGC shows a thickness of 5.6 ± 2.4 mm while a thickness of 10.3 ± 4.7 mm is an indication of AGC.

2.11 Conclusion and future developments

Considering that digestive disease can significantly impact the normal function of the GI tract and that GI cancer is one of the leading causes of death in the 21st century, the early diagnosis and subsequent treatment of GI disease is essential to reduce patient morbidity and mortality. Despite numerous technological advances in diagnosing and treating these diseases, the need for innovation still exists. This is partly due to the harsh, difficult–to–access environment that presents significant engineering challenges, but also to the increasing demand on health services by a growing population that has increasing disease prevalence. Therefore, there remains significant motivation for engineers in the biomedical field to find innovative, more sophisticated,

and minimally invasive technologies to access the GI tract. In order to develop effective devices, engineers need a broad spectrum of knowledge on the GI system, and so in this review, the fundamental properties of the GI system — focusing on the esophagus, stomach, small and large intestines — were described with the goal of presenting key information.

Developing disruptive medical devices for this region still has a number of major and open challenges. Firstly, the mechatronic design needs to be considered from the shape, dimensions, and materials of the device, to the research of innovative navigation strategies. The shape and dimensions must ensure safe and efficient passage through the tortuous and unstructured environment, while the material should be tailored to meet the friction, chemical resistance, and biocompatibility requirements (i.e. pH and microbiota of the environment). An innovative strategy for the device navigation is essential to ensure effective and real–time control and reduce the mean completion time of the procedure, which should at least be comparable with the existing procedure. This must be robust in an environment with numerous disturbances (i.e. respiration of the patient, peristaltic movements) and high variability between patients. To achieve this, localization, registration, and an effective locomotion mechanism (i.e. internal anchoring locomotion, external magnetic coupling locomotion or a novel hybrid combinations of internal and external locomotion) should be carefully considered depending on the context. Lastly, to bring added benefit, the device should provide effective diagnosis and or treatment. This should be accurately controlled with the device navigation and may be facilitated by context specific sensing, for example, combined time and pH measurements. In this context, the possibility of performing therapeutic functions, such as biopsy tissues, polyp ablation or drug delivery, is necessary. Therefore, enhanced and innovative devices have the potential to improve all these features, and thus, advance in the next decade, the medical and endoscopic field.

Chapter 3

The MFE: Magnetic Flexible Endoscope platform

This Chapter focuses on the lower GI tract, i.e. the large intestine. Herein, the clinical motivation for developing a robotic system for colonoscopy is explained and an overview of the main components of the MFE platform is provided.

3.1 Clinical motivation

Colonoscopy is an endoscopic procedure and, at the moment, the most important screening test employed for the inspection of the large intestine. The exam is performed by inserting a colonoscope from the anus through the entire colon to the ceacum (the end of the large intestine). In this first phase, the endoscopist focuses on reaching the ceacum as fast as possible. Upon reaching the ceacum, the scope is slowly withdrawn to visually inspect the colon wall, perform tissue biopsy or remove polyps.

The traditional colonoscope is a FE characterized by high stiffness and rigidity. This allows the clinician to push the colonoscope inside the patient's colon and navigate the bowel. However, the stiffness of the colonoscope causes a deformation of the shape of the colon which results in pain and discomfort for the patient. As a consequence of a painful and unpleasant procedure, patients are more reluctant to participate in prevention strategies which leads to an increase in the risk of tumor development [10].

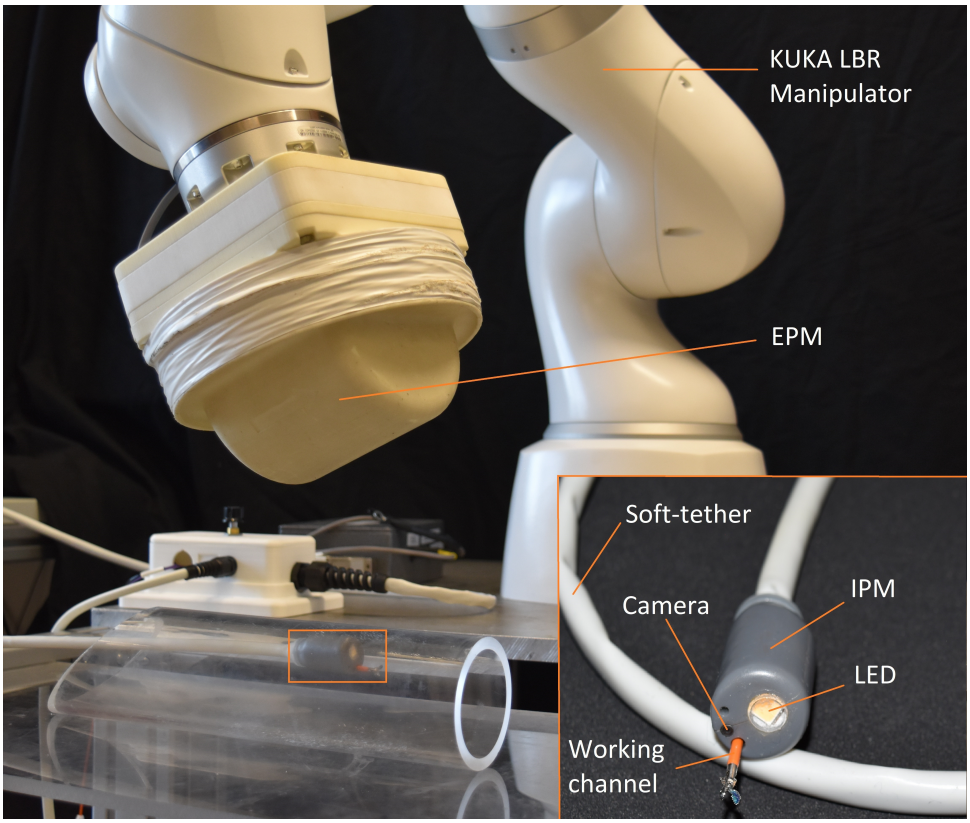

Figure 3.1: Overview of the Magnetic Flexible Endoscope platform.

3.2 MFE System overview

The Magnetic Flexible Endoscope (MFE) platform (Figure 3.1) is an alternative to the traditional FE [25]. The platform is composed of a highly flexible endoscope (MFE) guided by a robotic manipulator.

The MFE consists of an Internal Permanent Magnet (IPM) mounted in a 3-D printed shell and placed at the tip of the endoscope, which also contains a camera and LED to visualize and illuminate the colon. The IPM is a NdFeB N52 permanent magnet with a 11.10 mm diameter and 22.20 mm length. A flexible circuit, composed of an array of magnetic field sensors and Inertial Measurement Unit (IMU), is glued around the IPM and is used for the Localization algorithm described briefly in 3.2.2.

A soft and flexible tether contains cabling for on-board electrical components and channels for air and water, which permit the easy passage of the endoscope by insufflating the colon and the cleaning of the camera lens, respectively. A working channel is then used for inserting the instrument (i.e., forceps or needles for performing biopsies and snares for polyps removal) allowing the clinician to perform diagnostic and therapeutic tasks; this allows for the same

functionalities of a standard FE to be maintained.

A KUKA LBR Med R820[1], a collaborative 7-DoF robotic manipulator is used to control the 6-DoF of an External Permanent Magnet (EPM) (NdFeB N52 permanent magnet, 100.00 mm diameter and length), mounted at its EE. The control system is implemented using the Robotic Operating System (ROS) in Python, combined with an open-source KUKA to ROS integration package. A joystick is used by the clinician as input to impart a new pose to the endoscope given a visual feedback from the camera, embedded in the tip of the endoscope.

In the following, a summary of the major clinical needs and requirements for the MFE platform. The pose accuracy is the deviation between the required and current pose and, in this scenario, is a fundamental parameter to ensure the safety of the system. This is discussed in detail in Chapter 6 and is related to the localization accuracy detailed in 3.2.2. Since no established benchmarks were reported for accuracy in magnetic capsule endoscopy applications, the localization accuracy was based on two fundamentals [199]:

- the localization accuracy must be inferior to the well-known mean diameter of the colon.
- the performance of the localization algorithm needed to be proven competitive with respect to prior methods.

Regarding the maximum pressure that can be applied to the colon wall without causing any damage (e.g. perforation of the bowel) this has been reported to be 3 bar [200]. A colonoscopist usually applies a force in a range of $13.9 - 27.9$ N during a standard colonoscopy [201]. No detailed studies where conducted on this topic during the experiments reported in this thesis, however it was proven that during the retroflexion procedure [202], which is the procedure that induces more stress on the colon wall with the MFE, the maximum applied tissue stress was 0.249 bar, which is only 8.3% of the maximum applicable pressure.

3.2.1 Limitations of basic control

As briefly mentioned in Chapter 1, magnetic devices can be controlled using either coil-based systems [14–20], rotating permanent magnet-based systems [21, 22] or permanent magnet-based systems [23–27]. Herein, the main advantages and disadvantages of each actuation system are briefly considered. These play an important role in the choice of the controller.

[1] `https://www.kuka.com/en-gb/industries/health-care/kuka-medical-robotics`

Coil-based Systems The usage of multiple coils within a predefined workspace is one of the most investigated approaches. In fact, these systems generally have high controllability and accuracy, therefore, they can achieve accurate control of the magnetic field and gradient inside the workspace. On-the-other-hand, they are often more bulky, have a confined workspace, a high energy consumption and produce heat.

Rotating Permanent Magnets This approach employs the magnetic field generated by permanent magnets and solves the issue related to heating in coil-based systems. However, these systems are very similar to their coil-based counterparts and, therefore, they share the same limitations in terms of workspace.

Single Permanent Magnet Permanent magnet-based devices are actuated by a single permanent magnet, manipulated by a robotic manipulator. The main advantages of using permanent magnet-based devices over coil-based and rotating permanent magnet-based systems are the compact size and reduced energy consumption. However, this gain comes at the cost of reduced controllability, related to less accuracy in controlling the magnetic field and its gradient over the workspace. Therefore, efficacious control of the IPM is less trivial and the choice for suitable control techniques is crucial.

The MFE platform makes use of a single permanent magnet attached to the EE of a KUKA manipulator. Magnetic forces and torques are employed, in this context, to steer and guide the magnetic endoscope through the GI tract. However, due to the unintuitive nature of the interaction of the magnetic fields, the implementation of an intelligent and appropriate control technique is critical.

The inherited control strategy, developed from the previous group at the beginning of the project, was a standard Proportional-Integral-Derivative (PID) control which lacked two main elements:

- control over the 5th DoF i.e. the linear position of the endoscope along the gravity direction;
- control over the magnetic force which would guarantee the convergence of the force and improve the control properties.

Therefore, the main disadvantage of the inherited closed-loop control algorithm was that, if

placed in a realistic colon simulator, it would cause the MFE to get stuck in the folds of the colon tissue, as a consequence of not having control in the direction of gravity. Hence, a control approach able to levitate the endoscope, controlling the 5th DoF of the system i.e. the gravity direction, would solve the problem and achieve a smoother navigation of the endoscope.

Magnetic levitation is a phenomenon that can be achieved by counteracting the effects of the gravitational force by means of solely magnetic forces and torques. Moreover, since forces and torques are control inputs for magnetic agents, it is particularly efficacious to consider a quasi-static [14, 16] or a dynamic control approach [47]. Consequently, a dynamic control approach, that relates the IPM pose in the workspace to the magnetic forces and torques due to the magnetic field of the EPM, can be considered a suitable choice.

In this work the magnetic levitation has been achieved with two different approaches:

- Gravity compensation PID control
- Adaptive Backstepping control.

Both approaches, in contrast to the standard PID control, add an internal loop that aims to converge the actual force to the desired one. The latter, unlike the former, takes into account the dynamics of the IPM and is able to cope with parametric uncertainties and unknown bounded external disturbances.

On-the-other-hand, no control suitable for performing interventional tasks, such as biopsy or polyp removal, has been developed so far. Interventional tasks require precision and accuracy in order to be performed. Therefore, a model-based controller, which takes into account the main characteristics of the system and its dynamics, seems to be the best choice for these type of tasks. As a matter of fact, a model-based controller permits the analysis and synthesis of a control system based on a specific plant. Therefore, linearizing the plant on different and specific equilibria would enable the synthesis of different and effective controllers for each point of equilibrium, enhancing the overall performance of the controller.

3.2.2 Magnetic endoscope localization

Herein, the localization algorithm [199], inherited from the previous group, is briefly explained. In order to develop closed-loop control, a real-time localization algorithm must be incorporated into the control system. The following localization system is used in this thesis as the method

by which the real-time 6 DoF pose of the MFE is estimated. As a matter of fact, magnetic localization of the endoscope is essential to enable work on closed-loop control for navigation and stabilization of the magnetic endoscope, shown hereafter in the following chapters.

The following localization algorithm introduces a hybrid method that combines static and time-varying magnetic field sources. This approach has been introduced for solving the singularity of the problem. In fact, due to the symmetry of the cylindrical geometry of the EPM, the magnetic field creates a singularity plane normal to the magnetic moment of the EPM in which the system presents more than one solution and, thus, the endoscope pose cannot be estimated.

The information provided by the IMU, composed of an accelerometer and a gyroscope placed inside the endoscope, is fused by means of a Mahoney filter to compute roll and pitch angles. The yaw angle and the linear position are inferred comparing the information provided by the six Hall effect sensor, placed inside the endoscope, with a predefined map of the EPM magnetic field. The result is a probability distribution processed with a Particle filter.

Unfortunately, on the singularity plane, the system solution is not univocal. Therefore, the presence of an electromagnetic coil, orthogonal to the magnetic moment of the EPM, which generates an additional, orthogonal, time-varying magnetic field at 300 Hz is essential. The coil is treated as a permanent magnet and is considered separate from the EPM's magnetic field by means of a Goertzel's filter and the result is fed into the particle filter. This augments the dimension of the system, solving the singularity.

The current localization algorithm permits the estimation of the endoscope's pose with a positional accuracy of 5mm ($\pm$1 mm), and rotational accuracy of 5° ($\pm$0.8°), at 100 Hz.

3.2.3 Magnetic model and nomenclature

In the following, we discuss some basic concepts about magnetic actuation and define some of the variables used in this thesis. We consider IPM and EPM modeled as dipoles. We show how to compute the magnetic field B_m and magnetic force, f_m, and torque, τ_m.

Consider the vector between EE position (p_E) and IPM position (p_I), referred to as $p = p_E - p_I$. According to the dipole model, the magnetic field $B_m(p) \in R^3$ generated by the actuator magnet is

$$B_m = \left(\frac{||m_E||}{4\pi||p||^3} D(\hat{p})\hat{m}_E \right)$$

and the force and torque between EPM and IPM is

$$\begin{aligned} f_m &= \frac{3M}{||p||^4}(\hat{m}_E\hat{m}_I^T + \hat{m}_I\hat{m}_E^T + (\hat{m}_I^T Z\hat{m}_E)I)\hat{p} \\ \tau_m &= \frac{M}{||p||^3}\hat{m}_I \times D\hat{m}_E \end{aligned}$$

where $M = \frac{\mu_0||m_I||\ ||m_E||}{4\pi}$ with $m_I = ||m_I||\hat{m}_I$ and $m_E = ||m_E||\hat{m}_E$ *magnetic moments* of IPM and EPM, respectively; $\mu_0 = 4\pi 10^{-7}\frac{N}{A^2}$ permeability of vacuum, $\hat{p} = \frac{p}{||p||}$, $Z = I - 5\hat{p}\hat{p}^T$ and $D = 3\hat{p}\hat{p}^T - I$. Herein, $I \in \mathbb{R}^{3\times 3}$ is referred to as the *identity matrix* and $||\cdot||$ is the *Euclidean norm.*

It is well established that approximating the system with a dipole model leads to errors, which, in this scenario, are mainly related to the inter-magnetic distance between the two magnets. Following a trial-and-error process, the minimum and maximum inter-magnetic distances were determined to be 15 cm and 20 cm, respectively. The minimum value is the safest minimum distance of the EPM from the abdominal wall, the maximum is the distance at which the magnetic force and torque exerted on the MFE is still appreciable. However, the error on the dipole model at the mean distance can be consider negligible since was estimated to be less than 10% for both the IPM and EPM.

Chapter 4

Magnetic Levitation

This chapter presents the magnetic levitation of the MFE, a technique that aims to facilitate the inspection of the colon by reducing contact with the colon walls and, thus, achieve a smoother navigation of the endoscope, by avoiding to get stuck in the colon folds. Two different non-linear backstepping approaches are taken into account to achieve a successful levitation. Both control techniques were implemented by controlling the position of the endoscope along the gravity direction and adding a further internal loop, a force control aimed to converge the actual magnetic force to the desired one, guaranteeing the overall convergence of the entire system. Initially, a gravity compensation PID control was implemented to prove the feasibility of the magnetic levitation. In fact, counteracting the gravity allows the endoscope to levitate and maintain the center of the lumen, reducing the contact with the environment. The feasibility of this approach was theoretically proven with the Lyapunov approach. Therefore, a more suitable and sophisticated control approach, Adaptive Backstepping control strategy, was considered in order to provide confidence of stability and performance of the levitation technique. This second approach adds a further control loop which estimates the dynamics of the IPM considering the parametric uncertainties of the system and the possible external disturbances due to the interaction of the tether with the external environment. A theoretically proof of stability was provided with the Lypunov approach in order to strengthen the work.

Chapter source: Adaptive Dynamic Control for Magnetically Actuated Medical Robots, by Lavinia Barducci*, Giovanni Pittiglio*, Joseph C. Norton, Keith L. Obstein, & Pietro Valdastri, IEEE Robotics and Automation Letters volume 4, pages 3633-3640 (2019).

Other related papers: Magnetic Levitation for Soft-Tethered Capsule Colonoscopy Actuated With a Single Permanent Magnet: A Dynamic Control Approach, by Giovanni Pittiglio*, Lavinia Barducci*, James W. Martin, Joseph C. Norton, Keith L. Obstein, & Pietro Valdastri, IEEE Robotics and Automation Letters volume 4, pages 1224-1231 (2019).

4.1 Magnetic Levitation for Soft-Tethered Capsule Colonoscopy Actuated with a Single Permanent Magnet: a Dynamic Control Approach

4.1.1 Abstract

The present work investigates a novel control approach for magnetically driven soft-tethered capsules for colonoscopy - a potentially painless approach for colon inspection. The focus of this work is on a class of devices composed of a magnetic capsule endoscope actuated by a single external permanent magnet. Actuation is achieved by manipulating the external magnet with a serial manipulator, which in turn produces forces and torques on the internal magnetic capsule. We propose a control strategy which, counteracting gravity, achieves levitation of the capsule. This technique, based on a nonlinear backstepping approach, is able to limit contact with the colon walls, reducing friction, avoiding contact with internal folds and facilitating the inspection of non-planar cavities. The approach is validated on an experimental setup which embodies a general scenario faced in colonoscopy. The experiments show that we can attain 19.5 % of contact with the colon wall, compared to the almost 100 % of previously proposed approaches. Moreover, we show that the control can be used to navigate the capsule through a more realistic environment - a colon phantom - with reasonable completion time.

4.1.2 Introduction

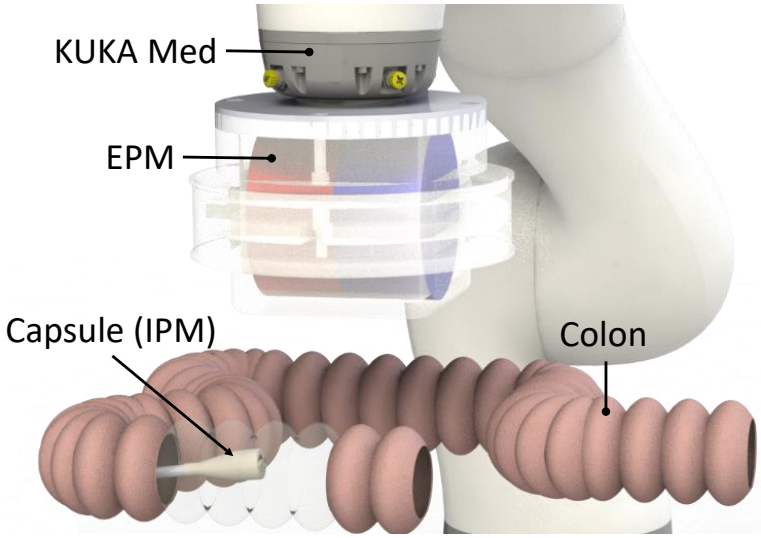

Figure 4.1: Schematic representation of the platform.

Over the last decade, magnetically actuated robotic platforms have had a significant impact

in the field of medical robotics, providing new tools to facilitate minimally invasive diagnosis and therapy in different regions of the human body. The main advantage of magnetically actuated robots is the application of functional forces and torques without the need for the alternative, often complex and bulky on-board locomotion mechanisms. Due to this advantage, these devices have been investigated for several endoscopic procedures such as *colonoscopy* [12, 23, 24], *gastroscopy* [26], *cardiac applications* [15, 203–206], *surgery* [20] and *bronchoscopy* [207].

In general, magnetically actuated endoscopic robots can be subdivided in terms of external actuation, between *coil-based* [14–19, 208], *rotating permanent magnets-based* [21, 22] and *permanent magnet-based* [12, 23, 24, 26, 209] devices. The first ones generate a magnetic field, generally, based on the usage of multiple coils within a predefined workspace. The second ones make use of rotating magnets instead of coils. Permanent magnet-based devices are actuated by a single permanent magnet, manipulated by a serial robot.

Systems that use multiple coils generally have higher controllability owing to the fine control over the magnetic field within the workspace. However, these systems are often more bulky, have a confined workspace, are expensive and have a high energy consumption that may hinder their practical use.

Rotating permanent magnets-based devices, permit 6 DoFs steering, when employing multiple magnets [22]. This approach avoids heating normally associated with using coils, but shares the same limitations in terms of workspace.

The focus of the present work is MFE actuated with single EPM [12, 23], shown in Fig. 4.1. This has been investigated as an alternative to standard colonoscopy, with the main advantages of being ease-of-use and reduced patient discomfort - two significant drawbacks with the current procedure. Standard colonoscopes, pushed from outside the body, advance through the colon by exerting pressure on the bowel wall. This environmental interaction is needed to steer the device and conform its shape to the tortuous lumen. On-the-other-hand, soft-tethered magnetic capsules are controlled by an externally applied force focused at the tip of the device. Therefore, in order to advance the capsule, there is no need to exert stress on the lumen; the forces are applied in the required direction only and the soft tether follows passively.

However, a potential limitation of this platform is the continuous attraction of the capsule to the EPM and lack of gravity compensation [29]. This may cause the capsule to become

trapped in the anatomically complex and unstructured environment of the colon and may hinder locomotion through a steeply sloping lumen. The method in [29] is able only to control 4 DoFs: 2 DoFs on the plane, pitch and yaw. However, magnetic coupling between 2 single-dipole permanent magnets inherently permits the actuation of 5 DoFs; due to the cylindrical symmetry of the magnetic field, capsule roll is not possible. Therefore, the goal of our contribution is to enhance current practice by adding the actuation of the 5th DoFs: the one along the gravity direction. This aims to reduce contact with the environment and facilitate locomotion. However, the fundamental challenge of the proposed approach is that the equilibrium between magnetic force and gravity is highly unstable and, therefore, the control design is nontrivial.

While levitation is technically easier to implement in coil-based systems [210], in this work we aim to show that accurate control can be used to counter the limited controllability of systems with a single EPM. We show that levitation (controlling the capsule in the gravity direction) is feasible and can be done in free-space, i.e. without the need for a fluid medium [4]. This is relevant in the context of colonoscopy because the lumen is routinely distended with a gas medium. This control strategy can bring significant benefit as it facilitates the avoidance of obstacles (eg. tissue folds), a reduction in contact force and therefore, a reduction in both friction and risk of trauma or discomfort. It may also assist with navigating sloped regions of the colon.

This work is organized as follows: in Section 4.1.3 we provide a general overview of the method, which is explored further in Section 4.1.4. Sections 4.1.5 and 4.1.6 present the experimental data, which aims to prove the strength of the proposed approach; the former discusses free space levitation in a L-shaped acrylic tube, the latter reports the results obtained in a more realistic colon phantom. Section 4.1.7 draws our main conclusions and discusses future work.

4.1.3 Method

In the following we aim to describe a general approach for magnetic capsule levitation using a single EPM. The EPM is controlled by a serial manipulator and the capsule contains a magnet, referred to as IPM[1]. This is shown in Fig. 4.1. Achieving accurate control with robotically actuated permanent magnets [26] is challenging, due largely to the high inertia related to the movements of the large EPM and serial manipulator, compared to current flow. Moreover,

[1]In the following we use the name Internal Permanent Magnet also in reference to the magnetic capsule.

when considering only a single magnetic source, point-wise control of the magnetic field and its gradient is not as straightforward as in using multiple coils.

In order to achieve levitation we need to guarantee that the force on the IPM counteracts gravity, in an equilibrium state that is highly unstable. The approach taken can either be to design a controller aware of the dynamics of the IPM or to design a suitable trajectory planner that does not require the dynamic equilibrium to be considered. Our initial approach was to purse the latter and avoid the use of the system dynamics. As is shown in subsequent sections, this is a feasible approach that achieves asymptotic stability.

The overall control strategy is based on the *backstepping technique* and the global stability is formally proved by means of a Lyapunov-based approach [211]. This is guaranteed under the assumption that the desired trajectory of the IPM is a *piecewise-constant* function of the time. This means that desired velocity and acceleration of the IPM can be neglected. In this condition, a PD controller can be designed to steer the IPM and achieve asymptotic convergence. The assumption made does not interfere with the design of the controller, nor is limiting in any case when a smooth planning can be achieved.

This control technique uses capsule localization (100 Hz, 4 mm accuracy) [199], where the pose and inferred force and torque are known.

4.1.4 Dynamic Control

We take into account a *back-stepping* approach [211] on two levels (or loops): pose loop (Section 4.1.4) and force loop (Section 4.1.4). The latter, considered as an internal loop, is designed to guarantee the convergence of the actual force on the IPM to the desired one, while the former aims to steer the IPM. The presence of the internal force loop improves the control properties, compared to previous approaches [26, 29], and it is fundamental for levitation. Given the unstable force equilibrium, it is essential to guarantee the stability of this internal loop before attempting to steer the IPM. This control strategy is summarized in Fig. 4.2.

In this work, we only consider the dynamics of the capsule subject to forces and torques exerted by the EPM. These forces and torques, embedded in the vector $\tau_m \in \mathbb{R}^n$, depend on the relative position between the IPM and EPM. In general, $n = 5$ for single external magnetic source and $n = 6$ for multiple magnetic sources [16]. We consider that the two permanent magnets can be approximated with the *dipole model*, which is enough accurate given their geometry and relative

distance. Possible errors related to dipole modelling are discussed along with the experimental data provided in Sections 4.1.5.

In the present work, the presence of a tether is considered an unmodeled disturbance. In the specific case under analysis, the tether is beneficial as it acts as a stabilizing damper on the dynamics along the gravity direction, improving stability in the system. There is no limitation in applying the proposed method to untethered capsules, but we expect the need for a faster control loop to handle the less damped dynamics.

Consider the nominal dynamics of the capsule

$$B(x)\ddot{x} + C(x,\dot{x})\dot{x} + G(x) = \tau_m(x,q), \tag{4.1}$$

where $x \in \mathbb{R}^n$ is the capsule pose (position and orientation) and $q \in \mathbb{R}^m$ embeds the robot joint variables; matrices $B(x),\ C(x,\dot{x}),\ G(x)$ are the respective *inertia*, *Coriolis matrix* and *gravity* [212]. Our aim is to find q such that x approaches a desired value x_d.

The relationship $\tau_m(x,q)$ is the magnetic dipole force and torque exerted by the EPM on the IPM. This relationship is highly nonlinear, confounding computation of q given the desired force and torque on the IPM. Therefore, we consider a time derivation of this function [29], which reads as

$$\dot{\tau}_m = \frac{\partial \tau(x,q)}{\partial x}\dot{x} + \frac{\partial \tau(x,q)}{\partial q}\dot{q} = J_x\dot{x} + J_q\dot{q}, \tag{4.2}$$

and turns τ_m into a state variable for the system we aim to control and $\dot{q}$ into the control input; matrices J_x and J_q are derived in [47]. The variables $\dot{q}$ can be integrated to control the robot through its DK [212]. The novelty of our control system, compared to [29], is that we apply a closed-loop control on τ_m.

The overall dynamics we aim to control reads as

$$\begin{cases} B(x)\ddot{x} + C(x,\dot{x})\dot{x} + G(x) &= \tau \\ \dot{\tau} &= J_x\dot{x} + J_q\dot{q} + \dot{\nu} \end{cases}, \tag{4.3}$$

where ν models the tether interaction with the environment, for example: drag, elastic behaviour and friction; τ is the actual force and torque on the capsule. The localization method [199] ensures that x and $\dot{x}$ can be measured. The robot joints are measured by the embedded

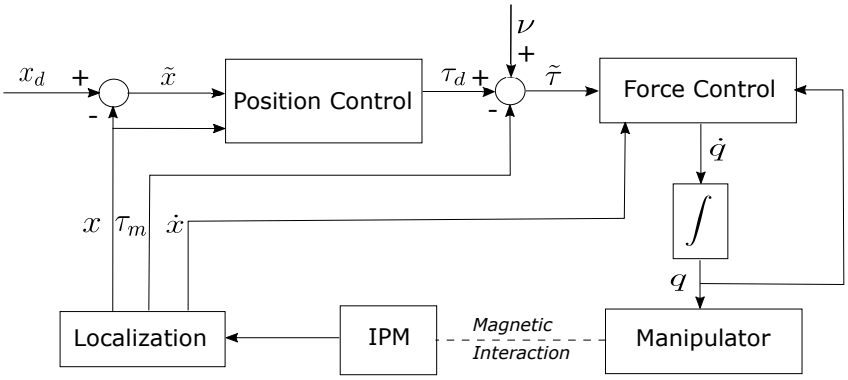

Figure 4.2: Control scheme.

encoders.

In the following sections we describe the main steps in the derivation of the controller and conclude by proving the stability of the controlled system, using Lemma 4.1 and Theorem 4.3.

Pose Control

Defining a pose controller that attempts to steer the IPM to a desired trajectory (x_d) is the first step and is achieved by first considering that τ can be deliberately set as a control input for the upper dynamics in 4.3. Because of the nonlinearities we attempt to find a set of desired forces and torques (referred to as τ_d). Afterwards, as described in the next section, we aim to control the actual torque (τ) to τ_d. The stability of this backstepping approach, as shown in Section 4.1.4, guarantees the overall convergence.

We want to prove that the *PD with gravity compensation*

$$\tau_d = G(x) + K_p\tilde{x} + K_d\dot{\tilde{x}}, \tag{4.4}$$

with $\tilde{x} = x_d - x$, guarantees $x \to x_d$ as $\tau \to \tau_d$. This is achieved under the following assumption.

Assumption 1. *The steering of the IPM is achieved by considering that:*

- *the force control, described in Section 4.1.4, is faster than the system dynamics in 4.1;*
- *the desired trajectory is a* piece-wise constant function of the time.

The former leads to assume that there exists an instant T, $0 < T \ll 1$, such that $\tau(t) = \tau_d(t),\ t \geq T$. In other words, we consider almost instantaneous convergence of force and torque. This simplification is used to prove the first step of the backstepping; Section 4.1.4 discusses the

case of a weaker assumption. The need for this assumption is justified by the following lemma, on which the final proof of this work (Theorem 4.3) is based.

Lemma 4.1. *Under Assumption 1, the pose controller in 4.4 achieves asymptotic stability of the error $\tilde{x}$, for any positive definite design gains K_p and K_d.*

Force Control

The second step in the design of the controller is to ensure that τ converges to τ_d and do so almost instantaneously (according to Assumption 1). The magnetic force and torque are computed from x and q by employing the localization data and dipole model.

In order to design an asymptotically stable controller for force and torque, we take into account 4.2 and search for $\dot{q}$ such that the dynamics for $\tilde{\tau} = \tau_d - \tau_m$ evolves as

$$\dot{\tilde{\tau}} = -K\tilde{\tau}, \tag{4.5}$$

with K positive definite design gain. This leads to asymptotic stability of the force and torque error dynamics.

By substituting 4.2 into 4.5 we obtain

$$\dot{\tau}_d - \dot{\tau}_m = -K\tilde{\tau}$$
$$\dot{\tau}_d - J_x\dot{x} - J_q\dot{q} = -K\tilde{\tau}$$

whose solution, with respect to $\dot{q}$, is

$$\dot{q} = J_q^{\dagger}(\dot{\tau}_d + K\tilde{\tau} - J_x\dot{x}). \tag{4.6}$$

Here $(\cdot)^{\dagger}$ stands for the *Moore-Penrose pseudoinverse* [212]. Note that the derivative of the desired torque τ_d can be analytically computed from the localization data.

Lemma 4.2. *Under the assumption that the disturbance $\nu \simeq 0$, any positive definite gain K achieves stability of the torque dynamics.*

Proof. Under the drawn assumption, $\tau \simeq \tau_m \to \tau_d$. □

Assuming the tether interactions to be negligible is justified by the fact that the tether used in our platform interacts with the environment with a very low friction coefficient - the tether and colon are both smooth and lubricated. Furthermore, considering that the tether is significantly stiffer than the colon, the elastic restoring forces would have minimal impact on capsule dynamics and any deformation would be seen primarily in the wall of the colon.

Overall Control

In the following, we describe the overall control strategy by considering the above results. In particular, we show that with the choice of $\dot{q}$

$$\begin{cases} \tau_d &= G(x) + K_p\tilde{x} + K_d\dot{\tilde{x}} \\ \dot{q} &= J_q^{\dagger}(\dot{\tau}_d + K\tilde{\tau} - J_x\dot{x} - \dot{x}) \end{cases}, \tag{4.7}$$

we can weaken Assumption 1. The new choice of $\dot{q}$ leads to

$$\dot{\tilde{\tau}} = -K\tilde{\tau} + \dot{x},$$

which achieves overall convergence, as discussed in Theorem 4.3. Therefore, the assumption under which we guarantee the overall convergence of the controlled system is the following.

Assumption 2. *The desired trajectory x_d is* piece-wise constant function *of the time and $\nu \simeq 0$.*

We can prove the convergence of the controlled dynamics, as in the following theorem.

Theorem 4.3. *Under Assumption 2, the controller defined in 4.7 achieves asymptotic stability of the dynamics 4.3, for any positive definite design gains K_p, K_d and K.*

This is elaborated in the Appendix section in [47].

4.1.5 Experimental analysis: Free space Levitation

The aim of the experimental work was to show that we can achieve levitation, including steering the capsule through inclined trajectories. This could be an essential tool for facilitating effective locomotion in the presence of obstacles and complex colon geometries.

The IPM was first placed into an acrylic tube with a realistic inner diameter of 60 mm [89], bent at an angle of 90 degrees in the center. Each half of the tube was 250 mm long. The

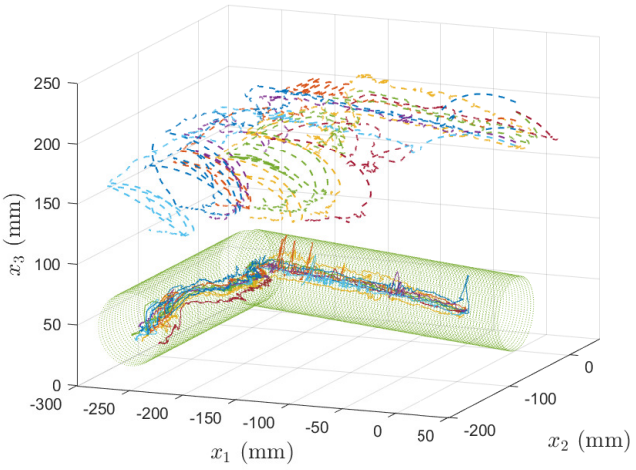

Figure 4.3: 3D tracking. The IPM (solid line) and EPM (dashed line) trajectories for all trials performed.

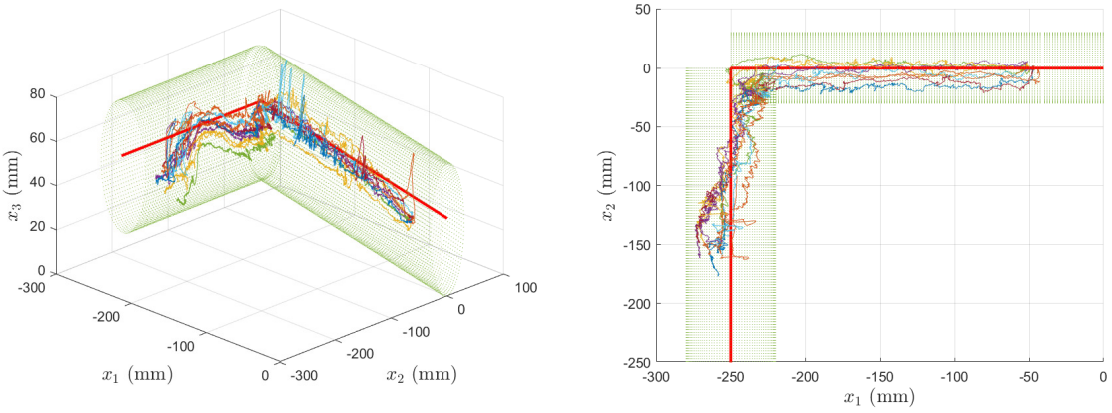

(a) 3D trajectories.

(b) Trajectories on x-y plan

Figure 4.4: 3D tracking. The desired IPM trajectory (red solid line) and actual trajectories for all trials performed.

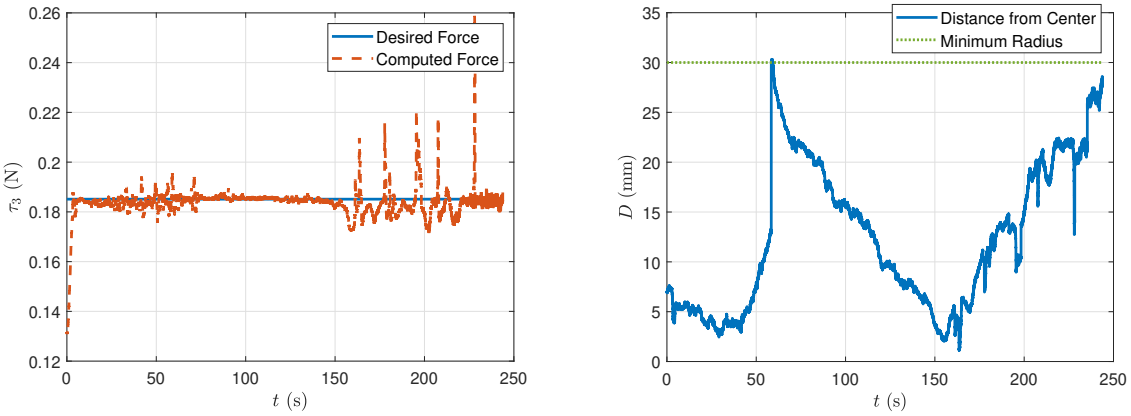

(a) Mean levitating force.

(b) Mean distance from wall.

Figure 4.5: Evaluation of levitating performance.

tube was inclined by approximately 20 mm over its length. This was chosen to show our controller performance when moving the capsule along the gravity direction (x_3). The referenced trajectory was computed off-line, via a trial and error technique, with a step size of 0.01 m. At half of the tube, where the trajectory rotates by a 90 degree angle, the orientation step size was chosen as 0.1 degree.

The IPM (axially magnetized, 21 mm diameter, 19 mm length, 15 g mass) is actuated using an EPM (axially magnetized, 101.6 mm diameter and length, 1.48T, N52) at the EE of a serial manipulator (KUKA LBR Med R820[2]). Localization [199] and control loop both run at approximately 100 Hz. The error in the dipole models were computed by considering [213] and the conditions during experiments. For the EPM, the maximum and mean error were 13 % and 3 % respectively. Whereas the corresponding errors for the IPM were 0.2 % and 0.06 % respectively. Magnetic interference was minimized by keeping the workspace free from ferromagnetic materials.

To show the efficacy of the control strategy, we commanded the capsule to traverse the acrylic tube in 10 trials. We report the 3D trajectories of the IPM and EPM in Fig. 4.3. In Fig. 4.4 we report the desired and actual IPM trajectories with a focus on the z direction 4.4(a) and on the x-y plan 4.4(b). The mean force along the gravity direction (τ_3), measured throughout the trajectories, is shown in Fig. 4.5(a). The mean distance between the capsule and the center of the tube (D), is shown in Fig. 4.5(b). These give an indication of the levitation performance; in-other-words, how effectively the system prevents the capsule from touching the surrounding walls.

We controlled the capsule to be in the center of the lumen on the $x_1 - x_2$ plane while maintaining the minimum height on the axis x_3 which achieves levitation - i.e. where τ_3 counteracts gravity. In the first part of the tube, this objective translates directly into levitating the capsule, as shown in Fig. 4.3 and 4.4. On-the-other-hand, in the second half of the path, the stiffness of the tether and acrylic tube leads to capsule-tube contact because of their large resistance to deformation, as shown in Fig. 4.4(b), 4.5(b). In this case the EPM is not able to exert enough force to counteract this resistance, in fact Fig. 4.5(a) shows force oscillations in the final part of the graph. Although the tether properties negatively impact simultaneous steering and levitation, the experiments show that the control strategy can resume capsule levitation

[2] `https://www.kuka.com/en-gb/industries/health-care/kuka-medical-robotics`

after moving past the corner.

Fig. 4.5(b) quantifies the amount of contact with the internal wall. The event of the capsule touching the wall is quantified by geometric constraints and real-time localization. The latter provides information about the position of the capsule inside the acrylic tube (upon an initial registration). The result is that, on average, the capsule is in contact with the tube 19.5 % of the time, compared to almost 100 % for previous methods [29]. Less contact with the environment can be equated to smoother locomotion.

4.1.6 Experimental analysis: Colon Phantom

In the following we describe an experiment performed on the M40 Colonoscope Training Simulator[3] in *standard configuration*. The aim was to show that the proposed method is able to control the IPM in a more realistic environment that is deformable, unstructured and contains obstacles. While quantitative feedback on capsule-environment contact could not be measured in this setup, the results show the feasibility of pursuing this control strategy.

These tests also validate our assumption of considering the tether dynamics as a disturbance, as the capsule is able to successfully traverse the complex environment despite tether-environment interaction. The colon has a low stiffness and provides little resistance to deformation from the comparatively stiffer tether.

We performed 5 trials in which the user (an individual with no prior endoscopic experience, but knowledge of the system) was tasked with traversing the colon phantom from sigmoid to ceacum. The user was provided with visual feedback from the capsule's on-board camera and could manipulate the capsule pose using a 3D mouse. The input from the user, via a 3D mouse, is discretize with respect to the maximum step size (0.01 m) to ensure a piece-wise constant trajectory. This setup is shown in Fig. 4.6. In Fig. 4.7 we show the colon phantom with all 5 trajectories overlaid.

The overall task had a mean completion time of 346.78 s with standard deviation of 119.37 s, for a path of approximately 0.85 m. This would equate to exploring a typical human colon in approximately 13 min, assuming an average colon length of 1.85m [89] and a mean capsule velocity of 2 mm/s seen in these experiments. In order to investigate the real performance of the proposed approach, a deeper analysis will be performed with expert users, as in [23].

[3] `https://www.kyotokagaku.com/products/detail01/m40.html`

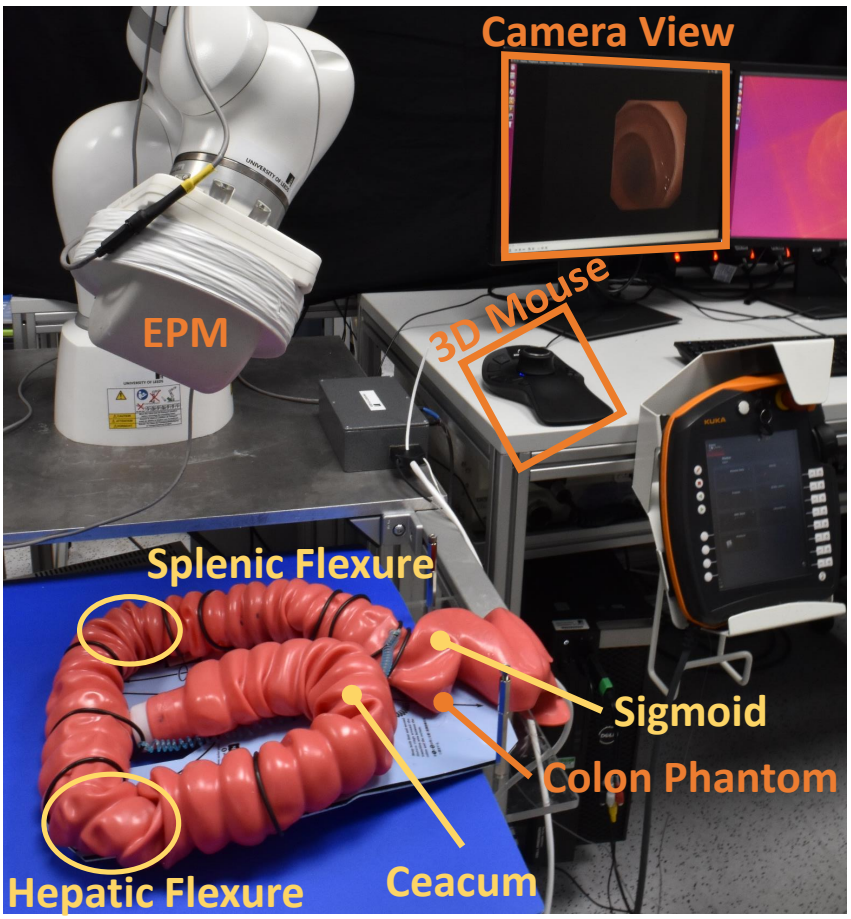

Figure 4.6: Experimental setup: colon simulator.

Increasing the velocity is related to two factors: the frequency of the control loop and the need for Assumption 2. The current localization frequency (100 Hz) is not fast enough to guarantee the capsule dynamics are handled completely and so increasing this would have a direct impact on system performance. Assumption 2 can be overcome by performing techniques which consider the system dynamics. These will be explored in future work.

4.1.7 Conclusions

The present work discussed a novel control technique for capsule levitation in magnetically driven capsule colonoscopy. This was motivated by the potential benefits of reduced friction, and obstacle avoidance, for improved locomotion in complex environments such as the colon. This is important as locomotion in this context is extremely challenging; devices are prone to becoming trapped in the soft folds of tissue and friction/drag can hinder progress. Although the magnetic system is inherently gentle, deforming the environment very little, the proposed control strategy improves this further and so may reduce clinical risks and patient discomfort. The

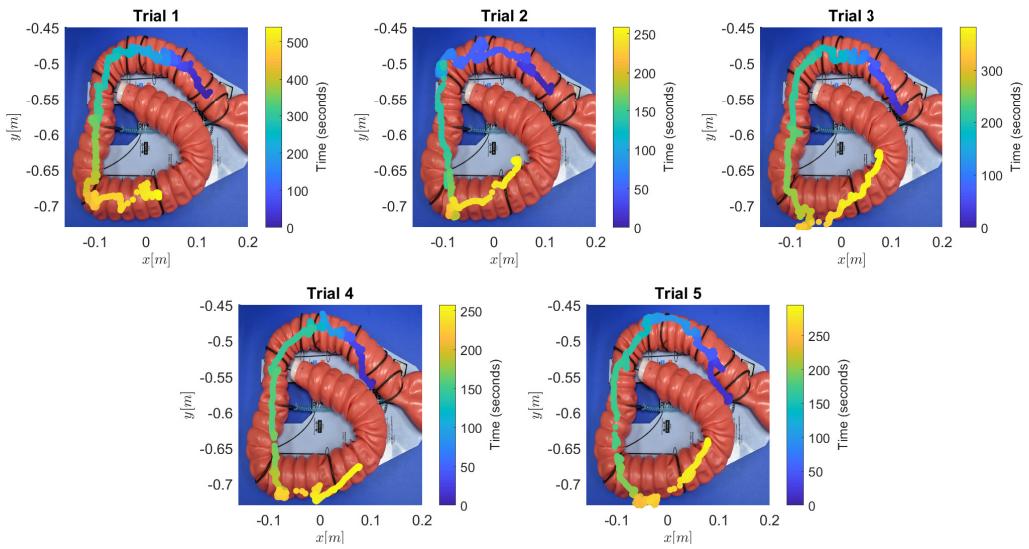

Figure 4.7: Trials on the colon simulator.

control strategy is based on a gravity compensation approach which attains capsule levitation and fine control along the gravity direction, while also permitting capsule steering.

The asymptotic stability of the proposed technique was proved by employing the Lyapunov approach and supported in the experimental results from tests in an acrylic tube. These results show that, while levitating, we are able to handle slopes and, compared to previous solutions, reduce contact with the cavity from approximately 100 % to 19.5 %. On the base of these results, we can conclude that the control approach is a promising technique for general application in magnetically driven capsule colonoscopy.

In order to strengthen this inference, we also performed colonoscopy on a phantom simulator for colonoscopy training. These results show that we can perform colonoscopy by employing the levitation technique. Due to the encouraging results obtained in the colon phantom, we aim to confirm our findings in more realistic experimental settings (i.e. animal and cadaver models) in the near future. Moreover, we will investigate the possibility of using the solely levitation or any combination of it with other control techniques.

One of the current limitations of the present work is assuming that tether-environment interactions are negligible disturbances. In our future works, we will also investigate how to integrate these interactions in out control scheme, possibly by embedding real-time shape sensors inside the tether.

4.2 Adaptive Dynamic Control for Magnetically Actuated Medical Robots

4.2.1 Abstract

In the present work we discuss a novel dynamic control approach for magnetically actuated robots, by proposing an *adaptive control* technique, robust towards parametric uncertainties and unknown bounded disturbances. The former generally arise due to partial knowledge of the robots' dynamic parameters, such as inertial factors, the latter are the outcome of unpredictable interaction with unstructured environments. In order to show the application of the proposed approach, we consider controlling the Magnetic Flexible Endoscope (MFE) which is composed of a soft-tethered Internal Permanent Magnet (IPM), actuated with a single External Permanent Magnet (EPM). We provide with experimental analysis to show the possibility of levitating the MFE - one of the most difficult tasks with this platform - in case of partial knowledge of the IPM's dynamics and no knowledge of the tether's behaviour. Experiments in an acrylic tube show a reduction of contact of the 32% compared to non-levitating techniques and 1.75 times faster task completion with respect to previously proposed levitating techniques. More realistic experiments, performed in a colon phantom, show that levitating the capsule achieves faster and smoother exploration and that the minimum time for completing the task is attained by the proposed approach.

4.2.2 Introduction

Magnetically actuated robots have been investigated during the last decades, particularly in the field of medical robotics. The main advantage of magnetically actuated robots is the potential miniaturization; this approach permits to overcome complex and bulky actuation system, achieving *minimally invasiveness*. This is generally equated to a reduction of patient discomfort and post-operative recovery time. Miniaturization is also feasible because functional forces can be maintained by balancing an arbitrarily small IPMs with a sufficiently large EPM.

Due to these advantages, this class of robot has been investigated for application to several fields of medicine, from endoscopic procedures, such as *colonoscopy* [23–25], *gastroscopy* [26] and *cardiac applications* [15, 203–206] to *microrobotics* [214]. Magnetic external actuation can vary from coil-based systems [14–20], rotating permanent magnet-based devices [21, 22]

and permanent magnet-based systems [23–27]. All these actuation mechanisms share similar control properties, in fact, actuation is based on employing the previously mentioned actuators for generating forces and torques focused on magnetic agents. Since the control inputs for these robots are forces and torques, it is particularly effecacious to consider a quasi-static [14, 16] or a dynamic control approach [47]. The latter has the advantage of considering the overall physical properties of the robots and permits faster and more accurate control.

We propose an *adaptive dynamic control* approach [215], able to cope with parametric uncertainties, such as inertial factors, and robust towards the presence of unknown bounded external disturbances. The former are, generally, related to partial knowledge of the robots' mechanical properties, the latter may be related to unstructured forces arising from the interaction with an unknown environment. This control technique employs the knowledge of the IPM pose, achieved by using an appropriate localization technique such as [199] or [216].

In order to discuss the application of the proposed technique, we focus on the control of the MFE [23], a innovative minimally invasive platform for colonoscopy. We consider the case of actuating a single *soft-tethered* IPM by employing a robotically manipulated EPM. Moreover, we consider partial knowledge of the mass and dimensions of the IPM and no information about the tether. While we focus on one platform, this proposed method could be applied to other actuation systems and untethered capsules [21].

Herein, we show successful *magnetic levitation* [47] which helps overcoming the major issue of previously proposed control techniques [29]: continuous attraction between the IPM and EPM. Successful levitation can encourage obstacle avoidance and a smoother navigation. It can also result in a reduction of pressure applied to the environment which will reduce discomfort for the patient and risk of adverse events.

This paper is organized as follows: in Section 4.2.3 we provide a general overview of the method, which is utilised and explored further in Section 4.2.4. Sections 4.2.5 and 4.2.6 present the experimental results, comparing the proposed approach with the ones discussed in [29, 47]; the former discusses free space levitation in a L-shaped acrylic tube, the latter reports the results obtained in a more realistic environment (a colon phantom). In Appendix 4.A, we discuss the basic concepts of the magnetic actuation, while Appendix 4.B reports proofs of lemmas and theorems employed in the paper.

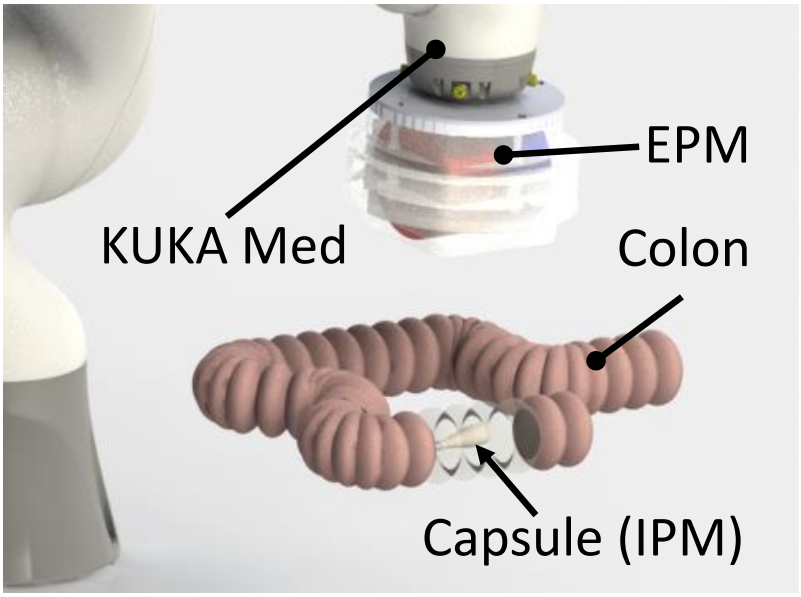

Figure 4.8: Schematic representation of the platform.

4.2.3 Control Overview

The dynamic control approach discussed in the following is achieved using a single EPM controlled by a serial manipulator. Another magnet, referred to as IPM[4] is housed within the capsule. This is shown in Fig. 4.8.

In this scenario, the most unstable equilibrium is the one along the gravity direction. In fact, we need to guarantee that the force on the IPM counteracts gravity in an equilibrium state that is highly unstable. A dynamic control approach takes into account all forces that act on the system. In particular, the coupling between magnets is directly expressed in terms of interaction (generalized) forces; levitation is the outcome of the equilibrium of these forces with gravity.

In our previous work [47], we proposed a dynamic control approach that allows the IPM to levitate in a realistic environment, such as a colon phantom. The main drawback of this technique lies in two main assumptions: the desired trajectory was considered as a *piece-wise constant function of the time* and IPM-tether interactions were assumed negligible. The former restricts velocity of the IPM movements, while the latter does not guarantee convergence in a general scenario. In this paper, we aim to weaken both assumptions by employing an *adaptive dynamic* control and by proving *ultimately uniform bounded stability* of the proposed approach.

Compared to the previously proposed solution [47], we present a novel approach which takes

[4]In the following the soft-tethered capsule is also referred to as Internal Permanent Magnet.

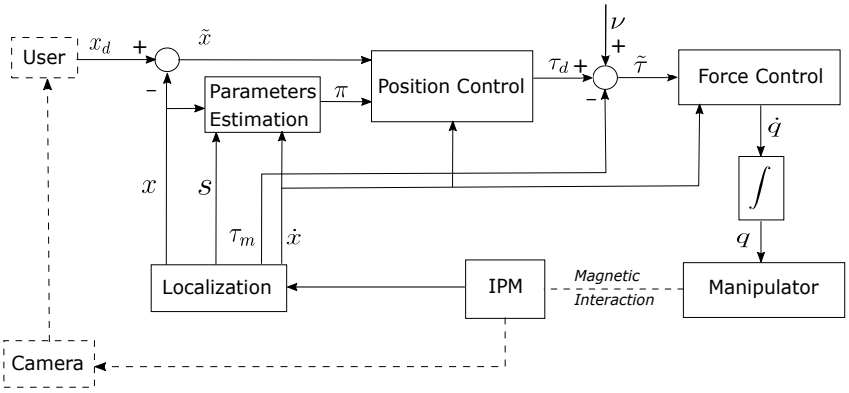

Figure 4.9: Control scheme.

into consideration the dynamics of IPM and deals with possible parametric uncertainties. The proposed technique is an *adaptive* control, which considers uncertainties such as the mass, dimensions of the IPM and the dynamics of the tether. In particular, the IPM mass is strongly affected by the tether. In fact, during levitation, a consistent section of the tether is lifted. The proposed control strategy autonomously modifies its parameters in order to adapt them to the actual system dynamics. Therefore, a further control loop has been inserted in the dynamic control in order to achieve convergence of the estimated dynamic parameters.

This control technique uses capsule localization (100 Hz, 4 mm accuracy) [199].

4.2.4 Dynamic Control

The control strategy proposed herein is based on the *backstepping technique* which, compared to [26, 29], adds a control loop on the force. This improves controller stability, as discussed in [47]. Moreover, as an advancement of [47], we added a further internal loop which estimates the dynamics of the IPM and takes into account the effect of the tether. The scheme in Fig. 4.9 shows the proposed control strategy (solid lines). The external loop (dashed lines) represents the user interface which is not investigated in the present work.

Therefore, the control has three key components: pose control (Section 4.2.4), parameters estimation (Section 4.2.4) and force control (Section 4.2.4). Pose control, considered as the external loop, aims to steer the IPM to the desired pose. The parameter estimation improves the controller properties, since this allows the assumptions to be weakened by the knowledge of the system dynamics. Force control, referred to also as “internal loop”, aims to converge the actual force to the desired one. The stability of this backstepping approach, as shown in Section 4.2.4, guarantees the overall convergence.

Fundamentally, the dynamics of the IPM is subjected to the magnetic interaction between EPM and IPM. The magnetic fields are approximated by the *dipole model* and are considered accurate for our purpose: given the geometry and relative distance between the two magnets, we can infer that the error does not significantly affect the control of the IPM. Possible errors related to dipole modelling are discussed in Section 4.2.5. The magnetic force and torque, exerted by the EPM on the IPM, can be written as a vector $\tau_m(x, q) \in \mathbb{R}^n$.

Consider the nominal dynamics of the IPM

$$B(x)\ddot{x} + C(x, \dot{x})\dot{x} + G(x) = \tau_m(x, q), \tag{4.8}$$

where $x \in \mathbb{R}^n$ is the IPM pose (i.e. position and orientation) and $q \in \mathbb{R}^m$ embeds the robot joint variables; $B(x)$, $C(x, \dot{x})$, $G(x)$ are referred to as *inertia*, *Coriolis matrix* and *gravity* [212] of the IPM, respectively. Our aim is to find q such that x approaches a desired value x_d.

This is achieved in two steps: first the value of the desired torque (τ_d) is found for $x \to x_d$, considering the dynamics of the unknown parameters, then we define $\dot{q}$ for which $\tau_m \to \tau_d$, according to the dynamics of the force and torque

$$\dot{\tau}_m = \frac{\partial \tau(x, q)}{\partial x}\dot{x} + \frac{\partial \tau(x, q)}{\partial q}\dot{q} = J_x\dot{x} + J_q\dot{q}. \tag{4.9}$$

The analytical computation of the matrices J_x and J_q is thoroughly explained in Appendix 4.A. The variables $\dot{q}$ can be integrated to control the robot through its DK [212]. The novelty of our control system, compared to [29], is that we apply a closed-loop control on τ_m, as in [47]. Compared to [47], we introduced a further control loop in which we guarantee the convergence of the unknown parameters of the dynamic system.

The proposed approach takes into consideration how the tether can affect the dynamics of the IPM. It is herein considered an unmodelled disturbance on the IPM dynamics, in order to underline the robustness of the proposed approach. However, we show the stability of the proposed technique (Theorem 4.6) also in absence of the tether, as in the case of untethered capsules [26]. We do not consider the case of known tether properties since, even in the case tether dynamics can be predicted, interaction with the environment would confound them. Therefore, we consider the most general case of dynamic control of a single IPM.

In order to consider possible parametric uncertainties, embedded in the parameters vector $\pi \in \mathbb{R}^p$, we rewrite the dynamics in 4.8 as

$$B(x)\ddot{x} + C(x,\dot{x})\dot{x} + G(x) = Y(x,\dot{x},\ddot{x})\pi, \tag{4.10}$$

where $Y(x,\dot{x},\ddot{x}) \in R^{n\times p}$ is the *dynamic regressor*, computed as in [217]. The update law of π allows the unknown parameters to converge to their real values, guaranteeing the robust asymptotic stability of the overall system. Appendix 4.B describes this in more detail.

The overall dynamics of the system we aim to control reads as

$$\begin{cases} Y(x,\dot{x},\ddot{x})\pi &= \tau \\ \dot{\tau} &= J_x\dot{x} + J_q\dot{q} + \dot{\nu} \end{cases}, \tag{4.11}$$

where ν models the tether interaction with the environment (such as: drag, elastic behaviour, friction and colon motions) and π embeds the uncertain parameters of the IPM, such as the mass, the length and the diameter. The localization method [199] measures x and $\dot{x}$, while the robot joints are measured by the embedded encoders.

Pose Control

As a first step, we define a pose controller that attempts to steer the IPM to a desired trajectory x_d. We aim to find a set of desired forces and torques, referred to as τ_d, that steer the IPM to the desired pose. Compared to [47], we consider partial knowledge of the dynamics of the system, using the *Adaptive Backstepping Control* [211, 215].

The control law can be determined directly through a standard Lyapunov approach, by defining

$$\begin{aligned} \tau_d &= \hat{B}(x)\ddot{x}_r + \hat{C}(x,\dot{x})\dot{x}_r + \hat{G}(x) - K_d s - \tilde{x} \\ &= Y(x,\dot{x},\dot{x}_r,\ddot{x}_r)\hat{\pi} - K_d s - \tilde{x} \end{aligned} \tag{4.12}$$

where $\hat{B}$, $\hat{C}$ and $\hat{C}$ are the estimated dynamic matrices, whose parameters are embedded in $\hat{\pi}$. The position error of the IPM is defined as $\tilde{x} = x_d - x$ and $s = \dot{\tilde{x}} + \Lambda\tilde{x} = \dot{x} - (\dot{x}_d - \Lambda\tilde{x}) = \dot{x} - \dot{x}_r$, with Λ symmetric, positive definite design matrix; $\dot{x}_r$ is referred to as the *reference velocity*, being the velocity the IPM is controlled to.

The present control loop guarantees $x \to x_d$, as $\tau \to \tau_d$. This statement holds under the

following assumption.

Assumption 3. *The steering of the IPM is achieved under these conditions:*

- *the force control, described in Section 4.2.4, is faster than the system dynamics in 4.8;*
- *the unknown parameters vector π in 4.10 is constant.*

The former leads to consider almost instantaneous convergence of force and torque; in fact, we assume there exists an instant T, $0 < T \ll 1$, such that $\tau(t) = \tau_d(t)$, for any $t \geq T$. This assumption is needed to prove Lemma 4.4 on which the final proof of this work (Theorem 4.6) is based. Furthermore, the need for $\pi = \text{const}$ is not limiting, since the inertial, Coriolis and gravity parameters do not generally vary over time.

Lemma 4.4. *Under Assumption 3, the pose controller in 4.12 achieves asymptotic stability of the error $\tilde{x}$, for any positive definite design gains K_d and Λ.*

Appendix 4.B includes further details on this.

Parameters Estimation

This internal loop estimates the unknown parameters of the IPM dynamics, such as the mass and the dimensions of the IPM; this allows us to adapt our controller to the real dynamics of the system.

The control law is derived from the Lyapunov theory, defining $\dot{\tilde{\pi}} = \dot{\pi} - \dot{\hat{\pi}} = -\dot{\hat{\pi}} = u_\pi$, under the assumption that the unknown parameters vector π is constant. The control law reads as

$$u_\pi = R^{-1} Y^T(x, \dot{x}, \dot{x}_r, \ddot{x}_r) s \tag{4.13}$$

where R is a positive, definite designed gain. The choice for u_π is justified by the proof of Lemma 4.4, reported in Appendix 4.B.

Force Control

As the third step, we design a controller that ensures the magnetic force (τ_m) converges on the desired force (τ_d). According to Assumption 3, this loop is required to converge almost instantaneously. The magnetic force and torque are computed from x and q by employing the localization output and dipole model.

According to 4.9, the choice for

$$\dot{q} = J_q^{\dagger}(\dot{\tau}_d + K\tilde{\tau} - J_x\dot{x}). \tag{4.14}$$

yields to

$$\dot{\tilde{\tau}} = \dot{\tau}_d - \dot{\tau}_m = -K\tilde{\tau}, \tag{4.15}$$

with K positive definite design gain [47]. This leads to asymptotic stability of the force and torque error dynamics.

Lemma 4.5 (from *[47]*)**.** *Any choice for the positive definite gain K achieves stability of the torque dynamics, if $\nu = 0$.*

Overall Control

In the following, we describe the overall control strategy by considering the previous sections. We show that the new choice of $\dot{q}$

$$\begin{cases} \tau_d &= Y(x, \dot{x}, \dot{x}_r, \ddot{x}_r)\hat{\pi} - K_d s - \tilde{x} \\ \dot{q} &= J_q^{\dagger}(\dot{\tau}_d + K\tilde{\tau} - J_x\dot{x} - \dot{x}) \\ u_\pi &= R^{-1}Y^T s \end{cases}, \tag{4.16}$$

leads to

$$\dot{\tilde{\tau}} = -K\tilde{\tau} + \dot{x},$$

which achieves overall convergence. This is is discussed in the following theorem.

Theorem 4.6. *Under the assumption $\pi = const$, the controller defined in 4.16 attains, for any positive definite design gains K_p, K_d and K,*

(a) asymptotic stability of $\tilde{x}$ if $\nu \simeq 0$;

(b) ultimately uniformly bounded error $\tilde{x}$ if ν is piece-wise constant*.*

This is discussed in Appendix 4.B , where we underline that, even in the presence of unknown unmodelled disturbances related to the tether dynamics, stability of the error is ensured. Moreover, in the absence of disturbances (e.g. untethered IPM), asymptotic stability is guaranteed.

Table 4.1: Mean error of the dipole model.

	Adaptive Backstepping	**Gravity compensating PD**	**PD**
EPM	3%	3.04%	2.5%
IPM	28.08%	27.8%	23.05%

4.2.5 Experimental analysis: Free space Levitation

The goal of this experimental work is to validate the control strategy and show that IPM height (i.e. levitation) can be controlled and compare its performance with the two previous control strategies mentioned in this paper [29, 47].

The IPM is a cylindrical permanent magnet with an axial magnetization of 1.48 T (N52), diameter and length of 10.16 mm and a mass of 15 g. The EPM is a permanent magnet with a diameter and length of 101.6 mm and an axial magnetization of 1.48 T (N52). The EPM is attached to the flange of a serial manipulator (KUKA LBR Med robot[5]). The mass, the radius and the length of the MFE are considered as the parameters to model in order to estimate the actual system dynamics. Previously reported data on these parameters are used as an initial estimate. Localization [199] and control loop both run at approximately 100 Hz. So far, no studies have been conducted on the speed of the system dynamics.

Table 4.1 reports the errors related to the dipole model, considering the mean distance between the two magnets during the experiments, described in [213].

To show how our control performs, we chose to navigate the IPM through an acrylic tube (Fig. 4.10) with an inner diameter of 60 mm and a 90 degrees bend in the middle. Each half of the tube has a length of 250 mm and the first part is inclined by approximately 20 mm over its length. In this case, the desired trajectory is a pre-planned path since we aim to objectively evaluate the levitating performance, without the user in the loop.

We compared this control approach with the techniques proposed in [47] and [29]. The latter imposes a continuous force along the gravity direction to maintain the magnetic coupling between the two magnets and therefore, imposes continuous contact with the environment; the former is able to levitate the IPM, but with limited velocity, due to the drawn assumptions. We performed 5 trials inside the tube with each method.

[5] `https://www.kuka.com/en-de/industries/healthcare/kuka-medical-robotics`

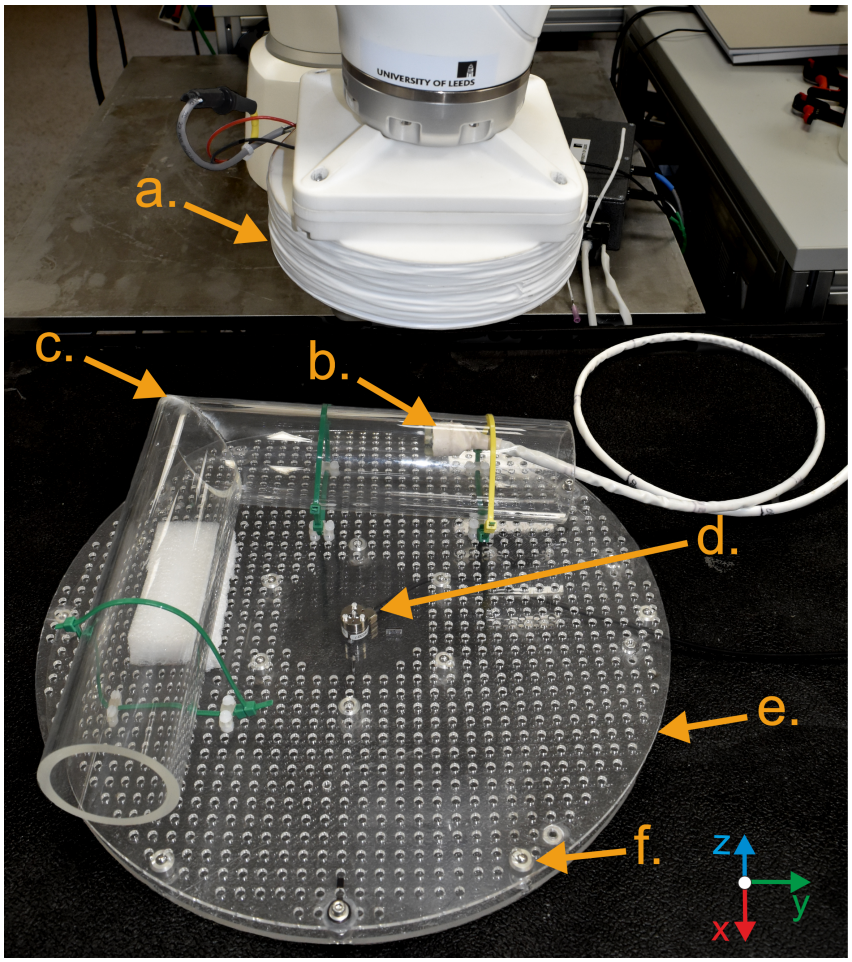

Figure 4.10: Sensorised platform. a. EPM, b. IPM, c. Environment (acrylic tube), d. Force/Torque sensor, e. Top acrylic sheet (constrained in negative z) and f. One of the ball transfer units

During the tests, we controlled the IPM to stay in the center of the lumen on the $x-y$ plane and to maintain levitation on the z axis. In the first tract of the tube, the main challenge for the controller is levitating the IPM, while in the second half of the tube, the stiffness of the tether and tube causes the IPM to maintain contact with the wall of the tube. However, the experiments show that the current control technique and the technique used in [47] are both able to resume IPM levitation after the disruption of moving past the corner.

To give a quantitative indication of the IPM's contact with the environment and, crucially, be able to compare the three control strategies, a custom sensorised force platform (Fig. 4.10) was used. The force sensor (6 axis Force/Torque sensor, Nano17, ATI) was secured between two acrylic sheets, with the top sheet constrained in the negative z direction but allowed to move freely in x, y and positive z due to the ball transfer units used to support it. The sensor was used to precisely record (via a National Instruments cDAQ 9171, 1kHz sampling frequency) all forces acting on the acrylic sheet through the environment (i.e. acrylic tube). This setup was chosen

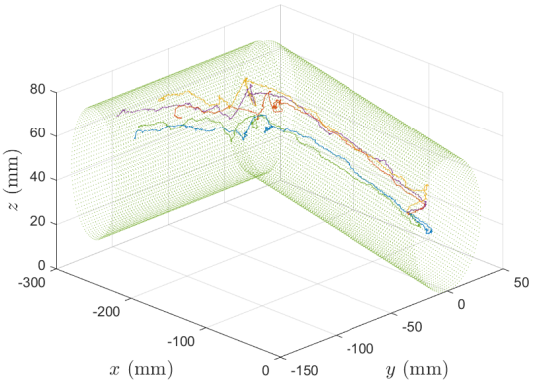

(a) Adaptive backstepping control.

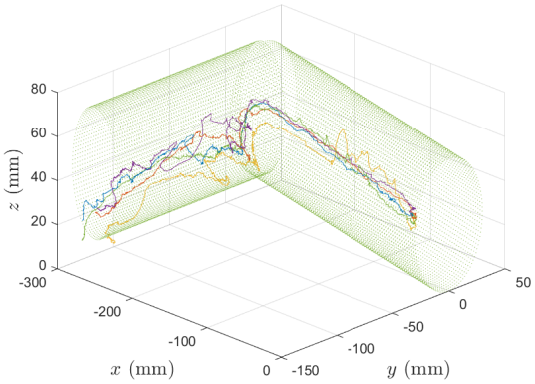

(b) Gravity compensating PD control [47].

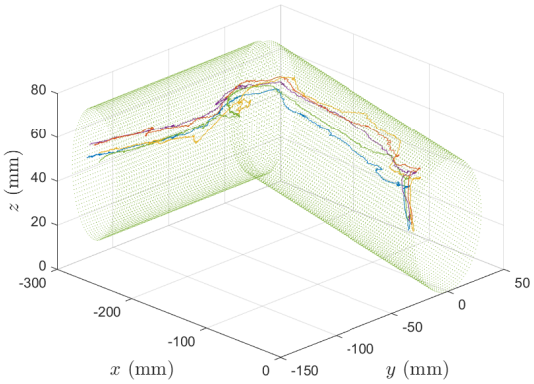

(c) PD control [29].

Figure 4.11: 3D tracking.

to allow flexibility in the tube layout and the use of an extremely precise sensor (resolving down to approximately 0.003N) that could be damaged if connected to an unconstrained platform.

In Fig. 4.11, we report the 3D trajectories of the IPM for each approach, while in Fig. 4.12 we report the force on the z direction (gravity direction), the norm of the lateral force (along x and y axis) and the overall contact between the IPM and the tube wall, expressed as norm of the force vector.

The results show that the amount of contact with the current method is comparable to the results obtained with the gravity compensating PD approach, but is reduced with respect to the amount of contact achieved with the PD method. In fact, the force along the gravity direction is significantly lower with the first two approaches. Fig. 4.12(a) shows a negative mean value for the force with the Adaptive backstepping control and the Gravity compensating PD control. This is due to the force transmitted by the tether on the negative z axis. In general,

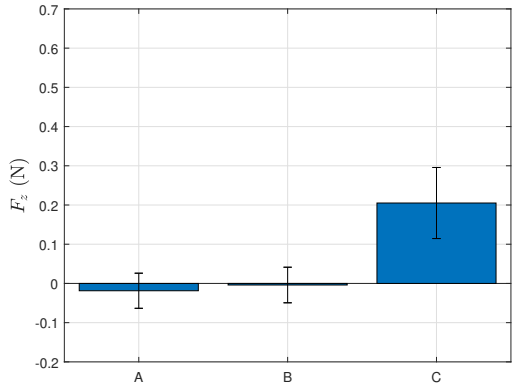

(a) Force along the z direction.

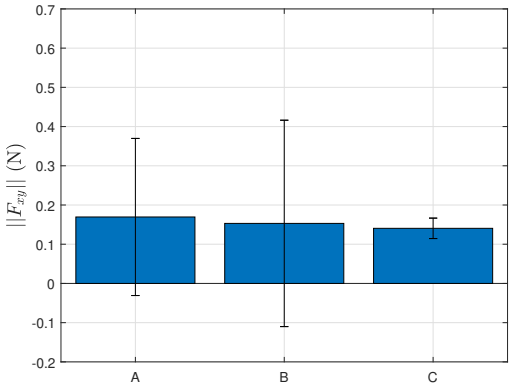

(b) Norm of the lateral forces.

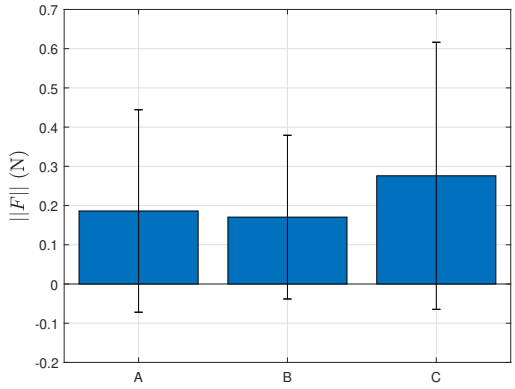

(c) Overall IPM-tube contact.

Figure 4.12: Overview of the IPM-tube contact. A. Adaptive backstepping control. B. Gravity compensating PD control. C. PD control.

we can infer that the IPM does not have contact with the tube wall; the limited contact with the tube is indicated from the standard deviation.

Moreover, due to the stiffness of the acrylic tube and the interaction of the tether, the norm of the overall force (i.e. taking into account force in the x and y direction) is significantly larger than the force in the z direction with the Adaptive Backstepping control and the Gravity compensating PD control approaches. This also underlines the robustness of the proposed approach towards significant interaction between the tether and the environment. On-the-other-hand, this issue is likely to be less significant in a more flexible environment, such as the colon. Therefore, the method is expected to attain a more satisfactory performance.

Moreover, in Fig. 4.11 we can notice that, with respect to the Gravity compensating PD control, the Adaptive backstepping control is able to maintain a better levitation also after the corner (where the rigidity of the tube and the stiffness of the tether affect the behaviour of the IPM).

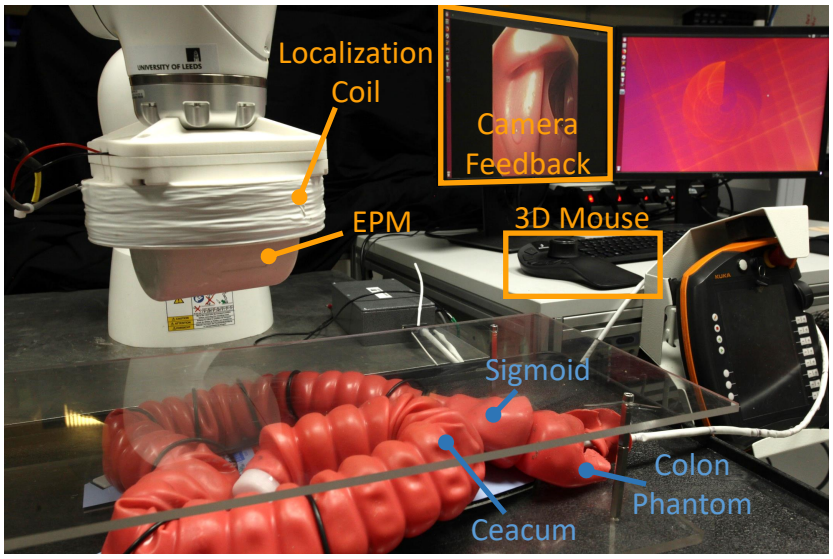

Figure 4.13: Setup for colon phantom experiments.

The gravity compensating PD control, instead, has more difficulty to exert necessary force to levitate the IPM while trying to reduce the IPM-tube contact.

Concerning the time to travel the tube and to resume the IPM levitation after the corner, we can infer that the Adaptive Backstepping control is faster than the gravity compensating PD method: with the Adaptive Backstepping control the IPM was able to traverse the tube in a mean time of 72 s with a standard deviation of 9.1 s, while the PD controller reports a mean time of 126.2 s with standard deviation of 23 s.

4.2.6 Experimental analysis: Colon Phantom

To show the practical feasibility of this approach we provide experiments in a more realistic environment. For this purpose, we used the M40 Colonoscope Training Simulator[6] in *standard configuration*. As the previous set of the experiments in Section 4.2.5, we compared the current approach with the method used in [47] and the PD control computed in [29].

We performed 5 trials with each approach to compare all techniques. The user (with no prior endoscopic experience, but knowledge of the platform) was able to guide the IPM to traverse the colon from the end of the sigmoid to the caecum. The IPM is equipped with a camera that provides a visual feedback to the user, which manipulates the IPM's desired pose (x_d) with a 3D mouse, as shown in Fig. 4.13.

In Fig. 4.14, we report the fastest trial with each approach. These experiments show that

[6] `https://www.kyotokagaku.com/products/detail01/m40.html`

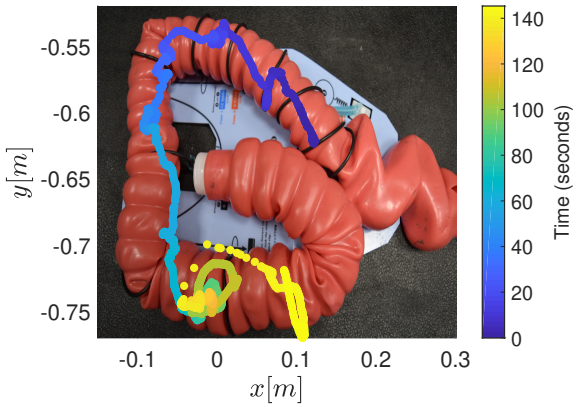

(a) Adaptive backstepping control.

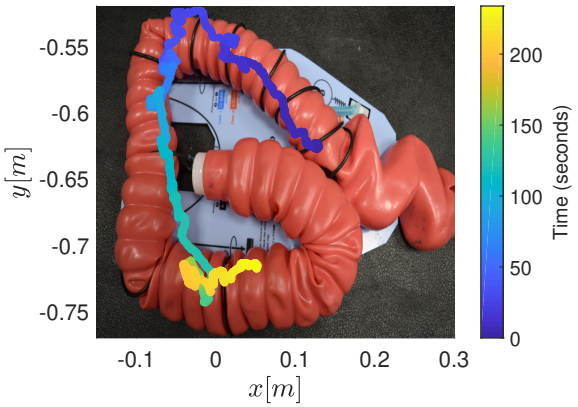

(b) Gravity compensating PD control [47].

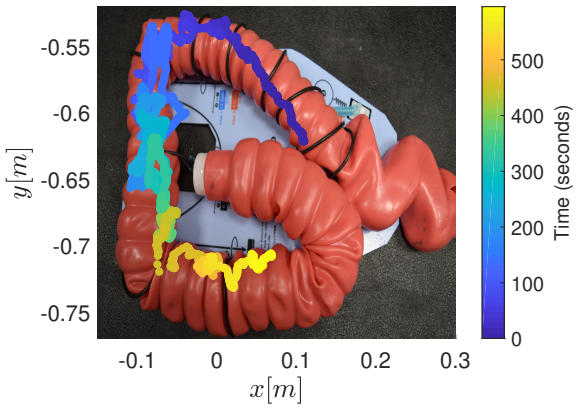

(c) PD control [29].

Figure 4.14: Trials on the colon simulator.

the current approach is able to reduce the mean completion time for the overall task (a path of approximately 0.85 m). The Adaptive Backstepping control achieves a mean completion time of 248.5 s with standard deviation of 31.8 s; the mean time achieved by the gravity compensating PD control [47] was 306.3 s with a standard deviation of 69.6 s; the PD control [29], instead, had a mean completion time of 551.9 s with standard deviation of 138.4 s. Moreover, since we set a maximum time for each trial of 600 s, the PD control failed two times over all five trials - the ceacum was not reached on time.

In order to levitate the capsule, the force exerted on the IPM along the z axis is reduced, compared to [29]; this leads to a lower functional steering force and the need for feeding the tether (i.e. assistance with overcoming tether drag). However, since the capsule is levitating, the friction related to environmental interaction is reduced and feeding the tether is more effective. A video of the experiment performed with the Adaptive backstepping control is reported in the

attached media of the paper.

Regarding the user learning curve, it was noted during the experiments that it varies depending on the technique used to perform colonoscopy. In particular, levitation techniques were observed to be easier to use, perhaps because of the ease and smoothness of guiding the endoscope inside the intestine, while levitating. On the other hand, the PID technique, which is unable to reduce contact with the environment and prevent the endoscope from being trapped in the folds of the colon, was considered more challenging by the user. However, no studies have been conducted on this aspect, so no data are reported here.

During these experiments, the sensorised platform was not used to measure the force that the IPM exerts on the environment. This was because the transmitted forces (from the IPM interactions to the sensor) were sufficiently low to be comparable with background noise. The attributing factor being the highly deformable environment that absorbs (dissipates) the low (<1N) contact forces. In the future, to investigate the real performance of the proposed approach, a deeper analysis will be performed with expert users.

A supplementary video shows the robustness of the control technique in the presence of external disturbances.

4.2.7 Conclusion

The present paper discusses a dynamic approach for the control of the magnetically actuated medical robots. In particular, we show the application of the proposed technique to the MFE [23]. We prove that proposed method is enough accurate to achieve levitation of the IPM, which is one of the most complex tasks with this type of platforms. Moreover, levitating the IPM leads to reduced contact with the environment, avoiding obstacles and folds. This can aid locomotion and reduce tissue stress (i.e. patient discomfort and risk of trauma).

The control strategy is based on the *Adaptive Backstepping Control*, which facilitates IPM levitation. The novelty of the current approach is the fact that we take into account the dynamics of the IPM, considering all the uncertainties the system is subjected to. This overcomes some of the assumptions drawn in [47]. In particular, the assumption that the desired trajectory is a *piece-wise constant function of the time* is weakened. This allows an increase in the velocity of the IPM, even if this is always subjected to the limitation of the IPM localization algorithm. In fact, the current localization frequency (100 Hz) is not fast enough to guarantee that the

IPM dynamics is handled completely and so increasing this would have a direct impact on system performance. Moreover, further studies on the dynamics of the system would help better understand the actual requirement on the localization and control loop.

To prove the strength of the current approach we performed two sets of experiments. The first set of experiments was developed in free space, using a sensorised platform to measure the forces the IPM exerted on the environment. The measured force can be read as a measure of the amount of contact between the IPM and the tube wall. The results demonstrate that our method is able to reduce the contact with the surrounding and increase the velocity of the IPM respect to the previous solutions [29, 47].

To prove the feasibility of our approach in a more realistic environment, we performed the second set of experiments in a colon phantom. These proved that with the current strategy the IPM was able to traverse the colon from the sigmoid to the caecum with a reasonable completion time. Prior work using a latex phantom and Olympus colonoscope demonstrates a median cecal intubation time (i.e. travelling from anus to cecum) of 150.19 s (115.68, 197.48) for 4 experted physicians [218]. Even if the proposed method is slower compared to the standard technique, it is worth mentioning that the lower invasiveness of the MFE has the potential for eliminating the need for anesthesia and so achieve an overall shorter procedure and recovery time.

In the future, we will investigate the performance of the current approach in a more realistic experimental setting (i.e animal and cadaver models). Moreover, we aim to investigate the application of the proposed control approach to multiple IPMs.

Appendix

4.A Magnetic Actuation

Consider the vector between EE position (p_E) and IPM position (p_I), referred to as $p = p_E - p_I$. According to the dipole model, the (generalized) force between EPM and IPM is

$$\tau_m = \begin{pmatrix} \frac{3M}{||p||^4}(\hat{m}_E\hat{m}_I^T + \hat{m}_I\hat{m}_E^T + (\hat{m}_I^T Z \hat{m}_E)I)\hat{p} \\ \frac{M}{||p||^3}\hat{m}_I \times D\hat{m}_E \end{pmatrix}$$

where $M = \frac{\mu_0||m_I||\ ||m_E||}{4\pi}$ with $m_I = ||m_I||\hat{m}_I$ and $m_E = ||m_E||\hat{m}_E$ *magnetic moments* of IPM and EPM, respectively; $\mu_0 = 4\pi 10^{-7}\frac{N}{A^2}$ permeability of vacuum, $\hat{p} = \frac{p}{||p||}$, $Z = I - 5\hat{p}\hat{p}^T$ and $D = 3\hat{p}\hat{p}^T - I$. Herein $I \in \mathbb{R}^{3\times 3}$ is referred to as the *identity matrix* and $||\cdot||$ is the *Euclidean norm*.

We consider the time derivative of τ_m [47]

$$\begin{aligned} \dot{\tau}_m &= \begin{pmatrix} \frac{\partial \tau_m}{\partial p} & \frac{\partial \tau_m}{\partial \hat{m}_E} \end{pmatrix} \begin{pmatrix} \dot{p}_E \\ \dot{\hat{m}}_E \end{pmatrix} - \begin{pmatrix} \frac{\partial \tau_m}{\partial p} & \frac{\partial \tau_m}{\partial \hat{m}_I} \end{pmatrix} \begin{pmatrix} \dot{p}_I \\ \dot{\hat{m}}_I \end{pmatrix} \\ &= \begin{pmatrix} \frac{\partial \tau_m}{\partial p} & \frac{\partial \tau_m}{\partial \hat{m}_E} \end{pmatrix} \begin{pmatrix} I & 0_{3,3} \\ 0_{3,3} & (\hat{m}_E)_\times^T \end{pmatrix} J\dot{q} - \begin{pmatrix} \frac{\partial \tau_m}{\partial p} & \frac{\partial \tau_m}{\partial \hat{m}_I} \end{pmatrix} \begin{pmatrix} I & 0_{3,3} \\ 0_{3,3} & (\hat{m}_I)_\times^T \end{pmatrix} \dot{x} \\ &= J_q\dot{q} + J_x\dot{x}, \end{aligned}$$

with J manipulator's Jacobian matrix.

4.B Proofs of Lemmas and Theorems

In the following we provide the proofs of Lemma 4.4 and Theorem 4.6.

Proof of Lemma 1. *Consider the positive definite Lyapunov function*

$$W(\tilde{x}, s, \tilde{\pi}, t) = \frac{1}{2}\tilde{x}^T\tilde{x} + \frac{1}{2}s^T B(x)s + \frac{1}{2}\tilde{\pi}^T R\tilde{\pi}.$$

with R is a positive definite gain. Since the unknown parameters are assumed constant, their error dynamics is $\dot{\tilde{\pi}} = \dot{\pi} - \dot{\hat{\pi}} = -\dot{\hat{\pi}} \stackrel{def}{=} -u_\pi$, for some choice for the update law u_π. The time derivative of the chosen Lyapunov function reads as

$$\begin{aligned}\dot{W} &= \tilde{x}^T\dot{\tilde{x}} + s^T B(x)\dot{s} + \frac{1}{2}s^T\dot{B}(x)s - \tilde{\pi}^T R u_\pi \\ &= \tilde{x}^T\dot{\tilde{x}} + s^T(B(x)\ddot{x} - B(x)\ddot{x}_r) + \frac{1}{2}s^T\dot{B}(x)s - \tilde{\pi}^T R u_\pi\end{aligned}$$

Summing and subtracting $s^T Cs$ we obtain

$$\dot{W} = \tilde{x}^T\dot{\tilde{x}} + s^T(-B(x)\ddot{x}_r - C(x,\dot{x})\dot{x}_r - G(x) + \tau) + \frac{1}{2}s^T(\dot{B}(x) - 2C(x,\dot{x}))s - \tilde{\pi}^T R u_\pi.$$

Due to the skew-symmetry *of $\dot{B}(x) - 2C(x,\dot{x})$, $\dot{s}^T(\dot{B}(x) - 2C(x,\dot{x}))\dot{s} = 0$ [212]. We define the generalized forces as*

$$\tau = \hat{B}(x)\ddot{x}_r + \hat{C}(x,\dot{x})\dot{x}_r + \hat{G}(x) - K_d s - \tilde{x}.$$

thus

$$\dot{W} = s^T Y\tilde{\pi} - s^T K_d s - \tilde{x}^T\Lambda\tilde{x} - \tilde{\pi}^T R u_\pi.$$

The update law $u_\pi = R^{-1}Y^T s$, for the parameters dynamics, yields to

$$\dot{W} = -s^T K_d s - \tilde{x}^T\Lambda\tilde{x}$$

and leads to conclude for, at least, uniform stability *of the origin.*

According to La Salle-Yoshizawa's theorem [219], since $\lim_{t\to\infty}\dot{W}(\tilde{x}, s, \tilde{\pi}) = 0$, $\lim_{t\to\infty}\tilde{x} = 0$ and asymptotic stability of $\tilde{x}$ is guaranteed.

Proof of Theorem 1. *Consider the positive definite Lyapunov function*

$$V(\tilde{x}, s, \tilde{\pi}, t, \tilde{\tau}) = W(\tilde{x}, s, \tilde{\pi}, t) + \frac{1}{2}\overline{\tau}^T\overline{\tau},$$

where $W(\tilde{x}, s, \tilde{\pi}, t)$ is the Lyapunov function defined in the proof of Lemma 4.4 and $\overline{\tau} = \tau_d - \tau$.

The time derivative of the chosen Lyapunov function is

$$\begin{aligned}\dot{V}(\tilde{x}, s, \tilde{\pi}, t, \tilde{\tau}) &= -s^T K_d s - \tilde{x}^T \Lambda \tilde{x} + (\tilde{\tau} + \nu)^T \dot{\tilde{\tau}} \\ &= -s^T K_d s - \tilde{x}^T \Lambda \tilde{x} - \tilde{\tau}^T K \tilde{\tau} - \nu^T K \tilde{\tau},\end{aligned}$$

under the assumption $\dot{\nu} \simeq 0$.

First, we prove statement (a). In absence of disturbances, i.e. $\nu = 0$*, by applying the La Salle-Yoshizawa's theorem [219], we can conclude for asymptotic stability of* $\tilde{x}$*, as in the proof of Lemma 4.4.*

We can also investigate the uniform ultimate boundedness of $\tilde{x}$ *(statement (b)), by showing that for any* $0 < \theta < 1$*,*

$$\begin{aligned}\dot{V}(\tilde{x}, s, \tilde{\pi}, t, \tilde{\tau}) = (1-\theta)(-s^T K_d s - \tilde{x}^T \Lambda \tilde{x} - \tilde{\tau}^T K \tilde{\tau}) + \\ \theta(-s^T K_d s - \tilde{x}^T \Lambda \tilde{x} - \tilde{\tau}^T K \tilde{\tau}) - \dot{\nu}^T K \tilde{\tau},\end{aligned}$$

therefore,

$$\dot{V}(\tilde{x}, s, \tilde{\pi}, t, \tilde{\tau}) \leq \overline{\lambda}(K_d, \Lambda, K)||\tilde{\xi}|| \forall 0 < \theta < 1,$$

if

$$||\tilde{\xi}|| = \frac{-\overline{\lambda}(K)||\dot{\nu}||}{\theta \overline{\lambda}(K_d, \Lambda, K)} \stackrel{def}{=} \mu.$$

Here $\tilde{\xi} = (s^T \tilde{x}^T \tilde{\tau}^T)^T$ *and* $\overline{\lambda}(A_1, A_2, \ldots, A_l)$ *is referred as the maximum eigenvalue of the matrices* $A_1, A_2, \ldots, A_l$*.*

Therefore, the ultimate bound is μ*.*

Chapter 5

Active Stabilization of Interventional Tasks utilizing a Magnetically Manipulated Endoscope

Chapter source: Active Stabilization of Interventional Tasks utilizing a Magnetically Manipulated Endoscope, by Lavinia Barducci, Bruno Scaglioni, James W. Martin, Keith L. Obstein, & Pietro Valdastri, Frontiers in Robotics and AI volume 2, (2022).

5.1 Abstract

Magnetically actuated robots have become increasingly popular in medical endoscopy over the past decade. Despite the significant improvements in autonomy and control methods, progress within the field of medical magnetic endoscopes has mainly been in the domain of enhanced navigation. Interventional tasks such as biopsy, polyp removal, and clip placement are a major procedural component of endoscopy. Little advancement has been done in this area due to the problem of adequately controlling and stabilizing magnetically actuated endoscopes for interventional tasks. In the present paper we discuss a novel *model-based* LPV control approach to provide stability during interventional maneuvers. This method linearizes the non-linear dynamic interaction between the external actuation system and the endoscope in a set of equilibria, associated to different distances between the magnetic source and the endoscope, and computes different controllers for each equilibrium. This approach provides the global stability

of the overall system and robustness against external disturbances. The performance of the LPV approach is compared to an intelligent teleoperation control method (based on a PID controller), on the MFE platform. Four biopsies in different regions of the colon and at two different system equilibria are performed. Both controllers are asked to stabilize the endoscope in the presence of external disturbances (i.e. the introduction of the biopsy forceps through the working channel of the endoscope). The experiments, performed in a benchtop colon simulator, show a maximum reduction of the mean orientation error of the endoscope of 45.8% with the LPV control compared to the PID controller.

5.2 Introduction

CRC is the third most common cancerous disease worldwide [220, 221]; therefore, prevention and early diagnosis of CRC are crucial. Although FEs have been at the forefront in detection and treatment of CRC [222], their main disadvantages are patient discomfort and complexity of use, both associated to the stiffness of the endoscope shaft [223, 224]. This leads to limitations in their ability to diagnose and treat CRC [12].

The demand for new, less invasive and more sophisticated technologies in the prevention of CRC has increased significantly in the last decades [13, 225]. Minimally invasive technologies (i.e. virtual endoscopy, WCEs) have become commercially available [12, 39, 226]. Albeit their encouraging results, their main limitation lies in the inability to perform interventional tasks such as biopsy and polyps removal [11, 12].

In the last decade, new advanced flexible endoscopes (or soft-tethered capsules), have been investigated to overcome WCEs limitations. The presence of a soft-tether enables the use of the endoscope as diagnostic and therapeutic instrument [41] and, thus, permits the use of advanced flexible endoscopes as a complete replacement for conventional endoscopes. Moreover, the soft-tether reduces the tissue stretching and, consequently, the discomfort for the patient.

In order to control and navigate an advanced flexible endoscope, an external or internal actuation mechanism is required; this has led to investigating magnetically actuated endoscopes [227]. These have major advantages of potential miniaturisation, avoiding complex and bulky internal actuation and achieving minimal invasiveness, leading to a reduction of patient discomfort and potentially decreasing post-operative recovery [11].

The control of magnetic endoscopes for colonoscopy has mainly been focused on navigation, with the aim of increasing the level of autonomy and reducing the operator burden [31, 47]; however, interventional procedures such as biopsy, polyp removal and clip placement, common in clinical colonoscopy [24, 57, 228], did not receive the same interest in the robotic community. Among interventional tasks, the most common is biopsy. In this procedure, an instrument is introduced through the operative channel to the endoscope tip, where a sample of tissue is collected thorough a pair of forceps.

For tethered devices, performing a biopsy involves passing a flexible instrument through the working channel, aligning the forceps to the target and grasping a portion of the tissue. Biopsies can be categorised in random sampling and targeted procedures [229]. Random biopsies are performed in multiple colon regions and at specific intervals, while targeted biopsies are performed on suspected lesions. Herein, we focus on targeted biopsies, which, having a precise positional target, requires greater accuracy in endoscope positioning and disturbance rejection.

Conventionally, an assistant inserts the forceps while the clinician stabilizes the endoscope. Maintaining a correct alignment between the biopsy forceps and the target is challenging because the endoscope stability is affected by the disturbance caused by the instrument insertion. Autonomously controlling the endoscope orientation during the biopsy procedure would enable the physician to perform a biopsy without the support of an assistant, accelerating the process, improving the accuracy and decreasing the burden on the team.

Few papers focus on robotic biospy: [230–232] propose different approaches in wireless devices, while [228, 233] developed semi-autonomous routines for performing biopsies, [228] focused on a crawler robot and [233] on a magnetic endoscope. However, no previous work could be found in literature on the topic of active stabilization of tethered robotic endoscopes. The task of active stabilization has been addressed only in the content of wireless capsules [234–236] and in the context of robotic surgery, by means of image-based algorithms that rely on the horizon stabilization principle. In this paper we propose an approach to control magnetic endoscopes during targeted biopsies based on localization sensors, capable of autonomously stabilizing the endoscope in the presence of external disturbances, with a focus on the disturbances created by the instrument insertion.

Magnetic manipulation is based on the interaction between magnetic fields, which is non-linear and varies significantly with the inter-magnetic distance (i.e. the distance between the actuating

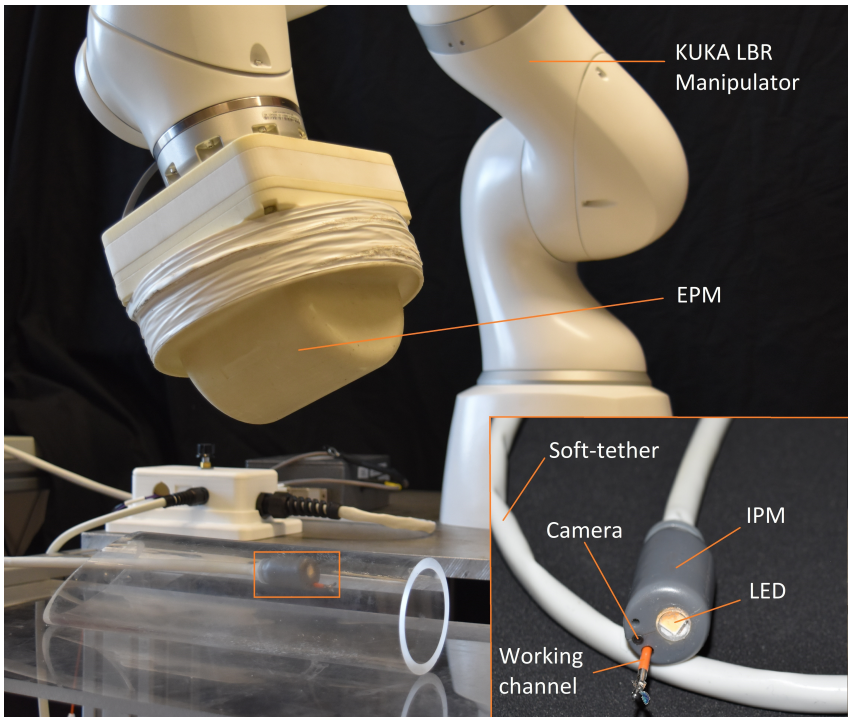

Figure 5.2.1: Overview of the MFE system. The magnetic endoscope (bottom right) contains a camera, LED, and a working channel. A KUKA LBR Med robotic arm actuates the MFE via manipulating an external permanent magnet mounted to its end-effector.

source of magnetic field and the driven magnet). To provide satisfactory results with a task such as stabilization at different distances, classical techniques like PID and linear controller synthesis would not provide sufficient performance: the PID controller, which needs to be tuned manually, is difficult to adapt to varying parameters and cannot manage multiple controlled variables simultaneously, on-the-other-hand, a classical linear regulator would not guarantee the stability of the overall system when far from the chosen linearization point.

Therefore, the Linear Parameter Varying (LPV) control strategy [237] is considered here. This control strategy involves obtaining linearized dynamic models for the non-linear system at different operating points, described by parameters which slowly vary with respect to the dynamics of the system; then, a LTI control law is designed to satisfy local performance objectives for each operating point. Tuning a controller for each point of equilibrium permits to optimize the closed-loop system in each condition and consequently achieve a general robust stability for the original non-linear system. As the parameters change, the control action is discontinuously switched between the various controllers. Under the condition of slowly changing parameters, the nonlinear system is guaranteed to be globally stable [238].

The technique is experimentally validated on the Magnetic Flexible Endoscope (MFE) [31], an

innovative magnetic colonoscope shown in Fig.5.2.1, with the aim of stabilizing the magnetic endoscope to perform biopsies. A single soft-tethered endoscope equipped with an IPM is actuated by means of a robotically manipulated EPM. Herein, a localization algorithm is embedded to localize the endoscope with respect to the base of the robotic manipulator [199].

This paper is organized as follows: in Section 5.3 we provide the theoretical formulation of the LPV method. Section 5.4 presents the experimental results and in Section 5.5 we discuss the results obtained and further developments of this approach.

5.3 Materials and Methods

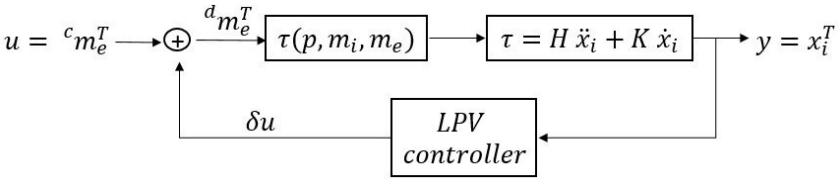

Figure 5.3.1: Control scheme. δu is the linearized input computed with the LPV controller and ${}^{c}m_e^T$ and ${}^{d}m_e^T$ are the current and desired EPM magnetic moment, respectively.

The dynamics of the endoscope is described as a family of parametrized linear systems as in Eq. 5.1, where $\rho(t)$ is the parameter, A, B, C, D are the matrices describing the system dynamics, $x(t)$ is the system state, $u(t)$ is the input and $y(t)$ is the output. The separation distance between the EPM and the endoscope plays a relevant role in the ability of the EPM to impart a meaningful torque on the IPM and stabilize the endoscope, therefore, it is chosen as time-varying parameter. The closed loop LPV system is described in Fig. 5.3.1 where the input u is the EPM magnetic moment and the controlled variable y is the IPM orientation. Herein, we consider the rotational part of the IPM dynamics, while the positional part is controlled by a PID controller since this plays an irrelevant role on the orientation of the MFE.

$$\begin{cases} \dot{x}(t) &= A(\rho(t))x(t) + B(\rho(t))u(t) \\ y(t) &= C(\rho(t))x(t) + D(\rho(t))u(t) \end{cases} \tag{5.1}$$

The dynamics of the IPM (and therefore of the endoscope) is subjected to magnetic interaction, approximated by the dipole-dipole magnetic model which assumes point-shaped sources and correctly approximates the real fields at a distance from the sources equal at least to the diameter of the magnets. In this context, the focus is on the magnetic torque exerted by the EPM on

the IPM, which can be written as a vector $\tau_m(p, x_i, x_e) \in \mathbb{R}^3$:

$$\tau_m(p, x_i, x_e) = \frac{M}{||p||^3} \hat{m}_I \times D\hat{m}_E \tag{5.2}$$

where $x_i \in \mathbb{R}^3$ is the IPM orientation, $x_e \in \mathbb{R}^3$ is the orientation of the EPM and $p = p_i - p_e$ is the relative distance between the IPM and EPM, all expressed in the world reference frame. $M = \frac{\mu_0 ||m_I||\ ||m_E||}{4\pi}$ with $m_I = ||m_I||\hat{m}_I$ and $m_E = ||m_E||\hat{m}_E$ are the magnetic moments of IPM and EPM, respectively; μ_0 is the magnetic permeability of vacuum, $\hat{p} = \frac{p}{||p||}$, $Z = I - 5\hat{p}\hat{p}^T$ and $D = 3\hat{p}\hat{p}^T - I$. Herein $I \in \mathbb{R}^{3\times3}$ is referred to as the *identity matrix* and $||\cdot||$ is the *Euclidean norm*.

Consider the rotational term of the nominal dynamics of the IPM

$$H(x_i)\ddot{x}_i + K(x_i, \dot{x}_i)\dot{x}_i = \tau_m(p, x_i, x_e), \tag{5.3}$$

$H(x_i),\ K(x_i, \dot{x}_i)$ are referred to as *inertia* and *Coriolis matrix* [212] of the IPM, respectively.

The goal is to find x_e such that x_i approaches a desired value x_d, even in the presence of external disturbances (i.e. respiration of the patient or insertion of the biopsy forceps inside the instrument channel).

The Inertia matrix, referred to the IPM frame, is inferred as the Inertial tensor of a cylinder with mass $m = 0.023$ Kg, radius $r = 0.01$ m, and height $h = 0.035$ m.

$$\mathbb{I} = \begin{bmatrix} \frac{1}{12}(3mr^2 + mh^2) & 0 & 0 \\ 0 & \frac{1}{12}(3mr^2 + mh^2) & 0 \\ 0 & 0 & \frac{1}{2}mr^2 \end{bmatrix} \tag{5.4}$$

The Inertia matrix is determined w.r.t. the world frame as $H = J^T\mathbb{I}J$ where J is defined as the Jacobian that links the angular velocity to the derivative of the angular orientation computed in the local frame.

The Coriolis matrix, $K(x)$ is derived from the Christoffel symbols, hence, each component can be written as:

$$c_{ij} = \frac{1}{2}\Big[\frac{\partial b_{ij}}{\partial x_k} + \frac{\partial b_{ik}}{\partial x_j} - \frac{\partial b_{jk}}{\partial x_i}\Big] \tag{5.5}$$

with the addition of a damping factor to the diagonal of the Coriolis matrix which takes into account the damping provided by the tissues interaction.

Therefore, considering the vector of the state variable as $x = [x_i, \dot{x}_i]^T = [x_1, x_2]^T$, the overall system, showed in Fig. 5.3.1, is modelled by:

$$\begin{cases} \dot{x}_1 &= x_2 \\ \dot{x}_2 &= H^{-1}(\tau_m - K\dot{x}_1) = H^{-1}(\tau_m - Kx_2) \end{cases} \tag{5.6}$$

Subsequently, the system is linearized with respect to the state variable x and the input $u = m_e^T = R_e^g m_e^{EPM}$, the direction of the magnetic moment of the EPM, where R_e^g is the rotation matrix of the EPM in world frame and m_e^{EPM} is the direction of the EPM magnetic moment in EPM frame. Eq. 5.7 shows the linearized matrices of the system.

$$\begin{aligned} A = \frac{\partial \dot{x}}{\partial x} = \begin{bmatrix} 0 & I \\ 0 & \frac{-K}{H} \end{bmatrix} \in \Re^{6\times 6}, \qquad B = \frac{\partial \dot{x}}{\partial u} \in \Re^{6\times 3} \\ C = \begin{bmatrix} 1 & 0 & 0 & 0 & 0 & 0 \\ 0 & 0 & 0 & 0 & 0 & 0 \\ 0 & 0 & 1 & 0 & 0 & 0 \end{bmatrix}, \qquad D = 0_{3\times 3} \end{aligned} \tag{5.7}$$

The system is linearized around more than one operating point with the aim of finding a controller corresponding to each equilibrium. No a priori information on the parameter is required other that its range of variation, which is assumed to vary with limited velocity. This assumption does not hinder the design of the control and guarantees the stability of the overall system [238, 239]. The relative orientation of the two permanent magnets is maintained constant and only the inter-magnetic distance on the z axis, expressed in world frame, is considered as a DoF of the system. This is a reasonable assumption, considering that it is always possible to bring the EPM on top of the endoscope before starting the procedure. The system is linearized in these equilibria:

- $m_e = [0, -1, 0]$
- $x_1 = [-\pi/2, 0, -\pi/2]$

- $x_2 = [0, 0, 0]$
- $p = [0, 0, \rho]$

As result, an array of systems, linearized in a different value of ρ, is obtained. The extremes of the parameter range are chosen as follows: the minimum value as the safest minimum distance of the EPM from the abdominal wall, the maximum as the distance at which the magnetic torque exerted on the MFE is still appreciable. At the minimum relative distance, the magnetic torque and, thus, the steerability of the endoscope are high; when the relative distance is at its maximum the magnetic torque decreases and in order to maintain the same performances, a controller that provides more energy is required. Therefore, employing different controllers at different points of equilibrium is essential.

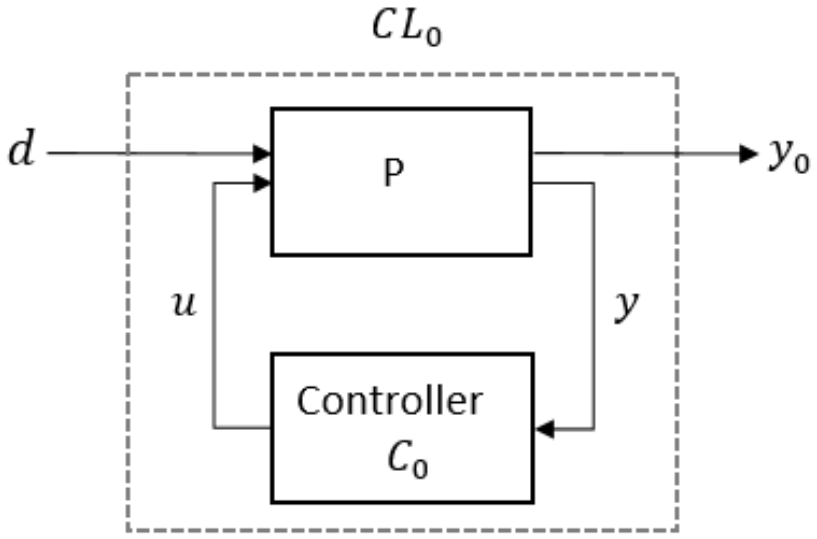

Figure 5.3.2: Control scheme represented as Linear-Fractional transformation (LFT) system.

To simplify the control system synthesis, the array of systems is expressed in the Standard form model, LPV LFT, as in Fig. 5.3.2. The LFT form enables to highlight the transfer functions between the disturbances and the system output and consequently synthesize a controller that modifies the effect of disturbances on the output. Here, d is referred to a piece-wise constant disturbance that needs to be attenuated and y_0, the output, has to be controlled. CL_0 is the closed-loop system computed given the parametrized LTI systems (defined as P) and the controllers C_0 is tuned with a non-smooth optimization algorithm [240, 241], available in the Matlab Control System Toolbox. The controllers gain-scheduled on the rho values are matrices 3×3, which multiplied to the output of the system (the MFE orientation), compute the desired input (EPM orientation) to reduce the orientation error of the endoscope.

In y_0, the orientation (pitch and yaw) of the IPM is considered. Due to the axial symmetry of the EPM [29], the roll angle is not controllable and, thus, is not considered. As a consequence, the new matrices B and C are computed as:

$$B_{new} = \left[\begin{array}{ccc|c} 1 & 0 & 0 & \\ 0 & 0 & 0 & B \\ 0 & 0 & 1 & \end{array}\right] \qquad C_{new} = \left[\begin{array}{cccccc} 1 & 0 & 0 & 0 & 0 & 0 \\ 0 & 0 & 0 & 0 & 0 & 0 \\ 0 & 0 & 1 & 0 & 0 & 0 \\ \hline 1 & 0 & 0 & 0 & 0 & 0 \\ 0 & 0 & 0 & 0 & 0 & 0 \\ 0 & 0 & 1 & 0 & 0 & 0 \end{array}\right] \tag{5.8}$$

All the conditions for the stabilization of the system and the attenuation of the disturbance d are defined appropriately. The disturbance, herein, is defined as a *piece-wise constant* disturbance. This means that velocity and acceleration of the disturbance can be neglected. The assumption made does not interfere nor limit the design of the controller. Considering the type of disturbance tackled in this work, associated with instrument insertion, this assumption is reasonable. In fact, considering a defined amount of time, the instrument insertion can be described as a locally constant disturbance.

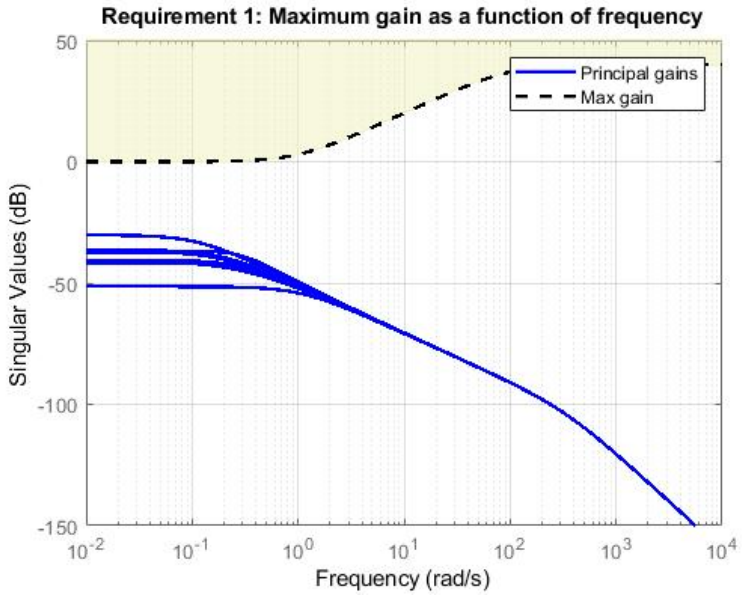

Figure 5.3.3: Magnitude Bode diagram of the transfer functions of the MIMO system. Simulation in Matlab with Systune.

The non-smooth optimization algorithm [241], implemented in the MATLAB-based tool SYS-

TUNE, is used to find a parametrized controller capable of achieving the required performances on the whole range of parameters. This means maintaining the response between the disturbance and the output of the system under a certain threshold specified by the following high-pass filter transfer function $g = 100\frac{(s+1)}{(s+100)}$, which ensures the attenuation of all low frequency signals. The response of the closed loop system is shown in Fig. 5.3.3. The blue lines represent the transfer functions of the closed loop MIMO system between the disturbance and the IPM orientation (Euler angles) of the endoscope. For each value of the parameter, considered herein as the inter-magnetic distance, different behaviours are shown in the diagram. It is worth noting that the Bode diagram of the input-output channels of the closed loop system is below the high-pass filter threshold and, thus, the overall non-linear system results as stabilized.

5.4 Experimental Validation and Results

The control strategy is validated on the MFE platform in a benchtop colon simulator. The platform is shown in Fig. 5.2.1 and a detail of the setup is shown in Fig. 5.4.1. The system is composed by a soft-tethered endoscope (the MFE) and a robotic manipulator to which an EPM is attached as the end-effector. The IPM is embedded in a 3D printed shell which comprises a LED, a camera and an instrument port. The soft-tether contains channels that provide insufflation, irrigation and a lumen dedicated to endoscopic instruments. The latter permits to insert tools such as biopsy forceps or polypectomy snares through the instrument port on the tip. The magnetic actuation is achieved by moving the EPM, attached to the flange of a serial manipulator (KUKA LBR Med R820) and, thus, imparting magnetic forces and torques on the MFE. The IPM is a cylindrical permanent magnet with an axial magnetization of 1.48 T (N52), diameter of 10.16 mm, length of 35 mm and a mass of 23 g. The EPM is a permanent magnet with a diameter and length of 101.6 mm and an axial magnetization of 1.48 T (N52). A flexible circuit, embedded in the MFE tip, is used for endoscope localization [199]. The localization algorithm estimates the MFE pose in real time (100 Hz) with a positional and rotational accuracy of 5 ± 1mm and $5 \pm 0.8^\circ$ [199].

We compared the control strategy described in Section 5.3 to the intelligent teleoperation control method (based on a PID controller) used in [31]. This control approach was used to successfully navigate the same endoscope in-vivo and represents the state of the art. Herein, the disturbance is proposed as the introduction of the biopsy forceps through the instrument port of the

endoscope; the control is asked to actively stabilize the endoscope, counteracting any negative effects on the orientation of the tip.

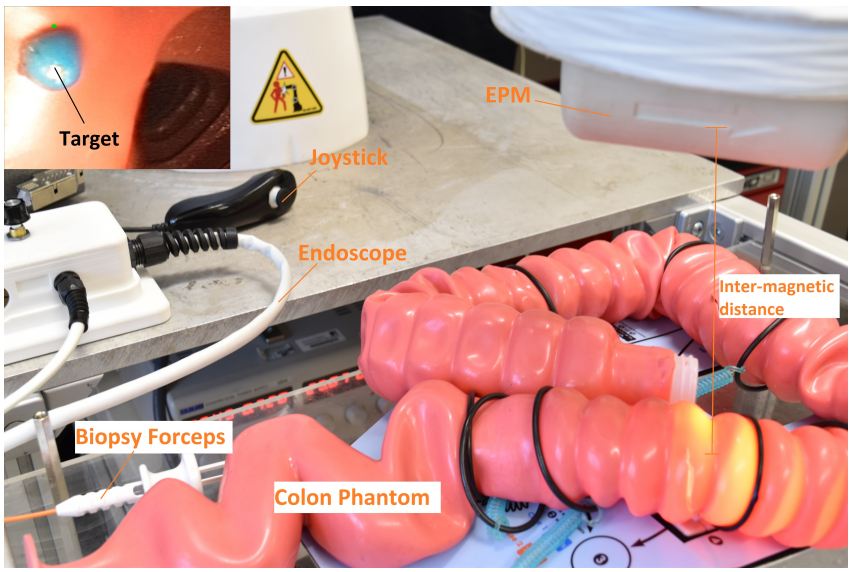

Figure 5.4.1: Experimental setup. The overall system is composed by an EPM, which actuates the MFE (placed inside the colon simulator), and a joystick to steer the endoscope. On the top left, the on-board camera shows a biopsy target inside a latex colonoscopy training phantom (M40, Kyoto Kagaku Co.).

We performed four biopsies on a Kyoto Kagaku M40 Colonoscope Training Simulator in *standard configuration*, Boston Scientific Single-Use Radial Jaw™ 4 Biopsy Forceps were used as endoscopic tool, as shown in Fig. 5.4.1. The target polyps were simulated with a blue colored polyvinyl acetate glue in different parts of the colon phantom (i.e. sigmoid, descending, transverse and ascending colon) and at different angles w.r.t. the MFE orientation. This setup aims to show that our approach can stabilize the endoscope and maintain a stable point of view of the MFE in a range of orientations that replicate the most commonly occurring cases in clinical practice. The experiments were repeated at two different inter-magnetic distances (15 cm and 20 cm), showing that at higher distances a more advanced controller is required to effectively stabilize the endoscope properly.

We performed 5 experiments at each inter-magnetic distance. At each experiment the user (with no prior endoscopic experience, but knowledge of the platform) was asked to perform four biopsies in four different regions of the colon. The endoscope was placed at the end of the ceacum and the user was instructed to withdraw the MFE and perform a biopsy every time a polyp was detected. Before performing the biopsy, the user was required to align the endoscope to the target by means of a joystick, using teleoperation algorithm [31]. The IPM orientation at the beginning of the biopsy procedure was recorded and used as the desired target orientation

in the stabilization phase.

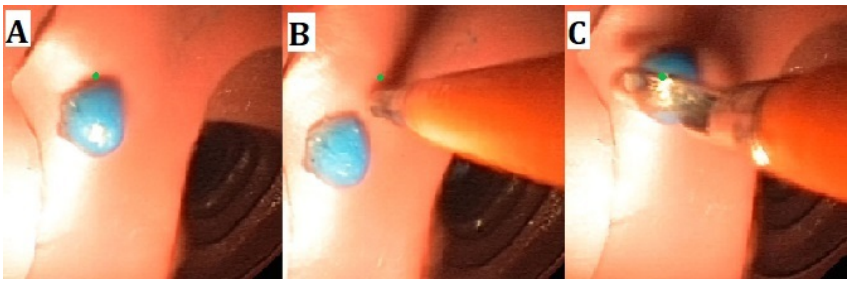

Figure 5.4.2: Targeted biopsy routine. (A) The polyp is detected by the user. The green dot is an estimated projection of the biopsy tool given an average distance of the endoscope from the target [233]. (B) The insertion of the biopsy forceps through the working channel leads to a deviation of the tip of the endoscope to the target. (C) The control algorithm generates a torque on the MFE to minimize the error between the target and the tool-tip.

In Fig. 5.4.2 the three main phases of the targeted biopsy routine are shown. When a polyp was detected, the user switched to the biopsy controller (i.e. LPV control) on the Graphical User Interface (GUI) and a green dot was visualized on the screen. This was an estimated projection of the biopsy tool given an average distance of the endoscope from the target tissue (this should be read as an indication of the position of the tip of the biopsy forceps when this is extruded from the tip of the endoscope, but it does not have any role in the control). While the instrument was inserted in the working channel a deviation of the tip of the endoscope from the target was induced. The control algorithm actuated the EPM, which was translated into a torque imparted on the MFE (based on the orientation error of the endoscope) that minimized the error between the target and the tool-tip. A video describing the experiments is attached. The experiments, showed in the video, are performed in the most similar possible conditions; this means same section of the colon and same position of the polyp inside the colon simulator. However, other factors such as the EPM position or the position of the tether influence the orientation of the endoscope. The video shows the PID controller is not always able to counteract the disturbance, which induces a deviation on the tip of the endoscope, resulting in fluctuation of the real IPM magnetic moment around the desired value.

Fig. 5.4.3A and Fig. 5.4.4A show the mean error (defined as $1/n \sum_{i=1}^{n} \tilde{x}_i$, where $\tilde{x}_i$ is the MFE orientation error at each cycle and n the number of cycles) along each axis, Fig. 5.4.3B and 5.4.4B the Euclidean norm of the error. In both figures, we compare the LPV approach with the algorithm discussed in [31]. In Fig. 5.4.3, the EPM is placed at the minimum height (0.15 m), while in Fig. 5.4.4 the inter-magnetic distance is set to the maximum (0.2 m). These values have been chosen as extremes of a safe window in which a possible collision with the patient

is avoided and simultaneously the transmittable torques are still significant. As expected, the inter-magnetic distance is correlated with the error in both cases. At the maximum distance, the steerability of the MFE decreases, especially when the biopsy tool is inserted inside the working channel. The tool increases the stiffness of the tether and, thus, the magnetic torque occasionally ineffectively orientates the MFE. However, although the mean error increases with the relative distance, our approach is able to effectively reduce the error compared to the PID controller. In particular, we observe a reduction on the norm of 18.1% and 45.8% at the lowest and the highest inter-magnetic distance, respectively. The difference is larger at higher inter-magnetic distance (Fig.5.4.4), showing that control adaptation with respect to distance can significantly improve performances. The z-test, applied to the experimental data, confirms the statistical significance of the results with a p-value < 0.05.

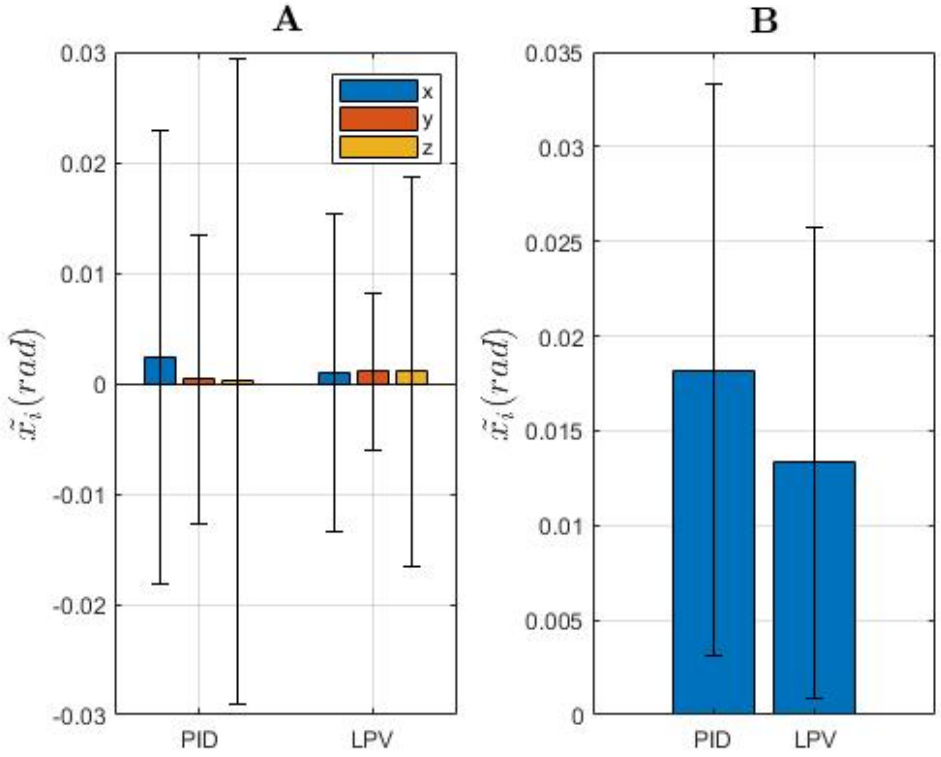

Figure 5.4.3: Overview of the IPM orientation error at 15 cm of inter-magnetic distance. (A) shows the mean and standard deviation of the orientation error. (B) shows the mean and the standard deviation of the euclidean norm of the mean orientation error.

Table 5.4.1 reports the absolute mean orientation error and the relative standard deviation on each axis, with both approaches. We notice that, at the lowest inter-magnetic distance (Fig. 5.4.3A), the absolute mean error is low and comparable with both approaches, while the standard deviation is substantially higher with the PID controller. The LPV controller

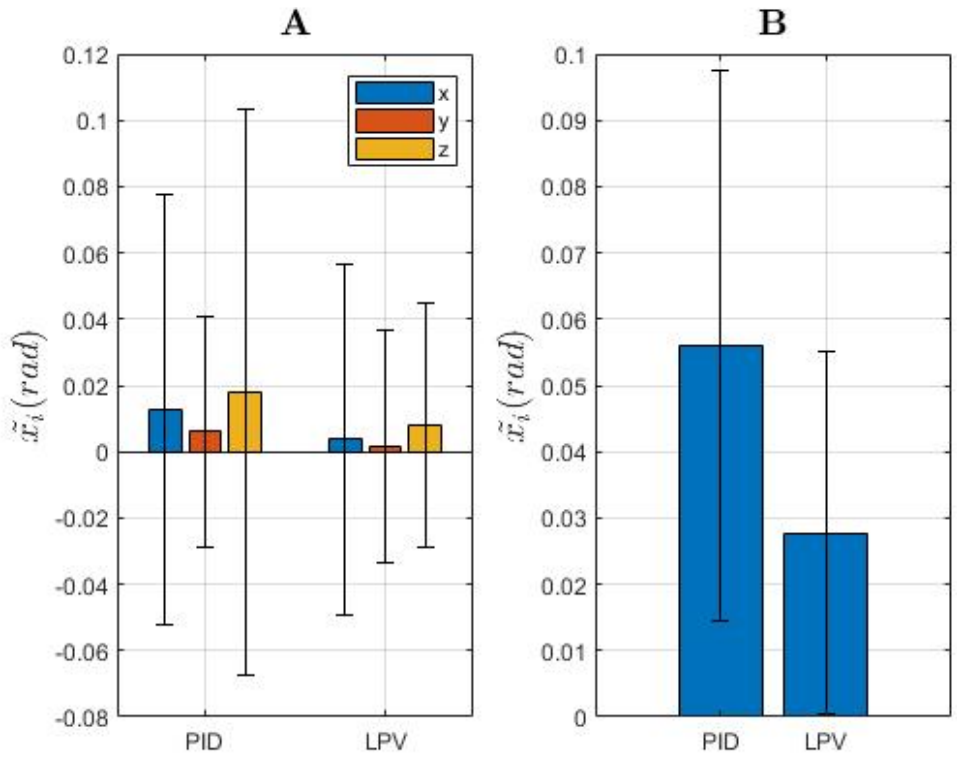

Figure 5.4.4: Overview of the IPM orientation error at 20 cm of inter-magnetic distance. (A) shows the mean and standard deviation of the orientation error. (B) shows the mean and the standard deviation of the euclidean norm of the mean orientation error.

presents a reduction of the relative percentage of the error on the x axis equal to 57.79%, but a higher relative percentage of the error on the y and z axis (175% and 250%). However, since the absolute mean values of the error, as reported in Table 5.4.1, are significantly low for both controllers, while the standard deviation is higher for the PID controller, the two approaches can be considered comparable.

On-the-other-hand, taking into account the highest inter-magnetic distance (Fig. 5.4.4A), we can notice that the mean error and the standard deviation are significantly reduced with the LPV controller compared to the PID, as reported in Table 5.4.1. In fact, at the highest inter-magnetic distance, our method obtains a reduction of 70.8%, 74.2% and 54.5% on the x, y and z axis, respectively, compared to the PID controller.

In Fig. 5.4.5 and 5.4.6 we compare the PID and LPV approaches by evaluating the measured and desired magnetic moment of the MFE, defined by the user by means of a joystick before switching to the biopsy controller on the GUI. The experiment that had the lowest mean error, at the highest inter-magnetic distance, for both approaches is shown. Both approaches are effective,

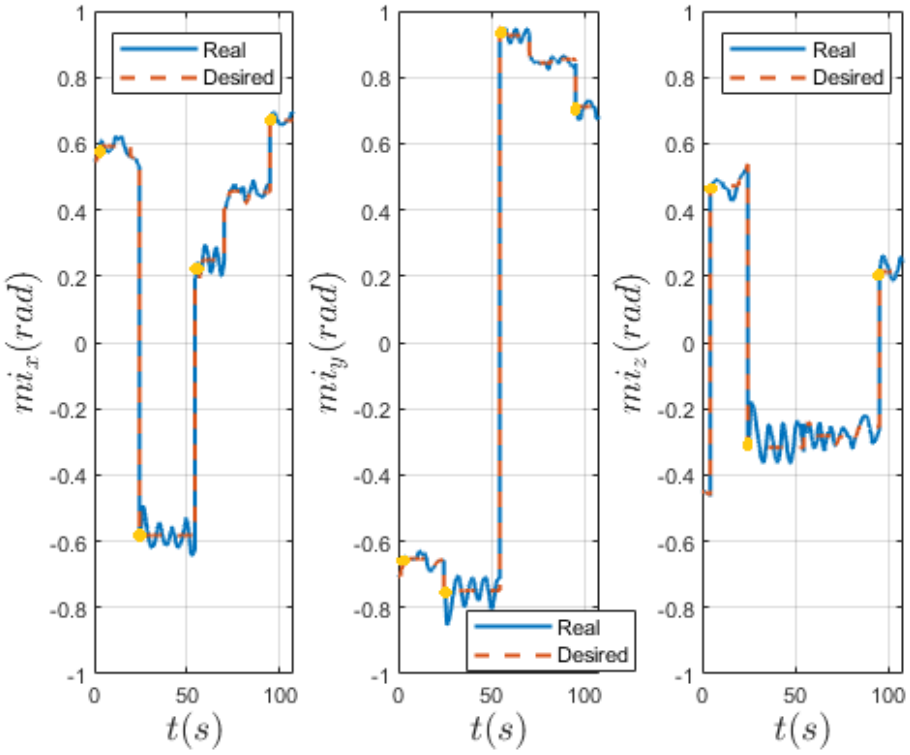

Figure 5.4.5: Real and desired IPM magnetic moment computed with PID controller. Desired (red) and real (blue) magnetic moment of the IPM in world frame. The yellow dots indicate the moment when the biopsy forceps is being introduced in the instrument port.

Table 5.4.1: Mean and standard deviation of the orientation error at different inter-magnetic distances.

ρ	axis	**PID (rad)**	**LPV (rad)**
0.15 m	x	0.002 ± 0.021	0.001 ± 0.0144
	y	0.0004 ± 0.013	0.001 ± 0.0071
	z	0.0002 ± 0.0292	0.0011 ± 0.0176
0.20 m	x	0.0129 ± 0.0650	0.0037 ± 0.0529
	y	0.0061 ± 0.0347	0.0016 ± 0.0351
	z	0.0178 ± 0.0853	0.0081 ± 0.0368

however, the PID controller presents more oscillations around the desired value, generated by external disturbances (i.e. insertion of the biopsy forceps inside the instrument port) and less effectively damped by the PID. Our approach presents lower oscillations, showing that our method is able to stabilize the system in the presence of external disturbances. In table 5.4.2, we quantify the fluctuations (i.e. standard deviation) of the measured magnetic moment around the desired value, with both approaches and the percentage reduction of the LPV approach w.r.t. the PID controller, with regard to the experiments reported in Fig. 5.4.5 and 5.4.6.

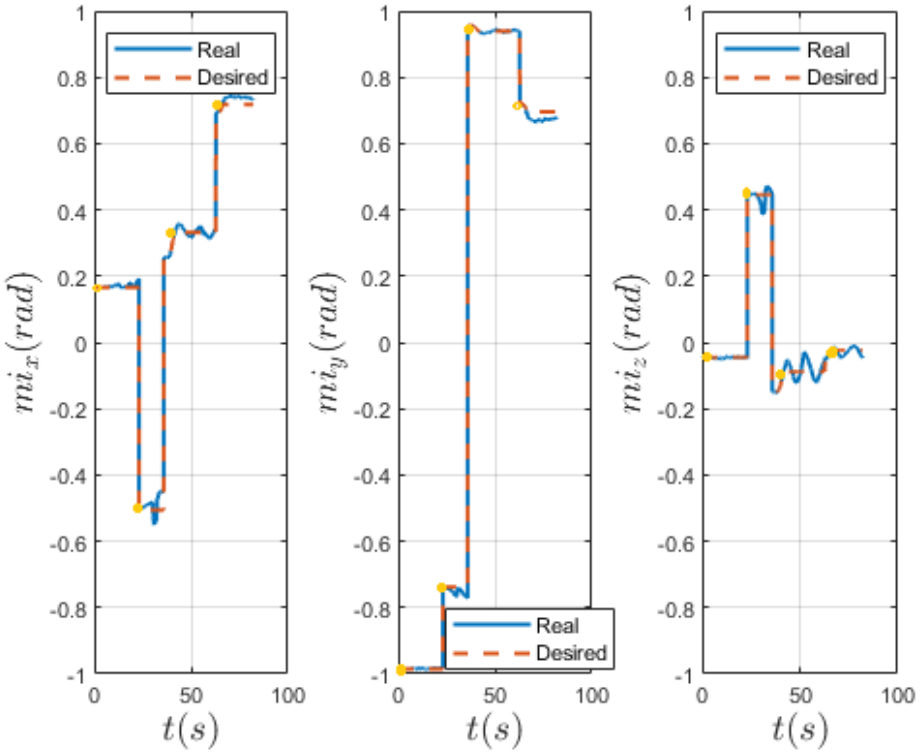

Figure 5.4.6: Real and desired IPM magnetic moment computed with LPV controller. Desired (red) and real (blue) magnetic moment of the IPM in world frame. The yellow dots indicate the moment when the biopsy forceps is being introduced in the instrument port.

Table 5.4.2: Quantitative analysis of the magnetic moment fluctuations.

axis	**PID (rad)**	**LPV (rad)**	reduction %
x	0.0738	0.0302	59.08%
y	0.0434	0.0255	41.32%
z	0.0740	0.0622	16.0%

Fig. 6.1.1 shows the variation of EPM magnetic moment with both controllers. It is worth noting that our approach significantly reduces the movements of the EPM showing that a more effective control action is computed with the LPV controller. Moreover, limiting the movement of the EPM permits to reduce the risk of the robot contact with the patient, avoiding potentially dangerous situations. The LPV control achieves a maximum reduction of the EPM oscillations of 58.1%, computed on the mean value of the magnetic moment, compared to the PID controller.

5.5 Discussion

This paper discusses a model-based LPV control approach with the aim of stabilizing a magnetically manipulated endoscope during interventional procedures such as biopsy, polyp removal

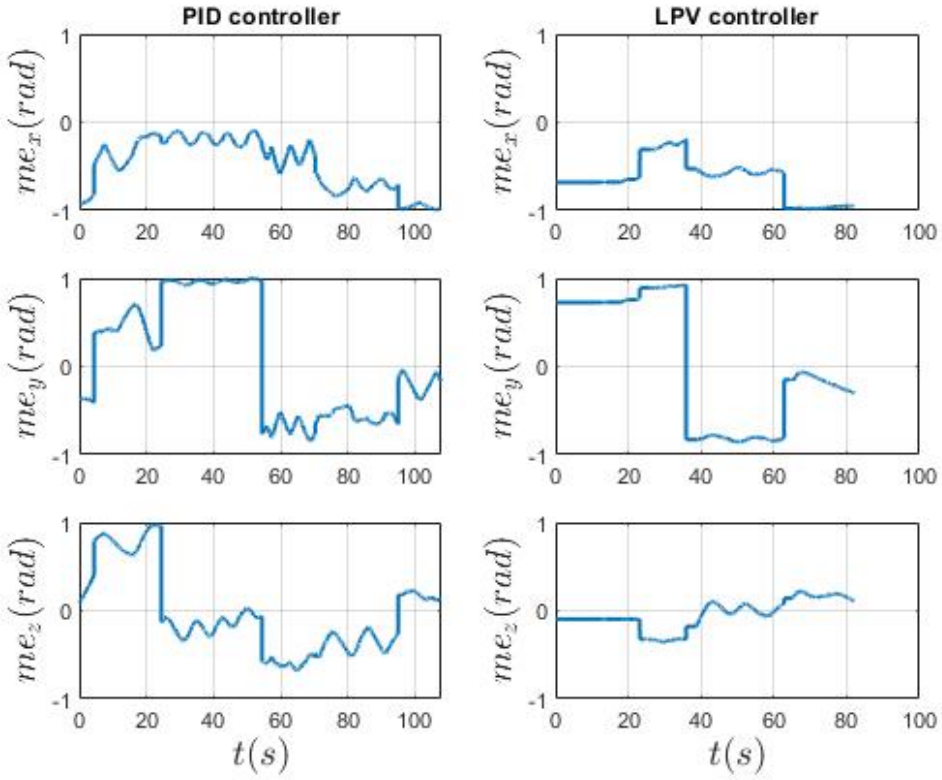

Figure 5.4.7: Real EPM magnetic moment in world frame. On the left the PID control and on the right the LPV controller. The EPM magnetic moment is computed by the controller, at each cycle, given the IPM magnetic moment error.

and clip placement. We show the application of the proposed technique on the MFE, used to perform targeted biopsies. We prove the proposed method is capable of stabilizing the endoscope in the presence of external disturbances (i.e., insertion of the tool in the instrument port) and provides enhanced performances with respect to the literature. This method can aid interventional tasks by enhancing the accuracy of the biopsy procedure. Moreover, the active stabilization of the endoscope allows a single user to perform each task autonomously and to reduce the number of people in the endoscopy room [242].

The control strategy is based on the LPV control that facilitates stabilization of the endoscope in the working environment. The novelty of this approach is the fact that linearizing the non-linear system in different equilibria (i.e. inter-magnetic distance between the two magnets) permits to cope with the different status of the non-linear system. In particular, the magnetic force and torque the EPM imparts on the IPM are strictly related to the relative distance between the two magnets: at higher inter-magnetic distances, due to various factors (i.e. different anatomies of the patients, position of the patient on the bed), the magnetic torque drops significantly. Therefore, a suitable robust controller able to cope with variations in the inter-

magnetic distance is crucial. To our knowledge, this is the first example of LPV control synthesis applied to a magnetic endoscope. Embedding this method in a clinical scenario could improve the clinical performance and ease-of-use of interventional tasks such as biopsy, polyp removal and clip placement.

To prove the strength of our approach, we performed 5 trials on a colon phantom. Four biopsies in different sections of the colon and at different orientation were taken using a biopsy forceps. The results show both approaches are effective, but the LPV approach was able to obtain a lower orientation error with respect to the PID controller. In particular, it is worth noting that at the maximum height, the oscillations around the desired magnetic moment direction are reduced by 45.8% with our method. Using an optimized and model-based controller, which takes into account different system equilibria, has the advantage of robustness, withstanding parameter variation still maintaining stability and performance goals. However, the main limitation of this work, as shown by Fig. 5.4.5 and 5.4.6 and the video attached to the paper, is the fact that a direct comparison of the experiments is not straightforward. In fact, the user inputs may vary and, thus, the experiments are not very repeatable. Nonetheless, the same conditions for each experiment were tried to replicate.

In the future, we will integrate our method with an AI [243] or a semi-autonomous routine [233] to target biopsies. Herein, the authors were able to track a target tissue, predict the projection of the tool channel outside the tip of the endoscope using a stereo-vision approach and align the magnetic endoscope to the polyps; however, no additional disturbances were taken into account. Combining [233] and our approach (i.e. the tracking of a tissue target and the active stabilization of the endoscope) we could achieve a completely autonomous procedure and reduce the personnel needed in the room. Although the discussion with clinical operators highlighted that the disturbances introduced by the instrument are the most disruptive, further works should investigate and adapt our approach in the context of additional disturbances such as patient breathing and peristalsis, that might require tracking of the tissues and target.

Chapter 6

Working towards clinical trials of the Robotic colonoscopy platform

The research done on the MFE platform resulted in the project being awarded funding to transition the entire platform towards first-in-human clinical investigation. This led to work with a consulting company in order to certify our platform and obtain MHRA certification.

In this context, the development of the platform saw a stage-gate process in which the project was managed and divided into several stages or phases interspersed with decision points or design reviews. In addition, risk management of the platform was carried out concurrently with the development and testing of the system. Risk management of the platform consists of risk identification or analysis, Failure Mode and Effect Analysis (FMEA) along with risk assessment. The latter involves the analysis of possible risk and consequently the analysis of possible control measures to reduce the risk. In more detail, the risk acceptability criteria is a probability calculated on the severity of the risk and the likelihood of the risk occurring. The risk assessment aims to reduce this probability by the means of design and risk control measures and to assess the overall acceptability of the residual risk. The major contributions of my thesis related to FMEA are the tests on the localization algorithm, protected workspace, and collision detection, described in the following sections. All of these are related to the system safety.

A V-model process [244] was adopted to evaluate and ensure the quality of the system, and therefore a system verification and validation process was implemented. This process consists of a few steps:

- identify the user requirements which are translated into functional requirements for the system;
- system design and project development;
- test functional and user requirements.

Therefore, the V-model is a structured method that establishes the relationships between each phase of the development life cycle and its associated phase of testing, as shown in Fig. 6.0.1. This results in not having a straightforward, linear process, but a procedure that alternates between development and testing phases. This allows the system to be refined and improved at any point in the process.

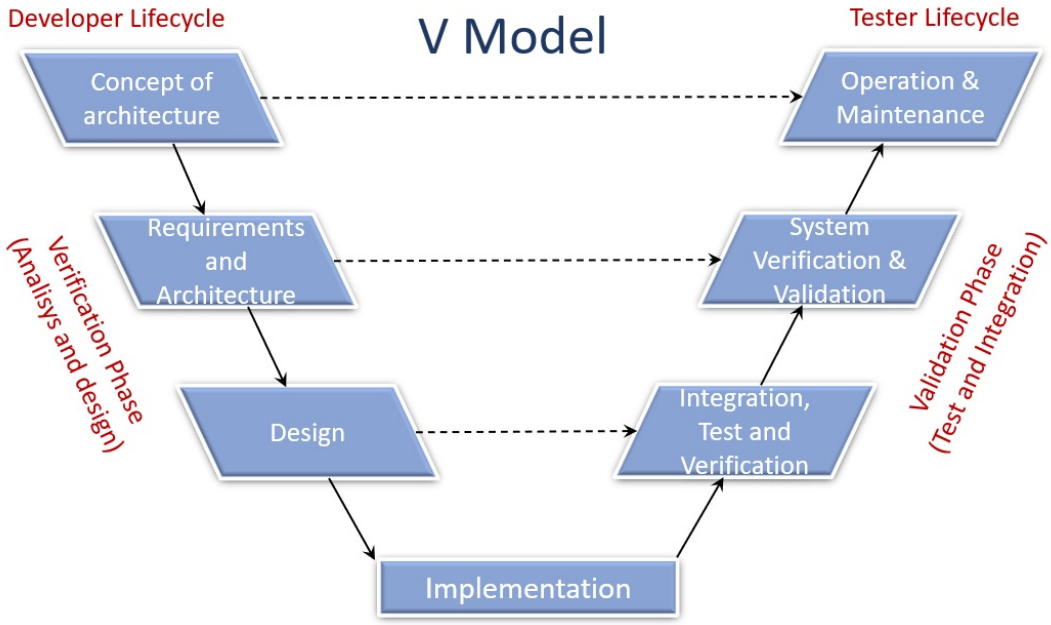

Figure 6.0.1: V-shaped process model

This work was done in collaboration with the software team of the MFE project with the goal of translating the platform into clinical research. Herein, a brief explanation of the main tests conducted in this context is provided.

6.1 Software development and testing

Testing the code in its entirety is necessary to certify the complete platform and obtain MHRA certification for the project. In this context, I worked on software certification and testing. This means developing a medical compliant software, adding code documentation, developing unit and integration tests and performing software component validation. The unit and integration

tests are implemented with the Robotic Operating System (ROS) platform, using the test function provided by python.

The safety of the platform is a crucial issue in transitioning the MFE platform towards clinical trials. Requirements on the workspace of the robotic manipulator, the collision detection and the localization of the magnetic endoscope were studied. Therefore, three main tests on these requirements have been performed at present. As mentioned, all of these tests have implications on the safety of the entire system and reduce the risk of the robot misbehaving in a way that could cause harm to the patient and/or other people/objects in the room (these are covered comprehensively in the Preliminary Hazard Analysis and FMEA documents for the MFE).

6.1.1 Protected workspace

The objective of this evaluation is to assess the correct functioning of the protected workspace, a constrained workspace where the KUKA robot can move freely without colliding with anything. This would secure the robot in a protected workspace and prevent the robot from hitting the patient and/or other people/objects in the room.

This protocol aims to evaluate the reliability of the protected workspace in a repeatable manner in order to ensure safe behaviour of the robot. Two types of workspaces were implemented; a “software” workspace (herein, referred to as ”soft” workspace) which was added to the code of our application and a “hardware” workspace (herein, referred to as ”hard” workspace and larger than the soft one) which was added onto the safety table of the KUKA robot.

The first one aims to prevent the robot from moving outside the protected “soft” workspace; the second one makes sure that the application on the smartpad of the manipulator is terminated as soon as the robot reaches the edges of the “hard” workspace (this means the soft workspace has been violated and for some reason the robot was not stopped before and, therefore, the robot is in a dangerous situation). To thoroughly test these scenarios, the protocol is split into two categories: non-disruptive and disruptive tests. Both tests aim at examining the reliability of the protected workspace in order to avoid the robot from moving outside the desired workspace and hitting the patient.

The non-disruptive test involves the use of our software, in which the soft limits for the protected workspace have been incorporated. This test evaluates the reliability of the code to prevent the EE from moving outside the protected workspace.

The disruptive test, on the other hand, takes into consideration the hard limits of the protected workspace and aims to verify that the smartpad controller stops the robot as soon as the robot reaches the edges of the hard protected workspace.

6.1.2 Collision Detection

This protocol aims to evaluate the collision detection functionality in order to ensure the safe behaviour of the robot. The KUKA medical robot is a collaborative robot. The term "collaborative robot" is used to mean a robot intended for direct interaction with the external environment and designed to physically interact with humans. A robot is considered collaborative when external torque sensors are applied at each joint of the robot itself. These permit to measure the external torque at each joint in order to be aware of the force/torque that the robot is applying to the external environment and to avoid applying any unacceptable force/torque on external objects and/or people.

The idea is to implement two different forms of collision detection, one "software" and one "hardware". The first one aims to move the EE of the KUKA robot away from the collision, when a "soft" collision has been detected. Conversely, the second one which is embedded in the safety table of the KUKA robot, aims to stop the robot and switch to hand-guiding control (i.e. manually move the robot to a safe position) after a dangerous collision could not be avoided for any reason. To thoroughly test these scenarios, the protocol is split into two categories: non-disruptive and disruptive tests.

The non-disruptive testing involves the use of our software, in which the soft limits for the collision detection are inserted. The idea is to have a test which checks that, when a collision is detected, the user is always able to move the robot away from the collision and return to a safe position with the help of the joystick.

The disruptive test, in contrast, takes into consideration the hard limits for collision detection and aims to verify that the smartpad controller stops the robot as soon as the collision has been detected, by reading the external joint torques. This allows the user to switch the controller to hand-guiding mode and manually move the robot away from the collision. This test was be conducted whilst the robot was moving and whilst it was stationary.

6.1.3 Localization

Localization is a fundamental part of the MFE system and has implications on safety. Incorrect localization data can result in harm if the user and/or robotic control system attempts to manipulate the endoscope based on this incorrect data.

The goal of this evaluation is to gain a high-level understanding of the current reliability of the localization and to obtain a quantitative evaluation of the localization error. "Reliability" in this context refers to the ability of the localization system to produce correct pose data in the presence of foreseeable environmental disturbances and prolonged use ($> 30min$). The main issues of localization systems might be obvious interference and drift (the localization output drifting through space despite a fixed pose of the endoscope in the real world).

These tests were performed using two KUKA LBR Med manipulators and an optical tracking system (Optitrack Prime 13 with 0.2 mm 3D accuracy, 1.3 MP (1280×1024) of resolution and 240 Hz frame rate)[1]. The primary robot (i.e. IIWA1), with the EPM mounted as a tool, aimed to localize the endoscope with the MFE localization algorithm, while the second manipulator (i.e. IIWA2) had the endoscope holder mounted as a tool. Two sets of four markers (Optitrack 6.4 mm ($\frac{1}{4}$ inches) M3 Markers) were attached to the EE of IIWA1 and to the endoscope holder secured to IIWA2. The purpose of the Optical tracking system is to obtain a ground truth for endoscope localization.

Two main localization tests were performed: static and dynamic. The test points, which represent the cartesian coordinates of the endoscope in the world frame of IIWA1, were chosen to test the localization algorithm in scenarios that frequently occur during clinical use.

Static tests involve the robotic manipulator and endoscope being placed in 5 predefined, fixed positions relative to each other and the surrounding equipment for a duration of 2 minutes each. In a second static test, from these fixed positions, metallic objects are brought close to the EPM and endoscope. This evaluates interference from internal (e.g. conductivity of the robot cart) and external (e.g. foreign metal objects) sources.

The dynamic tests were divided into two parts. In the first, the equipment is set up as in the static tests (i.e. with the EPM in a predefined, fixed position) but this time the endoscope is manipulated by IIWA2 to follow a predefined trajectory for 4 minutes. In a second dynamic

[1] https://optitrack.com/cameras/primex-13/specs.html

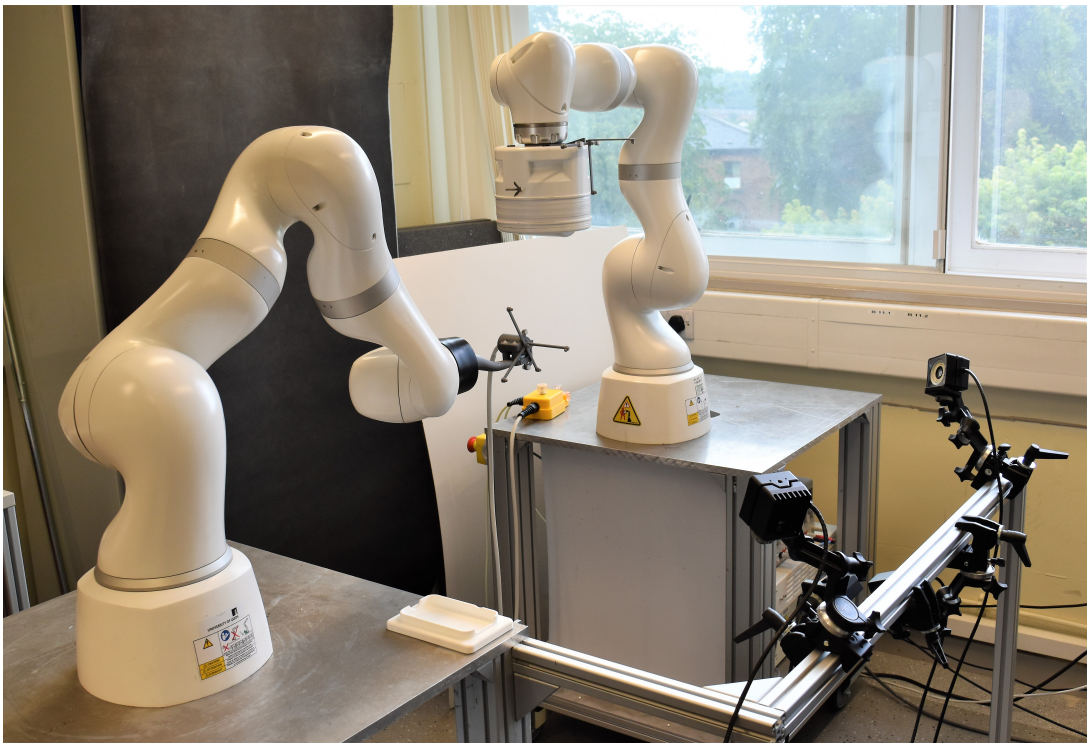

Figure 6.1.1: IIWA1 and IIWA2 with the EPM and the endoscope attached to the respectively EE. Optical tracking system to localize the MFE.

test, the endoscope is placed in a fixed pose and the EPM is moved in a repetitive way over the endoscope for a prolonged duration ($\sim$ 30 mins). These tests evaluate the localization reliability under dynamic conditions and during prolonged use, respectively.

During the tests, the output of the localization algorithm was compared with the output given by the optical tracking system and the error was computed. The outputs of the two localization methods were registered making use of appropriate ROS packages (i.e. rosbag and rostopic). The outputs were synchronized and the error was computed sampling the two signals at the same frequency (100 Hz). At the end of each test, the mean value and standard deviation of the pose error were computed and the tests were considered passed if the maximum position errors evaluated were less than 5 mm and the orientation errors were lower than 5°.

The tests considered above prove:

- the ability of the localization algorithm to estimate the pose of the endoscope with position errors lower than 5 mm and orientation errors below 5°;
- the ability of the software to provide a confident measure of the endoscope localization accuracy.

6.2 Summary

This chapter provides a brief analysis of the work carried out to certify the MFE platform and to obtain the MHRA certification in order to move the platform towards the clinical trials. The main tests performed in order to assess the quality of the system (i.e the Localization algorithm, workspace and collision tests) are briefly described.

Chapter 7

Conclusion and future directions

This chapter summarizes the main contributions of this thesis and the future directions of the project. Magnetic robotic endoscopes have proven to address all the major clinical needs for colonoscopy,[12, 13] thus providing a promising alternative for such complex procedures. In particular, they show the potential to reduce pain for the patient and, thus, the need for sedation; the possibility to fabricate disposable endoscopes, reducing the risk of infection; and finally, the improvement on the learning curve for the clinician due to its ease-of-use, lowering the cost to the healthcare provider. The benefits of this innovative technology are essential for preventing GI diseases, reducing the incidence of cancer such as CRC and improving the quality of life for people affected by chronic GI diseases such as IBD and IBS.

This work is a contribution to the adoption of the MFE in clinical practice. The main objective of this thesis is to help bridge the gap between the prototype and the wide range of needs in clinical application. On the basis of the main questions, detailed in Chapter 1, my work has progressed in the field of medical robotics control. The work of this thesis, therefore, started with an extensive literature review of the main characteristics and properties of the GI tract in order to provide engineers in the field with a comprehensive reference of the GI environment. As a consequence, the clinical motivations shaped the research section of this thesis. Moreover, due to the non-linear nature of the magnetic fields and the necessity of a more suitable control, the involvement of more intelligent forms of robotic control was considered essential. Therefore, an in-depth work on the control of the MFE is provided.

Hence, the contributions of this dissertation to the field of medical robotics are the following:

(1) a detailed literature review in collaboration with Prof. Benjamin Terry of University of Nebraska. This work addresses knowledge gaps in the field and provides a broad reference manual to engineers in the field of medical robotics who want to develop a more effective and innovative endoscope to inspect the GI tract;

(2) development of a suitable control approach to achieve magnetic levitation of the endoscope and reduce the contact between the endoscope and the colon wall;

(3) development of an appropriate control approach for stabilizing the orientation and viewpoint of the endoscope to perform interventional tasks, such as biopsy or polyp removal;

(4) aiding the transition into clinical use of the MFE platform by developing and testing the software and performing quality testing on the platform.

In further concluding this dissertation, a more in-depth summary of the contributions of this work is provided. Chapter 2 provides an in-depth literature review on the main properties and characteristics of the GI tract and a brief overview of the new technologies developed in the past decade. In fact, despite the numerous innovative medical devices developed, the number of open challenges in this field is still significant. Therefore, the need for new devices and suitable strategies for replacing the standard endoscopes used for the inspection of the GI environment, is still imperative. This was encouraging and motivated the investigation into new suitable control approaches able to achieve tasks autonomy in magnetic robotic endoscopy. Chapter 3 provides an overview of the MFE platform and the limitations inherited from basic robotic control. Moreover, an overview of a magnetic localization system [199], which allowed for the pose of the MFE to be accurately estimated, is given herein. Magnetic localization of the endoscope is essential to enable work on closed-loop control for navigation and stabilization of the magnetic endoscope. Chapter 4 and 5 represent the main body of the research work and, herein, an in-depth analysis of the techniques implemented to control the MFE is presented.

The inherited MFE platform includes a standard PID closed-loop control algorithm used to navigate the MFE inside the colon. The main disadvantage of this controller is the continuous attraction between the IPM and EPM. This results in continuous contact of the MFE with the colon walls, which would hinder smooth navigation of the endoscope. Chapter 4 demonstrates that a dynamic control approach is able to accurately compensate for gravity, achieving the magnetic levitation of the endoscope. This control technique has proven effective in enhancing

endoscope navigation, reducing the contact with the environment. This also reduces friction and, thus, pain for the patient.

Two main control techniques (i.e Gravity PID control and Adaptive Backstepping control), used to achieve the magnetic levitation of the endoscope, are described and the main results are shown in Chapter 4. Both techniques achieve the levitation of the endoscope by controlling the linear position of the MFE along the gravity direction and aid the performance of the overall control system by adding an internal control loop on the magnetic force. This guarantees the overall convergence and stability of the control system. The Adaptive Backstepping control, in contrast to the the Gravity PID control, adds a further loop which estimates the dynamics of the IPM, dealing with possible parametric uncertainties (i.e the effect of the tether on the dynamics of the MFE), and guarantees the robust asymptotic stability of the overall system.

Both approaches were validated in experimental environments. Free space levitation was shown in an L-shaped acrylic tube. A more realistic environment was then considered in order to demonstrate a successful levitation of the endoscope inside a colon phantom. Results showed that the dynamic control was able to reduce the contact of the endoscope with the environment, avoiding obstacles and folds. This facilitated locomotion, diminished tissue stress and reduced patient discomfort.

Despite the promising results obtained with both approaches and, in particular, with the Adaptive Backstepping control, the frequency limitation of the localization algorithm played an important role on the system's performance. In fact, the localization frequency (100 Hz) was not fast enough to ensure that the IPM dynamics were handled completely. Therefore, increasing the localization frequency would have a direct impact on the system's performance. As a next step, further experimental analysis in a more realistic environment, such as in vivo animal studies or cadaveric trials, would strengthen the validity of this approach, demonstrating that the proposed controllers can be applied in a clinical setting.

In Chapter 5, the next contribution from this thesis is presented on the topic of diagnostic and interventional autonomy for magnetic colonoscopy. To be clinically viable, magnetic endoscopes should be able to reproduce the main tasks of a colonoscopy procedure, such as biopsies and polyp removal. The focus of this chapter is on the targeted biopsies which are performed by the clinician on suspicious lesions. Having a precise positional target requires accuracy in the endoscope positioning and rejection of disturbance. To date, the control of magnetic endoscopes

has mainly been focused on navigation and no examples of active endoscope stabilization have been found in literature. In this chapter, a linear model-based control approach aimed at stabilizing the orientation of the MFE during interventional tasks and in the presence of external disturbances is presented. By linearizing the non-linear system at more than one equilibrium point, the LPV method allows for the synthesis of appropriate control for each equilibrium point while improving the stability of the overall control system.

The control technique was validated in an experimental setting using a benchtop colon simulator. The LPV control approach was compared with the standard PID control in terms of endoscope orientation error. The current technique showed a maximum reduction of the mean orientation error of 45.8% with respect to the standard PID control.

Further work will see the integration of this method with an AI [243] or a semi-autonomous routine [233] for target tracking. In fact, additional disturbances, specifically patient breathing and peristalsis, will cause movement of the biopsy target. Therefore, target tracking should be investigated along with the endoscope stabilization. The two techniques together would result in a fully autonomous procedure.

Chapter 6 briefly describes the work done to transition the MFE project through the clinical trials. The research work done on the platform over the past several years has been essential to advancing this technology into clinical use. To achieve this goal, work on the software development, software testing and quality management of the platform has been carried out to certify our platform and obtain the MHRA certification.

In summary, the control techniques developed in this work, with the purpose of performing smoother navigation and interventional tasks, are viable solutions and aim to reduce the cognitive load on the user. The next stage for this work would be to optimize the control techniques, described in Chapter 4 and 5, and to test them in a more realistic environment such as an animal or cadaver model. This would prove the effectiveness of the control approaches in more realistic and varied scenarios and may help transition the platform to clinical trails.

In conclusion, this technology may improve the patient experience of colonoscopy by reducing tissue stress, discomfort, and potentially eliminating the need for sedation. In addition, the improved autonomy of the MFE platform may also contribute to an enhanced operator experience, reducing operator burden.

References

1. Da Veiga, T., Chandler, J. H., Lloyd, P., Pittiglio, G., Wilkinson, N. J., Hoshiar, A. K., Harris, R. A. & Valdastri, P. Challenges of continuum robots in clinical context: A review. *Progress in Biomedical Engineering* **2.** ISSN: 25161091 (2020).
2. Peters, B. S., Armijo, P. R., Krause, C., Choudhury, S. A. & Oleynikov, D. Review of emerging surgical robotic technology. *Surgical Endoscopy* **32,** 1636–1655. ISSN: 1432-2218. https://doi.org/10.1007/s00464-018-6079-2 (2018).
3. Simaan, N., Yasin, R. M. & Wang, L. Medical Technologies and Challenges of Robot-Assisted Minimally Invasive Intervention and Diagnostics. *Annual Review of Control, Robotics, and Autonomous Systems* **1,** 465–490. https://doi.org/10.1146/annurev-control-060117-104956 (2018).
4. Taylor, R. H., Menciassi, A., Fichtinger, G. & Dario, P. in *Springer Handbook of Robotics* (eds Siciliano, B. & Khatib, O.) 1199–1222 (Springer Berlin Heidelberg, Berlin, Heidelberg, 2008). ISBN: 978-3-540-30301-5. https://doi.org/10.1007/978-3-540-30301-5{_}53.
5. Davies, B. A review of robotics in surgery. eng. *Proceedings of the Institution of Mechanical Engineers. Part H, Journal of engineering in medicine* **214,** 129–140. ISSN: 0954-4119 (Print) (2000).
6. Singh, P. & Krishna, C. M. Continuum Arm Robotic Manipulator: A Review. *Universal Journal of Mechanical Engineering* **2,** 193–198 (2014).
7. in. *Nonlinear Control Systems: An Introduction* (ed Isidori, A.) 178–253 (Springer Berlin Heidelberg, Berlin, Heidelberg, 1985). ISBN: 978-3-540-70747-9. https://doi.org/10.1007/BFb0006373.
8. *Canadian Cancer Society* www.cancer.ca.

9. Bray, F., Ferlay, J., Soerjomataram, I., Siegel, R. L., Torre, L. A. & Jemal, A. Global cancer statistics 2018: GLOBOCAN estimates of incidence and mortality worldwide for 36 cancers in 185 countries. *CA: A Cancer Journal for Clinicians* **68,** 394–424. ISSN: 1542-4863 (2018).

10. Joseph, D. A., Degroff, A. S., Hayes, N. S., Wong, F. L. & Plescia, M. The Colorectal Cancer Control Program: Partnering to increase population level screening. *Gastrointestinal Endoscopy* **73,** 429–434. ISSN: 00165107. http://dx.doi.org/10.1016/j.gie.2010.12.027 (2011).

11. Obstein, K. L. & Valdastri, P. Advanced endoscopic technologies for colorectal cancer screening. *World Journal of Gastroenterology* **19,** 431–439. ISSN: 10079327 (2013).

12. Valdastri, P., Simi, M. & Webster, R. J. r. Advanced technologies for gastrointestinal endoscopy. *Annual review of biomedical engineering* **14,** 397–429. ISSN: 1545-4274 (Electronic) (2012).

13. Slawinski, P. R., Obstein, K. L. & Valdastri, P. Emerging issues and future developments in capsule endoscopy. *Techniques in Gastrointestinal Endoscopy* **17,** 40–46. ISSN: 15585050 (2015).

14. Edelmann, J., Petruska, A. J. & Nelson, B. J. Magnetic control of continuum devices. *International Journal of Robotics Research* **36,** 68–85. ISSN: 17413176 (2017).

15. Chautems, C. & Nelson, B. J. The tethered magnet: Force and 5-DOF pose control for cardiac ablation. *Proceedings - IEEE International Conference on Robotics and Automation,* 4837–4842. ISSN: 10504729 (2017).

16. Petruska, A. J. & Nelson, B. J. Minimum Bounds on the Number of Electromagnets Required for Remote Magnetic Manipulation. *IEEE Transactions on Robotics* **31,** 714–722. ISSN: 15523098 (2015).

17. Chautems, C., Tonazzini, A., Floreano, D. & Nelson, B. J. A variable stiffness catheter controlled with an external magnetic field. *2017 IEEE/RSJ International Conference on Intelligent Robots and Systems (IROS),* 181–186. http://ieeexplore.ieee.org/document/8202155/ (2017).

18. Greigarn, T., Jackson, R., Liu, T. & Çavuşoğlu, M. C. *Experimental validation of the pseudo-rigid-body model of the MRI-actuated catheter* in *2017 IEEE International Conference on Robotics and Automation (ICRA)* (2017), 3600–3605.

19. Jeon, S., Hoshiar, A. K., Kim, K., Lee, S., Kim, E., Lee, S., Kim, J., Nelson, B. J., Cha, H., Yi, B. & Choi, H. A Magnetically Controlled Soft Microrobot Steering a Guidewire in a Three-Dimensional Phantom Vascular Network. *Soft Robotics* **0.** PMID: 30312145. eprint: https://doi.org/10.1089/soro.2018.0019. https://doi.org/10.1089/soro.2018.0019 (0).

20. Sikorski, J., Dawson, I., Denasi, A., Hekman, E. E. & Misra, S. Introducing BigMag - A novel system for 3D magnetic actuation of flexible surgical manipulators. *Proceedings - IEEE International Conference on Robotics and Automation,* 3594–3599. ISSN: 10504729 (2017).

21. Yim, S & Sitti, M. Design and Rolling Locomotion of a Magnetically Actuated Soft Capsule Endoscope. *IEEE Transactions on Robotics* **28,** 183–194. ISSN: 1552-3098 (2012).

22. Ryan, P. & Diller, E. Magnetic Actuation for Full Dexterity Microrobotic Control Using Rotating Permanent Magnets. *IEEE Transactions on Robotics* **33,** 1398–1409. ISSN: 15523098 (2017).

23. Arezzo, A., Menciassi, A., Valdastri, P., Ciuti, G., Lucarini, G., Salerno, M., Di Natali, C., Verra, M., Dario, P. & Morino, M. Experimental assessment of a novel robotically-driven endoscopic capsule compared to traditional colonoscopy. *Digestive and Liver Disease* **45,** 657–662. ISSN: 15908658. http://dx.doi.org/10.1016/j.dld.2013.01.025 (2013).

24. Valdastri, P, Quaglia, C, Susilo, E, Menciassi, A, Dario, P, Ho, C., Anhoeck, G & Schurr, M. Wireless therapeutic endoscopic capsule: in vivo experiment. *Endoscopy* **40,** 979–982. ISSN: 0013-726X. http://www.thieme-connect.de/DOI/DOI?10.1055/s-0028-1103424 (2008).

25. Valdastri, P, Ciuti, G, Verbeni, A, Menciassi, A, Dario, P, Arezzo, A & Morino, M. Magnetic air capsule robotic system: proof of concept of a novel approach for painless colonoscopy. *Surgical Endoscopy* **26,** 1238–1246. https://doi.org/10.1007/s00464-011-2054-x (2012).

26. Mahoney, A. W. & Abbott, J. J. Five-degree-of-freedom manipulation of an untethered magnetic device in fluid using a single permanent magnet with application in stomach capsule endoscopy. *The International Journal of Robotics Research* **35,** 129–147 (2016).

27. Tremblay, C., Conan, B., Loghin, D., Bigot, A. & Martel, S. *Fringe Field Navigation for Catheterization* in *6th European Conference of the International Federation for Med-*

ical and Biological Engineering (eds Lacković, I. & Vasic, D.) (Springer International Publishing, Cham, 2015), 379–382. ISBN: 978-3-319-11128-5.

28. Taddese, A. Z., Slawinski, P. R., Obstein, K. L. & Valdastri, P. Closed Loop Control of a Tethered Magnetic Capsule Endoscope. eng. *Robotics science and systems : online proceedings* **2016.** ISSN: 2330-7668 (Print) (2016).
29. Taddese, A. Z., Slawinski, P. R., Obstein, K. L. & Valdastri, P. *Nonholonomic closed-loop velocity control of a soft-tethered magnetic capsule endoscope* in *2016 IEEE/RSJ International Conference on Intelligent Robots and Systems (IROS)* (IEEE, 2016), 1139–1144. ISBN: 978-1-5090-3762-9. http://ieeexplore.ieee.org/document/7759192/.
30. Barducci, L., Pittiglio, G., Norton, J. C., Obstein, K. L. & Valdastri, P. Adaptive Dynamic Control for Magnetically Actuated Medical Robots. *IEEE Robotics and Automation Letters* **4,** 3633–3640 (2019).
31. Martin, J. W., Scaglioni, B., Norton, J. C., Subramanian, V., Arezzo, A., Obstein, K. L. & Valdastri, P. Enabling the future of colonoscopy with intelligent and autonomous magnetic manipulation. *Nature Machine Intelligence* **2,** 595–606. ISSN: 25225839. http://dx.doi.org/10.1038/s42256-020-00231-9 (2020).
32. Caffrey, C. M., Chevalerias, O., O'Mathuna, C. & Twomey, K. Swallowable-Capsule Technology, 23–29 (2008).
33. *National Institutes of Health (NIH)* https://www.nih.gov/health-information.
34. Tsai, S. P. A mortality and morbidity study of refinery and petrochemical employees in {Louisiana}. *Occupational and Environmental Medicine* **60,** 627–633. ISSN: 1351-0711. http://oem.bmj.com/cgi/doi/10.1136/oem.60.9.627 (2003).
35. Bray, F., Ferlay, J., Soerjomataram, I., Siegel, R. L., Torre, L. A. & Jemal, A. Global cancer statistics 2018: {GLOBOCAN} estimates of incidence and mortality worldwide for 36 cancers in 185 countries. *CA: A Cancer Journal for Clinicians* **68,** 394–424. ISSN: 00079235. http://doi.wiley.com/10.3322/caac.21492 (2018).
36. CDC. {*CDC*} {*VitalSigns*} - {*Colorectal*} {*Cancer*} 2011. https://www.cdc.gov/vitalsigns/cancerscreening/colorectalcancer/index.html.
37. Bujanda, L., Sarasqueta, C., Zubiaurre, L., Cosme, A., Muñoz, C., Sánchez, A., Martín, C., Tito, L., Piñol, V., Castells, A., Llor, X., Xicola, R. M., Pons, E., Clofent, J., De Castro, M. L., Cuquerella, J., Medina, E., Gutierrez, A., Arenas, J. I. & Jover, R. Low

adherence to colonoscopy in the screening of first-degree relatives of patients with colorectal cancer. *Gut* **56,** 1714–1718. ISSN: 00175749 (2007).

38. Li, B., Meng, M. Q.-H. & Lau, J. Y. W. Computer-aided small bowel tumor detection for capsule endoscopy. *Artificial Intelligence in Medicine* **52,** 11–16. ISSN: 09333657. https://linkinghub.elsevier.com/retrieve/pii/S0933365711000042 (2011).
39. Brambs, H. J. & Juchems, M. S. Virtual endoscopy using CT scan. *Minimally Invasive Therapy and Allied Technologies* **12,** 207–216. ISSN: 13645706 (2003).
40. Kumar, R. R., Joseph, J., Vidya, P. V., Pournami, C & John, N. J. *Virtual colonoscopy: {A} plausible alternative to conventional colonoscopy* in *2017 {IEEE} {Region} 10 {Symposium} ({TENSYMP})* (IEEE, Cochin, India, 2017), 1–5. ISBN: 978-1-5090-6255-3. http://ieeexplore.ieee.org/document/8070107/.
41. Slawinski, P. R., Obstein, K. L. & Valdastri, P. Capsule endoscopy of the future: What's on the horizon? *World Journal of Gastroenterology* **21,** 10528–10541. ISSN: 22192840 (2015).
42. Liao, Z., Hou, X., Lin-Hu, E. Q., Sheng, J. Q., Ge, Z. Z., Jiang, B., Hou, X. H., Liu, J. Y., Li, Z., Huang, Q. Y., Zhao, X. J., Li, N., Gao, Y. J., Zhang, Y., Zhou, J. Q., Wang, X. Y., Liu, J., Xie, X. P., Yang, C. M., Liu, H. L., Sun, X. T., Zou, W. B. & Li, Z. S. Accuracy of Magnetically Controlled Capsule Endoscopy, Compared With Conventional Gastroscopy, in Detection of Gastric Diseases. *Clinical Gastroenterology and Hepatology* **14,** 1266–1273.e1. ISSN: 15427714 (2016).
43. Nam, S. J., Lee, H. S. & Lim, Y. J. Evaluation of gastric disease with capsule endoscopy. *Clinical Endoscopy* **51,** 323–328. ISSN: 22342443 (2018).
44. Riccioni, M. E. Colon capsule endoscopy: Advantages, limitations and expectations. Which novelties? *World Journal of Gastrointestinal Endoscopy* **4,** 99. ISSN: 1948-5190. http://www.wjgnet.com/1948-5190/full/v4/i4/99.htm (2012).
45. Ciuti, G., Menciassi, A. & Dario, P. Capsule {Endoscopy}: {From} {Current} {Achievements} to {Open} {Challenges}. *IEEE Reviews in Biomedical Engineering* **4,** 59–72. ISSN: 1937-3333, 1941-1189. http://ieeexplore.ieee.org/document/6041014/ (2011).
46. Liu, L., Towfighian, S. & Hila, A. A {Review} of {Locomotion} {Systems} for {Capsule} {Endoscopy}. *IEEE Reviews in Biomedical Engineering* **8,** 138–151. ISSN: 1937-3333, 1941-1189. http://ieeexplore.ieee.org/document/7140757/ (2015).

47. Pittiglio, G., Barducci, L., Martin, J. W., Norton, J. C., Avizzano, C. A., Obstein, K. L. & Valdastri, P. Magnetic Levitation for Soft-Tethered Capsule Colonoscopy Actuated with a Single Permanent Magnet: A Dynamic Control Approach. *IEEE Robotics and Automation Letters* **4,** 1224–1231. ISSN: 23773766 (2019).

48. Zhang, P., Li, J., Hao, Y., Ciuti, G., Arai, T., Huang, Q. & Dario, P. *A compensation strategy for accurate orientation of a tethered robotic capsule endoscope* in *2017 IEEE International Conference on Cyborg and Bionic Systems (CBS)* (2017), 257–261.

49. Glass, P., Sitti, M., Pennathur, A. & Appasamy, R. A Swallowable Tethered Capsule Endoscope for Diagnosing Barrett's Esophagus. *Gastrointestinal Endoscopy* **69,** AB106. ISSN: 0016-5107. https://doi.org/10.1016/j.gie.2009.03.072 (2009).

50. Gora, M. J., Sauk, J. S., Carruth, R. W., Gallagher, K. A., Suter, M. J., Nishioka, N. S., Kava, L. E., Rosenberg, M., Bouma, B. E. & Tearney, G. J. Tethered capsule endomicroscopy enables less invasive imaging of gastrointestinal tract microstructure. *Nature Medicine* **19,** 238–240. ISSN: 1078-8956, 1546-170X. http://www.nature.com/articles/nm.3052 (2013).

51. Caprara, R., Obstein, K. L., Scozzarro, G., Natali, C. D., Beccani, M., Morgan, D. R. & Valdastri, P. A {Platform} for {Gastric} {Cancer} {Screening} in {Low}- and {Middle}-{Income} {Countries}. *IEEE Transactions on Biomedical Engineering* **62,** 1324–1332. ISSN: 0018-9294, 1558-2531. http://ieeexplore.ieee.org/document/6999943/ (2015).

52. Dehghani, H., Welch, C. R., Pourghodrat, A., Nelson, C. A., Oleynikov, D., Dasgupta, P. & Terry, B. S. Design and preliminary evaluation of a self-steering, pneumatically driven colonoscopy robot. *Journal of Medical Engineering & Technology* **41,** 223–236. ISSN: 0309-1902, 1464-522X. https://www.tandfonline.com/doi/full/10.1080/03091902.2016.1275853 (2017).

53. Mapara, S. S. & Patravale, V. B. Medical capsule robots: A renaissance for diagnostics, drug delivery and surgical treatment. *Journal of Controlled Release* **261,** 337–351. ISSN: 18734995. https://doi.org/10.1016/j.jconrel.2017.07.005 (2017).

54. Toennies, J. L., Tortora, G, Simi, M, Valdastri, P & Webster, R. J. Swallowable medical devices for diagnosis and surgery: The state of the art. *Proceedings of the Institution of Mechanical Engineers, Part C: Journal of Mechanical Engineering Science* **224,** 1397–1414. https://doi.org/10.1243/09544062JMES1879 (2010).

55. Beccani, M., Di Natali, C., Aiello, G., Benjamin, C., Susilo, E. & Valdastri, P. A Magnetic drug delivery Capsule based on a coil actuation mechanism. *Procedia Engineering* **120,** 53–56. ISSN: 18777058. http://dx.doi.org/10.1016/j.proeng.2015.08.564 (2015).

56. Kyoung-chul Kong, Jinhoon Cha, Doyoung Jeon & Dong-il Dan Cho. *A rotational micro biopsy device for the capsule endoscope* in *2005 {IEEE}/{RSJ} {International} {Conference} on {Intelligent} {Robots} and {Systems}* (IEEE, Edmonton, Alta., Canada, 2005), 1839–1843. ISBN: 978-0-7803-8912-0. http://ieeexplore.ieee.org/document/1545441/.

57. Norton, J. C., Slawinski, P. R., Lay, H. S., Martin, J. W., Cox, B. F., Cummins, G., Desmulliez, M. P., Clutton, R. E., Obstein, K. L., Cochran, S. & Valdastri, P. Intelligent magnetic manipulation for gastrointestinal ultrasound. *Science Robotics* **4,** 1–14. ISSN: 24709476 (2019).

58. Hounnou, G., Destrieux, C., Desmé, J., Bertrand, P. & Velut, S. Anatomical study of the length of the human intestine. *Surgical and Radiologic Anatomy* **24,** 290–294. ISSN: 09301038 (2002).

59. McKay, D. M. & Bienenstock, J. The interaction between mast cells and nerves in the gastrointestinal tract. *Immunology Today* **15,** 533–538. ISSN: 01675699 (1994).

60. Soybel, D. I. Anatomy and Physiology of the Stomach. *Surgical Clinics of North America* **85.** Gastric Surgery, 875–894. ISSN: 0039-6109. https://www.sciencedirect.com/science/article/pii/S0039610905000848 (2005).

61. Gelberg, H. B. Comparative anatomy, physiology, and mechanisms of disease production of the esophagus, stomach, and small intestine. *Toxicologic Pathology* **42,** 54–66. ISSN: 01926233 (2014).

62. Helander, H. F. & Fändriks, L. Surface area of the digestive tract-revisited. *Scandinavian Journal of Gastroenterology* **49,** 681–689. ISSN: 15027708 (2014).

63. Ødegaard, S., Nesje, L. B., Lærum, O. D. & Kimmey, M. B. High-frequency ultrasonographic imaging of the gastrointestinal wall. *Expert Review of Medical Devices* **9,** 263–273. ISSN: 17434440 (2012).

64. Kuo, B. & Urma, D. Esophagus - anatomy and development. *GI Motility online (2006).* https://www.nature.com/gimo/contents/pt1/full/gimo6.html (2006).

65. Ambe, P., Weber, S. A., Schauer, M. & Knoefel, W. T. Swallowed foreign bodies in adults. *Deutsches Arzteblatt International* **109,** 869–875. ISSN: 18660452 (2012).

66. Ikenberry, S. O., Jue, T. L., Anderson, M. A., Appalaneni, V., Banerjee, S., Ben-Menachem, T., Decker, G. A., Fanelli, R. D., Fisher, L. R., Fukami, N., Harrison, M. E., Jain, R., Khan, K. M., Krinsky, M. L., Maple, J. T., Sharaf, R., Strohmeyer, L. & Dominitz, J. A. Management of ingested foreign bodies and food impactions. *Gastrointestinal Endoscopy* **73,** 1085–1091. ISSN: 10976779 (2011).

67. Bekkerman, M., Sachdev, A. H., Andrade, J., Twersky, Y. & Iqbal, S. Endoscopic Management of Foreign Bodies in the Gastrointestinal Tract: A Review of the Literature. *Gastroenterology Research and Practice* **2016.** ISSN: 1687630X (2016).

68. Xia, F., Mao, J., Ding, J. & Yang, H. Observation of normal appearance and wall thickness of esophagus on CT images. *European Journal of Radiology* **72,** 406–411. ISSN: 0720048X (2009).

69. Moss, A. A., Schnyder, P., Thoeni, R. F. & Margulis, A. R. Esophageal carcinoma: Pretherapy staging by computed tomography. *American Journal of Roentgenology* **136,** 1051–1056. ISSN: 0361803X (1981).

70. Chaudhry, S. R., Liman, M. N. P. & Peterson, D. C. Anatomy, {Abdomen} and {Pelvis}, {Stomach}. `https://www.ncbi.nlm.nih.gov/books/NBK482334/`.

71. Ramkumar, d. & Schulze, k. s. The pylorus. *Neurogastroenterology and Motility* **17,** 22–30. ISSN: 1350-1925, 1365-2982. `http://doi.wiley.com/10.1111/j.1365-2982.2005.00664.x` (2005).

72. Doran, S., Jones, K. L., Andrews, J. M. & Horowitz, M. Effects of meal volume and posture on gastric emptying of solids and appetite. *Am J Physiol Regulatory Integrative Comp Physiol* **275,** R1712–1718. ISSN: 0002-9513. `http://ajpregu.physiology.org/cgi/content/abstract/275/5/R1712` (1998).

73. Moore, J. G., Datz, F. L., Christian, P. E., Greenberg, E & Alazraki, N. Effect of body posture on radionuclide measurements of gastric emptying. *Digestive Diseases and Sciences* **33,** 1592–1595. ISSN: 0163-2116. `http://dx.doi.org/10.1007/BF01535951{\%}5Cnhttp://download.springer.com/static/pdf/959/art{\%}3A10.1007{\%}2FBF01535951.pdf?originUrl=http://link.springer.com/article/10.1007/BF01535951{\&}token2=exp=1458738837{~}acl=/static/pdf/959/art{\%}253A10.10` (1988).

74. Sanaka, M., Anjiki, H., Tsutsumi, H., Abe, K., Kawakami, T., Saitoh, M., Yamamoto, T., Ishii, T. & Kuyama, Y. Effect of cigarette smoking on gastric emptying of solids in

Japanese smokers: A crossover study using the 13C-octanoic acid breath test. *Journal of Gastroenterology* **40,** 578–582. ISSN: 09441174 (2005).

75. Bennink, R., Peeters, M., Van Den Maegdenbergh, V., Geypens, B., Rutgeerts, P., De Roo, M. & Mortelmans, L. Comparison of total and compartmental gastric emptying and antral motility between healthy men and women. *European Journal of Nuclear Medicine* **25,** 1293–1299. ISSN: 03406997 (1998).

76. Vasavid, Pataramon Chaiwatanarat, T., Pusuwan, P., Sritara, C., Roysri, K., Namwongprom, S., Kuanrakcharoen, P., Premprabha, T., Chunlertrith, K., Thongsawat, S., Sirinthornpunya, S., Ovartlarnporn, B., Kachintorn, U., Leelakusolvong, S., Kositchaiwat, C., Chakkaphak, S. & Gonlachanvit, S. Normal Solid Gastric Emptying Values Measured by Scintigraphy Using Asian-style Meal:A Multicenter Study in Healthy Volunteers. *Journal of Neurogastroenterology and Motility* **20,** 371–378. ISSN: 2093-0879, 2093-0887. `http://www.jnmjournal.org/journal/view.html?doi=10.5056/jnm13114` (2014).

77. Suk, K. T., Lim, D. W., Kim, M. Y., Park, D. H., Kim, K. H., Kim, J. M., Kim, J. W., Kim, H. S., Kwon, S. O., Baik, S. K. & Park, S. J. Thickening of the gastric wall on transabdominal sonography: {A} sign of gastric cancer. *Journal of Clinical Ultrasound* **36,** 462–466. ISSN: 00912751, 10970096. `http://doi.wiley.com/10.1002/jcu.20450` (2008).

78. Huh, C. H., Bhutani, M. S., Farfán, E. B. & Bolch, W. E. Individual variations in mucosa and total wall thickness in the stomach and rectum assessed via endoscopic ultrasound. *Physiological Measurement* **24.** ISSN: 09673334 (2003).

79. Kararli, T. T. Comparison of the gastrointestinal anatomy, physiology, and biochemistry of humans and commonly used laboratory animals. *Biopharmaceutics & Drug Disposition* **16,** 351–380. ISSN: 1099081X (1995).

80. Collins, J. T., Nguyen, A. & Badireddy, M. Anatomy, {Abdomen} and {Pelvis}, {Small} {Intestine}. `https://www.ncbi.nlm.nih.gov/books/NBK459366/`.

81. Meyers, M. A. Treitz redux: the ligament of Treitz revisited. *Abdominal Imaging* **20,** 421–424. ISSN: 09428925 (1995).

82. Ellis, H. Anatomy of the small intestine (jejunum and ileum). *Surgery* **29,** 355–357. ISSN: 18781764. `http://dx.doi.org/10.1016/j.mpsur.2011.05.013` (2011).

83. Cronin, C. G., Delappe, E., Lohan, D. G., Roche, C. & Murphy, J. M. Normal small bowel wall characteristics on MR enterography. *European Journal of Radiology* **75,** 207–211. ISSN: 0720048X. http://dx.doi.org/10.1016/j.ejrad.2009.04.066 (2010).

84. Weaver, L. T., Austin, S. & Cole, T. J. Small intestinal length: A factor essential for gut adaptation. *Gut* **32,** 1321–1323. ISSN: 00175749 (1991).

85. Hosseinpour, M. & Behdad, A. Evaluation of small bowel measurement in alive patients. *Surgical and Radiologic Anatomy* **30,** 653–655. ISSN: 09301038 (2008).

86. Uro, D. D. Overview of short bowel syndrome and intestinal transplantation. *Colombia Médica* **38,** 5 (2007).

87. Kahai, P., Mandiga, P., Wehrle, C. J. & Lobo, S. Anatomy, {Abdomen} and {Pelvis}, {Large} {Intestine}. https://www.ncbi.nlm.nih.gov/books/NBK470577/.

88. Eickhoff, A., Pickhardt, P. J., Hartmann, D. & Riemann, J. F. Colon anatomy based on CT colonography and fluoroscopy: Impact on looping, straightening and ancillary manoeuvres in colonoscopy. *Digestive and Liver Disease* **42,** 291–296. ISSN: 15908658 (2010).

89. Alazmani, A., Hood, A., Jayne, D., Neville, A. & Culmer, P. Quantitative assessment of colorectal morphology: Implications for robotic colonoscopy. *Medical Engineering & Physics* **38,** 148 –154. ISSN: 1350-4533. http://www.sciencedirect.com/science/article/pii/S1350453315002763 (2016).

90. Sadahiro, S., Ohmura, T., Yamada, Y., Saito, T. & Taki, Y. Analysis of length and surface area of each segment of the large intestine according to age, sex and physique. *Surgical and Radiologic Anatomy* **14,** 251–257. ISSN: 09301038 (1992).

91. Wiesner, W., Mortelé, K. J., Ji, H. & Ros, P. R. Normal colonic wall thickness at CT and its relation to colonic distension. *Journal of Computer Assisted Tomography* **26,** 102–106. ISSN: 03638715 (2002).

92. Trefts, E., Gannon, M. & Wasserman, D. H. The liver. *Current Biology* **27,** R1147–R1151. ISSN: 09609822. https://linkinghub.elsevier.com/retrieve/pii/S0960982217311831 (2017).

93. Turumin, J. L., Shanturov, V. A. & Turumina, H. E. The role of the gallbladder in humans. *Revista de Gastroenterología de México* **78,** 177–187. ISSN: 03750906. https://linkinghub.elsevier.com/retrieve/pii/S0375090613000323 (2013).

94. Longnecker, D. S. *Anatomy and {Histology} of the {Pancreas}* tech. rep. (The University of Michigan Library). http://pancreapedia.org/?q=node/8098.

95. Coffey, J. C. Surgical anatomy and anatomic surgery – {Clinical} and scientific mutualism. *The Surgeon* **11,** 177–182. ISSN: 1479666X. https://linkinghub.elsevier.com/retrieve/pii/S1479666X13000371 (2013).

96. Byrnes, K. G., Walsh, D., Dockery, P., McDermott, K. & Coffey, J. C. Anatomy of the mesentery: {Current} understanding and mechanisms of attachment. *Seminars in Cell & Developmental Biology.* ISSN: 10849521. https://linkinghub.elsevier.com/retrieve/pii/S1084952118302052 (2018).

97. White, E. J., Cunnane, E. M., McMahon, M., Walsh, M. T., Coffey, J. C. & O'Sullivan, L. Mechanical characterisation of porcine non-intestinal colorectal tissues for innovation in surgical instrument design. *Proceedings of the Institution of Mechanical Engineers, Part H: Journal of Engineering in Medicine* **232,** 796–806. ISSN: 20413033 (2018).

98. Kimmey, M. B., Martin, R. W., Haggitt, R. C., Wang, K. Y., Franklin, D. W. & Silverstein, F. E. Histologic correlates of gastrointestinal ultrasound images. *Gastroenterology* **96,** 433–441. ISSN: 00165085. http://dx.doi.org/10.1016/0016-5085(89)91568-0 (1989).

99. Nylund, K., Hausken, T., Ødegaard, S., Eide, G. E. & Gilja, O. H. Gastrointestinal wall thickness measured with transabdominal ultrasonography and its relationship to demographic factors in healthy subjects. *Ultraschall in der Medizin* **33,** 225–232. ISSN: 01724614 (2012).

100. Marchesini, R., Pignoli, E., Tomatis, S., Fumagalli, S., Sichirollo, A. E., Palma, S. D., Fante, M. D., Spinelli, P., Croce, A. C. & Bottiroli, G. Ex vivo optical properties of human colon tissue. *Lasers in Surgery and Medicine* **15,** 351–357. ISSN: 10969101 (1994).

101. Lai, S. K., Wang, Y. Y., Wirtz, D. & Hanes, J. Micro- and macrorheology of mucus. *Advanced Drug Delivery Reviews* **61,** 86–100. ISSN: 0169409X. http://dx.doi.org/10.1016/j.addr.2008.09.012 (2009).

102. Pelaseyed, T., Bergström, J. H., Gustafsson, J. K., Ermund, A., Birchenough, G. M. H., Schütte, A., van der Post, S., Svensson, F., Rodríguez-Piñeiro, A. M., Nyström, E. E. L., Wising, C., Johansson, M. E. V. & Hansson, G. C. The mucus and mucins of the goblet cells and enterocytes provide the first defense line of the gastrointestinal tract and interact

with the immune system. *Immunological Reviews* **260,** 8–20. ISSN: 01052896. http://doi.wiley.com/10.1111/imr.12182 (2014).

103. Cone, R. A. Barrier properties of mucus. *Advanced Drug Delivery Reviews* **61,** 75–85. ISSN: 0169409X. http://dx.doi.org/10.1016/j.addr.2008.09.008 (2009).

104. Leal, J., Smyth, H. D. C. & Ghosh, D. Physicochemical properties of mucus and their impact on transmucosal drug delivery. *International Journal of Pharmaceutics* **532,** 555–572. ISSN: 03785173. https://linkinghub.elsevier.com/retrieve/pii/S0378517317308736 (2017).

105. Lock, J. Y., Carlson, T. L. & Carrier, R. L. Mucus models to evaluate the diffusion of drugs and particles. *Advanced Drug Delivery Reviews* **124,** 34–49. ISSN: 0169409X. https://linkinghub.elsevier.com/retrieve/pii/S0169409X17302405 (2018).

106. Boegh, M. & Nielsen, H. M. Mucus as a barrier to drug delivery - Understanding and mimicking the barrier properties. *Basic and Clinical Pharmacology and Toxicology* **116,** 179–186. ISSN: 17427843 (2015).

107. Johansson, M. E., Sjövall, H. & Hansson, G. C. The gastrointestinal mucus system in health and disease. *Nature Reviews Gastroenterology and Hepatology* **10,** 352–361. ISSN: 17595045 (2013).

108. Gustafsson, J. K., Ermund, A., Johansson, M. E., Schütte, A., Hansson, G. C. & Sjövall, H. An ex vivo method for studying mucus formation, properties, and thickness in human colonic biopsies and mouse small and large intestinal explants. *American Journal of Physiology - Gastrointestinal and Liver Physiology* **302,** 430–438. ISSN: 01931857 (2012).

109. Lindahl, A., Ungell, A. L., Knutson, L. & Lennernäs, H. *Characterization of fluids from the stomach and proximal jejunum in men and women* 1997.

110. Evans, D. F., Pye, G., Bramley, R., Clark, A. G., Dyson, T. J. & Hardcastle, J. D. Measurement of gastrointestinal pH profiles in normal ambulant human subjects. *Gut* **29,** 1035–1041. ISSN: 00175749 (1988).

111. McDougall, C. J., Wong, R., Scudera, P., Lesser, M. & DeCosse, J. J. Colonic mucosal pH in humans. *Digestive Diseases and Sciences* **38,** 542–545. ISSN: 01632116 (1993).

112. Tutuian, R. & Castell, D. O. Gastroesophageal reflux monitoring: pH and impedance. *GI Motility online (2006).* https://nature.com/gimo/contents/pt1/full/gimo31.html (2006).

113. Singh, H., Ye, A. & Horne, D. Structuring food emulsions in the gastrointestinal tract to modify lipid digestion. *Progress in Lipid Research* **48,** 92–100. ISSN: 01637827. http://dx.doi.org/10.1016/j.plipres.2008.12.001 (2009).

114. Boland, M. Human digestion - a processing perspective. *Journal of the Science of Food and Agriculture* **96,** 2275–2283. ISSN: 10970010 (2016).

115. Stevenson C E RLW. Chemical digestion and absorption: a closer look. https://courses.lumenlearning.com/suny-ap2/chapter/chemical-digestion-and-absorption-a-closer-look/.

116. Akshintala, V. S., Talukdar, R., Singh, V. K. & Goggins, M. The Gut Microbiome in Pancreatic Disease. *Clinical Gastroenterology and Hepatology* **17,** 290–295. ISSN: 15427714. https://doi.org/10.1016/j.cgh.2018.08.045 (2019).

117. Nishida, A., Inoue, R., Inatomi, O., Bamba, S., Naito, Y. & Andoh, A. Gut microbiota in the pathogenesis of inflammatory bowel disease. *Clinical Journal of Gastroenterology* **11,** 1–10. ISSN: 1865-7257, 1865-7265. http://link.springer.com/10.1007/s12328-017-0813-5 (2018).

118. Ley, R. E., Peterson, D. A. & Gordon, J. I. Ecological and evolutionary forces shaping microbial diversity in the human intestine. *Cell* **124,** 837–848. ISSN: 00928674 (2006).

119. Di Pilato, V., Freschi, G., Ringressi, M. N., Pallecchi, L., Rossolini, G. M. & Bechi, P. The esophageal microbiota in health and disease: {Esophageal} microbiota and disease. *Annals of the New York Academy of Sciences* **1381,** 21–33. ISSN: 00778923. http://doi.wiley.com/10.1111/nyas.13127 (2016).

120. Bik, E. M., Eckburg, P. B., Gill, S. R., Nelson, K. E., Purdom, E. A., Francois, F., Perez-Perez, G., Blaser, M. J. & Relman, D. A. Molecular analysis of the bacterial microbiota in the human stomach. *Proceedings of the National Academy of Sciences* **103,** 732–737. ISSN: 0027-8424. http://www.pnas.org/cgi/doi/10.1073/pnas.0506655103 (2006).

121. Zoetendal, E. G., Raes, J., Van Den Bogert, B., Arumugam, M., Booijink, C. C., Troost, F. J., Bork, P., Wels, M., De Vos, W. M. & Kleerebezem, M. The human small intestinal microbiota is driven by rapid uptake and conversion of simple carbohydrates. *ISME Journal* **6,** 1415–1426. ISSN: 17517362. http://dx.doi.org/10.1038/ismej.2011.212 (2012).

122. Eckburg, P. B., Bik, E. M., Bernstein, C. N., Purdom, E., Dethlefsen, L., Sargent, M., Gill, S. R., Nelson, K. E. & Relman, D. A. Microbiology: Diversity of the human intestinal microbial flora. *Science* **308,** 1635–1638. ISSN: 00368075. arXiv: NIHMS150003 (2005).

123. Jandhyala, S. M., Talukdar, R., Subramanyam, C., Vuyyuru, H., Sasikala, M. & Reddy, D. N. Role of the normal gut microbiota. *World Journal of Gastroenterology* **21,** 8836–8847. ISSN: 22192840 (2015).

124. Krishnan, S., Alden, N. & Lee, K. Pathways and functions of gut microbiota metabolism impacting host physiology. *Current Opinion in Biotechnology* **36,** 137–145. ISSN: 18790429. http://dx.doi.org/10.1016/j.copbio.2015.08.015 (2015).

125. Egorov, V. I., Schastlivtsev, I. V., Prut, E. V., Baranov, A. O. & Turusov, R. A. Mechanical properties of the human gastrointestinal tract. *Journal of Biomechanics* **35,** 1417–1425. ISSN: 00219290. arXiv: S0021-9290(02)00084-2 (2002).

126. Lim, Y. J., Deo, D., Singh, T. P., Jones, D. B. & De, S. In situ measurement and modeling of biomechanical response of human cadaveric soft tissues for physics-based surgical simulation. *Surgical Endoscopy and Other Interventional Techniques* **23,** 1298–1307. ISSN: 09302794 (2009).

127. Egorov, V. I., Schastlivtsev, V., Turusov, R. A. & Baranov, A. O. Participation of the intestinal layers in supplying of the mechanical strength of the intact and sutured gut. *European Surgical Research* **34,** 425–431. ISSN: 0014312X (2002).

128. Vanags, I., Petersons, A., Ose, V., Ozolanta, I., Kasyanov, V., Laizans, J., Vjaters, E., Gardovskis, J. & Vanags, A. Biomechanical properties of oesophagus wall under loading. *Journal of Biomechanics* **36,** 1387–1390. ISSN: 00219290. https://linkinghub.elsevier.com/retrieve/pii/S002192900300160X (2003).

129. Yang, W., Fung, T. C., Chian, K. S. & Chong, C. K. Viscoelasticity of esophageal tissue and application of a QLV model. *Journal of Biomechanical Engineering* **128,** 909–916. ISSN: 01480731 (2006).

130. Jia, Z. G., Li, W. & Zhou, Z. R. Mechanical characterization of stomach tissue under uniaxial tensile action. *Journal of Biomechanics* **48,** 651–658. ISSN: 18732380 (2015).

131. Tan, R., Liu, H., Su, G., Zhang, C., Li, H. & Wang, Y. Experimental investigation of the small intestine's viscoelasticity for the motion of capsule robot. *2011 IEEE International Conference on Mechatronics and Automation, ICMA 2011,* 249–253 (2011).

132. O'Connor, A. & O'Moráin, C. Digestive {Function} of the {Stomach}. **32,** 186–191 (2014).

133. Sanders, K. M., Koh, S. D., Ro, S. & Ward, S. M. Regulation of gastrointestinal motility—insights from smooth muscle biology. *Nature Reviews Gastroenterology & Hepatology* **9,** 633–645. ISSN: 1759-5045, 1759-5053. http://www.nature.com/articles/nrgastro.2012.168 (2012).

134. Takaki, M. Gut Pacemaker Cells: the Interstitial Cells of Cajal (ICC). *Journal of Smooth Muscle Research* **39,** 137–161. ISSN: 0916-8737. https://www.jstage.jst.go.jp/article/jsmr/39/5/39{_}5{_}137/{_}article (2003).

135. Hinder, R. A. & Kelly, K. A. Human gastric pacesetter potential. *The American Journal of Surgery* **133,** 29–33. ISSN: 00029610. https://linkinghub.elsevier.com/retrieve/pii/0002961077901878 (1977).

136. O'Grady, G., Du, P., Egbuji, J. U., Lammers, W. J. E. P., Wahab, A., Pullan, A. J., Cheng, L. K. & Windsor, J. A. A novel laparoscopic device for measuring gastrointestinal slow-wave activity. *Surgical Endoscopy* **23,** 2842–2848. ISSN: 0930-2794, 1432-2218. http://link.springer.com/10.1007/s00464-009-0515-2 (2009).

137. Cheng, L. K. Slow wave conduction patterns in the stomach: From Waller's foundations to current challenges. *Acta Physiologica* **213,** 384–393. ISSN: 17481716 (2015).

138. Vilariño, F., Spyridonos, P., Deiorio, F., Vitria, J., Azpiroz, F. & Radeva, P. Intestinal motility assessment with video capsule endoscopy: Automatic annotation of phasic intestinal contractions. *IEEE Transactions on Medical Imaging* **29,** 246–259. ISSN: 02780062 (2010).

139. Vu, H., Echigo, T., Sagawa, R., Yagi, K., Shiba, M., Higuchi, K., Arakawa, T. & Yagi, Y. Detection of contractions in adaptive transit time of the small bowel from wireless capsule endoscopy videos. *Computers in Biology and Medicine* **39,** 16–26. ISSN: 00104825 (2009).

140. Fleckenstein, P. Migrating electrical spike activity in the fasting human small intestine. *The American Journal of Digestive Diseases* **23,** 769–775. ISSN: 15732568 (1978).

141. SK, S. Colonic Motility in Health. *Morgan & Claypool Life Sciences, San Rafael, CA.* https://ncbi.nlm.nih.gov/books/NBK53471/.

142. Rao, S. S., Sadeghi, P., Beaty, J., Kavlock, R. & Ackerson, K. Ambulatory 24-h colonic manometry in healthy humans. *American Journal of Physiology - Gastrointestinal and Liver Physiology* **280,** 629–639. ISSN: 01931857 (2001).

143. O'Grady, G., Du, P., Cheng, L. K., Egbuji, J. U., Lammers, W. J., Windsor, J. A. & Pullan, A. J. Origin and propagation of human gastric slow-wave activity defined by high-resolution mapping. *American Journal of Physiology - Gastrointestinal and Liver Physiology* **299,** 585–592. ISSN: 01931857 (2010).

144. Bassotti, G & Gaburri, M. Manometric investigation of high-amplitude propagated contractile activity of the human colon. *American Journal of Physiology-Gastrointestinal and Liver Physiology* **255,** G660–G664. ISSN: 0193-1857, 1522-1547. https://www.physiology.org/doi/10.1152/ajpgi.1988.255.5.G660 (1988).

145. WorsØe, J., Fynne, L., Gregersen, T., Schlageter, V., Christensen, L. A., Dahlerup, J. F., Rijkhoff, N. J. M., Laurberg, S. & Krogh, K. Gastric transit and small intestinal transit time and motility assessed by a magnet tracking system. *BMC Gastroenterology* **11.** ISSN: 1471230X (2011).

146. Degen, L. P. & Phillips, S. F. Variability of gastrointestinal transit in healthy women and men. *Gut* **39,** 299–305. ISSN: 0017-5749. http://gut.bmj.com/cgi/doi/10.1136/gut.39.2.299 (1996).

147. Maurer, A. H. Gastrointestinal Motility, Part 2: Small-Bowel and Colon Transit. *Journal of Nuclear Medicine Technology* **44,** 12–18. ISSN: 0091-4916. http://tech.snmjournals.org/cgi/doi/10.2967/jnumed.113.134551 (2016).

148. Miller, M. A., Parkman, H. P., Urbain, J.-L. C., Brown, K. L., Donahue, D. J., Knight, L. C., Maurer, A. H. & Fisher, R. S. Comparison of {Scintigraphy} and {Lactulose} {Breath} {Hydrogen} {Test} for {Assessment} of {Orocecal} {Transit} ({Lactulose} {Accelerates} {Small} {Bowel} {Transit}). *Digestive Diseases and Sciences* **42,** 9 (1997).

149. Camilleri, M, Colemont, L. J., Phillips, S. F., Brown, M. L., Thomforde, G. M., Chapman, N & Zinsmeister, A. R. Human gastric emptying and colonic filling of solids characterized by a new method. *American Journal of Physiology-Gastrointestinal and Liver Physiology* **257,** G284–G290. ISSN: 0193-1857. http://www.physiology.org/doi/10.1152/ajpgi.1989.257.2.G284 (1989).

150. Krevsky, B, Maurer, A. H., Niewiarowski, T & Cohen, S. Effect of verapamil on human intestinal transit. *Digestive Diseases and Sciences* **37,** 919–924. ISSN: 0163-2116, 1573-2568. http://link.springer.com/10.1007/BF01300391 (1992).

151. Cummings, J. H., Jenkins, D. J. & Wiggins, H. S. Measurement of the mean transit time of dietary residue through the human gut. *Gut* **17,** 210–218. ISSN: 0017-5749. http://gut.bmj.com/cgi/doi/10.1136/gut.17.3.210 (1976).

152. Deloose, E., Janssen, P., Depoortere, I. & Tack, J. The migrating motor complex: Control mechanisms and its role in health and disease. *Nature Reviews Gastroenterology and Hepatology* **9,** 271–285. ISSN: 17595045 (2012).

153. Takahashi, T. Interdigestive migrating motor complex -its mechanism and clinical importance. *Journal of smooth muscle research = Nihon Heikatsukin Gakkai kikanshi* **49,** 99–111. ISSN: 18848796 (2013).

154. Jouet, P., Coffin, B., Lémann, M., Gorbatchef, C., Franchisseur, C., Jian, R., Rambaud, J. C. & Flourie, B. Tonic and phasic motor activity in the proximal and distal colon of healthy humans. *American Journal of Physiology - Gastrointestinal and Liver Physiology* **274,** 459–464. ISSN: 01931857 (1998).

155. Ferrua, M. J. & Singh, R. P. Modeling the {Fluid} {Dynamics} in a {Human} {Stomach} to {Gain} {Insight} of {Food} {Digestion}. *Journal of Food Science* **75,** R151–R162. ISSN: 00221147. http://doi.wiley.com/10.1111/j.1750-3841.2010.01748.x (2010).

156. Milo, R., Jorgensen, P., Moran, U., Weber, G. & Springer, M. {BioNumbers}—the database of key numbers in molecular and cell biology. *Nucleic Acids Research* **38,** D750–D753. ISSN: 0305-1048, 1362-4962. https://academic.oup.com/nar/article-lookup/doi/10.1093/nar/gkp889 (2010).

157. Malbrain, M. L., De Laet, I. E., De Waele, J. J. & Kirkpatrick, A. W. Intra-abdominal hypertension: Definitions, monitoring, interpretation and management. *Best Practice and Research: Clinical Anaesthesiology* **27,** 249–270. ISSN: 1532169X. http://dx.doi.org/10.1016/j.bpa.2013.06.009 (2013).

158. Balogh, Z., Jones, F., D'Amours, S., Parr, M. & Sugrue, M. Continuous intra-abdominal pressure measurement technique. *American journal of surgery* **188,** 679–684. ISSN: 00029610 (2004).

159. De Keulenaer, B. L., De Waele, J. J., Powell, B. & Malbrain, M. L. What is normal intra-abdominal pressure and how is it affected by positioning, body mass and positive end-expiratory pressure? *Intensive Care Medicine* **35,** 969–976. ISSN: 03424642 (2009).

160. Neumann, P & Gill, V. Pelvic {Floor} and {Abdominal} {Muscle} {Interaction}: {EMG} {Activity} and {Intra}-abdominal {Pressure}. *International Urogynecology Journal* **13,** 125–132. ISSN: 0937-3462, 1433-3023. http://link.springer.com/10.1007/s001920200027 (2002).

161. Miftahof, R. & Akhmadeev, N. Dynamics of intestinal propulsion. *Journal of Theoretical Biology* **246,** 377–393. ISSN: 00225193 (2007).

162. Arshak, A., Arshak, K., Waldron, D., Morris, D., Korostynska, O., Jafer, E. & Lyons, G. Review of the potential of a wireless MEMS and TFT microsystems for the measurement of pressure in the GI tract. *Medical Engineering and Physics* **27,** 347–356. ISSN: 13504533 (2005).

163. Bertuzzi, A, Salinari, S, Mancinelli, R & Pescatori, M. Peristaltic transport of a solid bolus. *Journal of Biomechanics* **16,** 459–464. ISSN: 00219290. https://linkinghub.elsevier.com/retrieve/pii/0021929083900593 (1983).

164. Miftahof, R. & Fedotov, E. Intestinal propulsion of a solid non-deformable bolus. *Journal of Theoretical Biology* **235,** 57–70. ISSN: 00225193 (2005).

165. Miftahof, R. N. The wave phenomena in smooth muscle syncytia. eng. *In silico biology* **5,** 479–498. ISSN: 1386-6338 (Print) (2005).

166. Terry, B. S., Schoen, J. A. & Rentschler, M. E. Characterization and experimental results of a novel sensor for measuring the contact force from myenteric contractions. *IEEE Transactions on Biomedical Engineering* **59,** 1971–1977. ISSN: 00189294 (2012).

167. Terry, B. S., Schoen, J. A. & Rentschler, M. E. Measurements of the contact force from myenteric contractions on a solid bolus. *Journal of Robotic Surgery* **7,** 53–57. ISSN: 18632483 (2013).

168. Terry, B. S., Francisco, M. M., Schoen, J. A. & Rentschler, M. E. Sensor for Measuring the Contact Force From Human Myenteric Contractions for In Vivo Robotic Capsule Endoscope Mobility. *Journal of Medical Devices* **7,** 030911. ISSN: 1932-6181. http://medicaldevices.asmedigitalcollection.asme.org/article.aspx?doi=10.1115/1.4024477 (2013).

169. Terry, B. S., Lyle, A. B., Schoen, J. A. & Rentschler, M. E. Preliminary Mechanical Characterization of the Small Bowel for In Vivo Robotic Mobility. *Journal of Biomechanical Engineering* **133,** 091010. ISSN: 01480731. http://biomechanical.asmedigitalcollection.asme.org/article.aspx?articleid=1430373 (2011).

170. Caliò, R., Camboni, D., Alcaide, J. O., Oddo, C. M., Carrozza, M. C., Menciassi, A., Ciuti, G. & Dario, P. Robotic endoscopic capsule for closed-loop force-based control and safety strategies. *2017 IEEE International Conference on Cyborg and Bionic Systems, CBS 2017* **2018-Janua,** 253–256 (2018).

171. King, M. Experimental models for studying mucociliary clearance. *European Respiratory Journal* **11,** 222–228. ISSN: 09031936 (1998).

172. Terry, B. S., Passernig, A. C., Hill, M. L., Schoen, J. A. & Rentschler, M. E. Small intestine mucosal adhesivity to in vivo capsule robot materials. *Journal of the Mechanical Behavior of Biomedical Materials* **15,** 24–32. ISSN: 17516161. http://dx.doi.org/10.1016/j.jmbbm.2012.06.018 (2012).

173. Varum, F. J., Veiga, F., Sousa, J. S. & Basit, A. W. An investigation into the role of mucus thickness on mucoadhesion in the gastrointestinal tract of pig. *European Journal of Pharmaceutical Sciences* **40,** 335–341. ISSN: 09280987 (2010).

174. Kern, M. D., Ortega Alcaide, J. & Rentschler, M. E. Soft material adhesion characterization for in vivo locomotion of robotic capsule endoscopes: {Experimental} and modeling results. *Journal of the Mechanical Behavior of Biomedical Materials* **39,** 257–269. ISSN: 17516161. https://linkinghub.elsevier.com/retrieve/pii/S1751616114002380 (2014).

175. Dodou, D., Van Den Berg, M., Van Gennip, J., Breedveld, P. & Wieringa, P. A. Mucoadhesive films inside the colonic tube: Performance in a three-dimensional world. *Journal of the Royal Society Interface* **5,** 1353–1362. ISSN: 17425662 (2008).

176. Dodou, D., Girard, D., Breedveld, P. & Wieringa, P. A. Intestinal locomotion by means of mucoadhesive films. *2005 International Conference on Advanced Robotics, ICAR '05, Proceedings* **2005,** 352–359 (2005).

177. Pensabene, V., Valdastri, P., Tognarelli, S., Menciassi, A., Arezzo, A. & Dario, P. Mucoadhesive film for anchoring assistive surgical instruments in endoscopic surgery: In vivo assessment of deployment and attachment. *Surgical Endoscopy* **25,** 3071–3079. ISSN: 14322218 (2011).

178. Dodou, D., Breedveld, P. & Wieringa, P. A. Stick, unstick, restick sticky films in the colon. *Minimally Invasive Therapy and Allied Technologies* **15,** 286–295. ISSN: 13645706 (2006).

179. Sliker, L. J., Ciuti, G., Rentschler, M. E. & Menciassi, A. Frictional resistance model for tissue-capsule endoscope sliding contact in the gastrointestinal tract. *Tribology International* **102,** 472–484. ISSN: 0301679X. http://dx.doi.org/10.1016/j.triboint.2016.06.003 (2016).

180. Kim, J. S., Sung, I. H., Kim, Y. T., Kim, D. E. & Jang, Y. H. Analytical model development for the prediction of the frictional resistance of a capsule endoscope inside an intestine. *Proceedings of the Institution of Mechanical Engineers, Part H: Journal of Engineering in Medicine* **221,** 837–845. ISSN: 09544119 (2007).

181. Woo, S. H., Kim, T. W., Mohy-Ud-Din, Z., Park, I. Y. & Cho, J.-H. Small intestinal model for electrically propelled capsule endoscopy. *BioMedical Engineering OnLine* **10,** 108. ISSN: 1475-925X. http://biomedical-engineering-online.biomedcentral.com/articles/10.1186/1475-925X-10-108 (2011).

182. Baek, N. K., Sung, I. H. & Kim, D. E. Frictional resistance characteristics of a capsule inside the intestine for microendoscope design. *Proceedings of the Institution of Mechanical Engineers, Part H: Journal of Engineering in Medicine* **218,** 193–201 (2004).

183. Zhang, C., Liu, H., Tan, R. & Li, H. Modeling of {Velocity}-dependent {Frictional} {Resistance} of a {Capsule} {Robot} {Inside} an {Intestine}. *Tribology Letters* **47,** 295–301. ISSN: 1023-8883, 1573-2711. http://link.springer.com/10.1007/s11249-012-9980-1 (2012).

184. Lyle, A. B., Luftig, J. T. & Rentschler, M. E. A tribological investigation of the small bowel lumen surface. *Tribology International* **62,** 171–176. ISSN: 0301679X. https://linkinghub.elsevier.com/retrieve/pii/S0301679X12003738 (2013).

185. Lyle, A. B., Terry, B. S., Schoen, J. A. & Rentschler, M. E. Preliminary friction force measurements on small bowel lumen when eliminating sled edge effects. *Tribology Letters* **51,** 377–383. ISSN: 10238883 (2013).

186. Kim, J. S., Sung, I. H., Kim, Y. T., Kwon, E. Y., Kim, D. E. & Jang, Y. H. Experimental investigation of frictional and viscoelastic properties of intestine for microendoscope application. *Tribology Letters* **22,** 143–149. ISSN: 10238883 (2006).

187. Wang, K. D. & Yan, G. Z. Research on measurement and modeling of the gastro intestine's frictional characteristics. *Measurement Science and Technology* **20,** 15803. ISSN: 0957-0233, 1361-6501. http://stacks.iop.org/0957-0233/20/i=1/a=015803?key=crossref.e28536288b99479d9d07ef19d6849144 (2009).

188. Jiwoon Kwon, Sukho Park, Byungkyu Kim & Jong-Oh Park. *Bio-{Material} {Property} {Measurement} {System} for {Locomotive} {Mechanism} in {Gastro}-{Intestinal} {Tract}* in *Proceedings of the 2005 {IEEE} {International} {Conference} on {Robotics} and {Automation}* (IEEE, Barcelona, Spain, 2005), 1303–1308. ISBN: 978-0-7803-8914-4. http://ieeexplore.ieee.org/document/1570295/.

189. Wang, X. & Meng, M. Q. An experimental study of resistant properties of the small intestine for an active capsule endoscope. *Proceedings of the Institution of Mechanical Engineers, Part H: Journal of Engineering in Medicine* **224,** 107–118. ISSN: 09544119 (2010).

190. Kwon, J., Cheung, E., Park, S. & Sitti, M. Friction enhancement via micro-patterned wet elastomer adhesives on small intestinal surfaces. *Biomedical Materials* **1,** 216–220. ISSN: 17486041 (2006).

191. Xiaona Wang & Meng, M.-H. *Study of {Frictional} {Properties} of the {Small} {Intestine} for {Design} of {Active} {Capsule} {Endoscope}* in *The {First} {IEEE}/{RAS}-{EMBS} {International} {Conference} on {Biomedical} {Robotics} and {Biomechatronics}, 2006. {BioRob} 2006.* (IEEE, Pisa, Italy, 2006), 124–129. ISBN: 978-1-4244-0040-9. http://ieeexplore.ieee.org/document/1639071/.

192. Bai, J. P. F., Burckart, G. J. & Mulberg, A. E. Literature {Review} of {Gastrointestinal} {Physiology} in the {Elderly}, in {Pediatric} {Patients}, and in {Patients} with {Gastrointestinal} {Diseases}. *Journal of Pharmaceutical Sciences* **105,** 476–483. ISSN: 00223549. https://linkinghub.elsevier.com/retrieve/pii/S0022354915001616 (2016).

193. Salminen, S, Bouley, C, Boutron, M.-C., Cummings, J. H., Franck, A, Gibson, G. R., Isolauri, E, Moreau, M.-C., Roberfroid, M & Rowland, I. Functional food science and gastrointestinal physiology and function. *British Journal of Nutrition* **80,** S147–S171. ISSN: 0007-1145, 1475-2662. https://www.cambridge.org/core/product/identifier/S0007114598001226/type/journal{_}article (1998).

194. Gajendran, M., Loganathan, P., Jimenez, G., Catinella, A. P., Ng, N., Umapathy, C., Ziade, N. & Hashash, J. G. A comprehensive review and update on ulcerative colitis.

Disease-a-Month **65,** 100851. ISSN: 00115029. https://linkinghub.elsevier.com/retrieve/pii/S0011502919300318 (2019).

195. Effinger, A., O'Driscoll, C. M., McAllister, M. & Fotaki, N. Impact of gastrointestinal disease states on oral drug absorption - implications for formulation design - a {PEARRL} review. *Journal of Pharmacy and Pharmacology* **71,** 674–698. ISSN: 00223573. http://doi.wiley.com/10.1111/jphp.12928 (2019).

196. Sasaki, Y, Hada, R, Nakajima, H, Fukuda, S & Munakata, A. Improved localizing method of radiopill in measurement of entire gastrointestinal pH profiles: colonic luminal pH in normal subjects and patients with Crohn's disease. eng. *The American journal of gastroenterology* **92,** 114–118. ISSN: 0002-9270 (Print) (1997).

197. Tojo, R. Intestinal microbiota in health and disease: {Role} of bifidobacteria in gut homeostasis. *World Journal of Gastroenterology* **20,** 15163. ISSN: 1007-9327. http://www.wjgnet.com/1007-9327/full/v20/i41/15163.htm (2014).

198. Liao, Z., Liu, H. & Komaki, R. Target delineation for esophageal cancer. *Journal of Women's Imaging* **5,** 177–186. ISSN: 1084824X (2003).

199. Taddese, A. Z., Slawinski, P. R., Pirotta, M., De Momi, E., Obstein, K. L. & Valdastri, P. Enhanced real-time pose estimation for closed-loop robotic manipulation of magnetically actuated capsule endoscopes. *The International Journal of Robotics Research* **37,** 890–911. eprint: https://doi.org/10.1177/0278364918779132. https://doi.org/10.1177/0278364918779132 (2018).

200. Moshkowitz, M, Hirsch, Y, Carmel, I, Duvdevany, T, Fabian, I, Willenz, E. P. & Cohen, J. A novel device for rapid cleaning of poorly prepared colons. *Endoscopy* **42,** 834–836. ISSN: 0013726X (2010).

201. Johnson, S., Schultz, M., Scholze, M., Smith, T., Woodfield, J. & Hammer, N. How much force is required to perforate a colon during colonoscopy? An experimental study. eng. *Journal of the mechanical behavior of biomedical materials* **91,** 139–148. ISSN: 1878-0180 (Electronic) (2019).

202. Slawinski, P. R., Taddese, A. Z., Musto, K. B., Obstein, K. L. & Valdastri, P. Autonomous Retroflexion of a Magnetic Flexible Endoscope. *IEEE Robotics and Automation Letters* **2,** 1352–1359. ISSN: 2377-3766. http://ieeexplore.ieee.org/document/7852481/ (2017).

203. Faddis, M. N., Blume, W., Finney, J., Hall, A., Rauch, J., Sell, J., Bae, K. T., Talcott, M. & Lindsay, B. Novel, magnetically guided catheter for endocardial mapping and radiofrequency catheter ablation. *Circulation* **106,** 2980–2985. ISSN: 00097322 (2002).

204. Toggweiler, S., Leipsic, J., Binder, R. K., Freeman, M., Barbanti, M., Heijmen, R. H., Wood, D. A. & Webb, J. G. Management of vascular access in transcatheter aortic valve replacement: Part 2: Vascular complications. *JACC: Cardiovascular Interventions* **6,** 767–776. ISSN: 19368798 (2013).

205. Hilai, S. K., Jost Michelsen, W., Driller, J. & Leonard, E. Magnetically Guided Devices for Vascular Exploration and Treatment. *Radiology* **113.** PMID: 4428036, 529–540. eprint: https://doi.org/10.1148/113.3.529. https://doi.org/10.1148/113.3.529 (1974).

206. Ernst, S., Ouyang, F., Linder, C., Hertting, K., Stahl, F., Chun, J., Hachiya, H., Bänsch, D., Antz, M. & Kuck, K.-H. Initial Experience With Remote Catheter Ablation Using a Novel Magnetic Navigation System. *Circulation* **109,** 1472–1475. eprint: https://www.ahajournals.org/doi/pdf/10.1161/01.CIR.0000125126.83579.1B. https://www.ahajournals.org/doi/abs/10.1161/01.CIR.0000125126.83579.1B (2004).

207. Casarella, W. J., Driller, J. & Hilal, S. K. The magnetically guided bronchial catheter of modified POD design: A new approach to selective bronchoscopy. *Radiology* **93,** 930–932 (1969).

208. Edelmann, J., Petruska, A. J. & Nelson, B. J. Estimation-Based Control of a Magnetic Endoscope without Device Localization. *Journal of Medical Robotics Research* **03,** 1850002. ISSN: 2424-905X. http://www.worldscientific.com/doi/abs/10.1142/S2424905X18500022 (2018).

209. Ciuti, G., Valdastri, P., Menciassi, A. & Dario, P. Robotic magnetic steering and locomotion of capsule endoscope for diagnostic and surgical endoluminal procedures. *Robotica* **28,** 199. ISSN: 0263-5747 (2010).

210. Miyasaka, M. & Berkelman, P. Magnetic levitation with unlimited omnidirectional rotation range. *Mechatronics* **24,** 252–264. ISSN: 09574158. http://dx.doi.org/10.1016/j.mechatronics.2014.02.001 (2014).

211. Khalil, H. K. *Nonlinear systems* ISBN: 9780023635410. https://books.google.co.uk/books?id=RVHvAAAAMAAJ (Macmillan Pub. Co., 1992).

212. Siciliano, B., Sciavicco, L., Villani, L. & Oriolo, G. *Robotics: Modelling, Planning and Control* 1st. ISBN: 1846286417, 9781846286414 (Springer Publishing Company, Incorporated, 2008).

213. Petruska, A. J. & Abbott, J. J. Optimal Permanent-Magnet Geometries for Dipole Field Approximation. *IEEE Transactions on Magnetics* **49,** 811–819. ISSN: 0018-9464 (2013).

214. Diller, E., Giltinan, J., Lum, G. Z., Ye, Z. & Sitti, M. Six-degree-of-freedom magnetic actuation for wireless microrobotics. *International Journal of Robotics Research* **35,** 114–128. ISSN: 17413176 (2016).

215. Zhou, J. & Wen, C. *Adaptive backstepping control of uncertain systems: Nonsmooth nonlinearities, interactions or time-variations* (Springer, 2008).

216. Turan, M., Shabbir, J., Araujo, H., Konukoglu, E. & Sitti, M. A deep learning based fusion of RGB camera information and magnetic localization information for endoscopic capsule robots. *International Journal of Intelligent Robotics and Applications* **1,** 442–450. ISSN: 2366-598X. https://doi.org/10.1007/s41315-017-0039-1 (2017).

217. Gabiccini, M., Bracci, A., De Carli, D, Fredianelli, M & Bicchi, A. *Explicit Lagrangian formulation of the dynamic regressors for serial manipulators* in *Proceedings of the XIX Aimeta Congress* (2009).

218. Obstein, K. L., Patil, V. D., Jayender, J., Estpar, R. S. J., Spofford, I. S., Lengyel, B. I., Vosburgh, K. G. & Thompson, C. C. Evaluation of colonoscopy technical skill levels by use of an objective kinematic-based system. *Gastrointestinal Endoscopy* **73,** 315–321.e1. ISSN: 10976779. http://dx.doi.org/10.1016/j.gie.2010.09.005 (2011).

219. Spooner, J. T., Maggiore, M., Ordonez, R. & Passino, K. M. *Stable Adaptive Control and Estimation for Nonlinear Systems- Neural and Fuzzy Approximator Techniques* (John Wiley & Sons, 2002).

220. Sung, H., Ferlay, J., Siegel, R. L., Laversanne, M., Soerjomataram, I., Jemal, A. & Bray, F. Global Cancer Statistics 2020: GLOBOCAN Estimates of Incidence and Mortality Worldwide for 36 Cancers in 185 Countries. *CA: A Cancer Journal for Clinicians* **71,** 209–249. https://acsjournals.onlinelibrary.wiley.com/doi/abs/10.3322/caac.21660 (2021).

221. Joseph, D. A., Meester, R. G., Zauber, A. G., Manninen, D. L., Winges, L., Dong, F. B., Peaker, B. & van Ballegooijen, M. Colorectal cancer screening: Estimated fu-

ture colonoscopy need and current volume and capacity. *Cancer* **122,** 2479–2486. ISSN: 10970142 (2016).

222. Comas, M., Mendivil, J., Andreu, M., Hernández, C. & Castells, X. Long-term prediction of the demand of colonoscopies generated by a population-based colorectal cancer screening program. *PLoS ONE* **11,** 1–13. ISSN: 19326203 (2016).

223. Larsen, S., Kalloo, A. & Hutfless, S. The hidden cost of colonoscopy including cost of reprocessing and infection rate: the implications for disposable colonoscopes. *Gut* **69,** 197–200. ISSN: 0017-5749. https://gut.bmj.com/content/69/2/197 (2020).

224. Spier, B. J., Benson, M., Pfau, P. R., Nelligan, G., Lucey, M. R. & Gaumnitz, E. A. Colonoscopy training in gastroenterology fellowships: determining competence. *Gastrointestinal endoscopy* **71,** 319–324. ISSN: 1097-6779 (Electronic) (2010).

225. Barducci, L., Norton, J. C., Sarker, S., Mohammed, S., Jones, R., Valdastri, P. & Terry, B. S. Fundamentals of the gut for capsule engineers. *Progress in Biomedical Engineering* **2,** 42002. https://doi.org/10.1088/2516-1091/abab4c (2020).

226. Kumar, R. R., Joseph, J., Vidya, P. V., Pournami, C. & John, N. J. Virtual colonoscopy: A plausible alternative to conventional colonoscopy. *TENSYMP 2017 - IEEE International Symposium on Technologies for Smart Cities* (2017).

227. Sliker, L., Ciuti, G., Rentschler, M. & Menciassi, A. Magnetically driven medical devices: A review. *Expert Review of Medical Devices* **12,** 737–752. ISSN: 17452422 (2015).

228. Zhang, Q., Prendergast, J. M., Formosa, G. A., Fulton, M. J. & Rentschler, M. E. Enabling Autonomous Colonoscopy Intervention Using a Robotic Endoscope Platform. *IEEE Transactions on Biomedical Engineering* **68,** 1957–1968 (2021).

229. Peixoto, A., Silva, M., Pereira, P. & Macedo, G. Biopsies in Gastrointestinal Endoscopy: When and How. *GE Portuguese journal of gastroenterology* **23,** 19–27. ISSN: 2341-4545. https://pubmed.ncbi.nlm.nih.gov/28868426https://www.ncbi.nlm.nih.gov/pmc/articles/PMC5580003/ (2015).

230. Simi, M., Gerboni, G., Menciassi, A. & Valdastri, P. Magnetic Torsion Spring Mechanism for a Wireless Biopsy Capsule. *Journal of Medical Devices* **7.** ISSN: 1932-6181. https://doi.org/10.1115/1.4025185 (2013).

231. Hoang, M. C., Le, V. H., Nguyen, K. T., Nguyen, V. D., Kim, J., Choi, E., Bang, S., Kang, B., Park, J.-O. & Kim, C.-S. A Robotic Biopsy Endoscope with Magnetic 5-

DOF Locomotion and a Retractable Biopsy Punch. *Micromachines* **11.** ISSN: 2072-666X. https://www.mdpi.com/2072-666X/11/1/98 (2020).

232. Yim, S., Gultepe, E., Gracias, D. H. & Sitti, M. Biopsy using a Magnetic Capsule Endoscope Carrying, Releasing, and Retrieving Untethered Microgrippers. *IEEE Transactions on Biomedical Engineering* **61,** 513–521 (2014).

233. Martin, J. W., Barducci, L., Scaglioni, B., Norton, J. C. & Winters, C. Robotic Autonomy for Magnetic Endoscope Biopsy Robotic Autonomy for Magnetic Endoscope Biopsy. *IEEE Transactions on Medical Robotics and Bionics* [**under review**]. https://www.dropbox.com/s/wm0bdg3zaxo7ce2/TMRB-06-21-OA-0349_Proof_hi.pdf?dl=0 (2021).

234. Warren, A., Mountney, P., Noonan, D. & Yang, G.-Z. Horizon Stabilized—Dynamic View Expansion for Robotic Assisted Surgery (HS-DVE). *International Journal of Computer Assisted Radiology and Surgery* **7,** 281–288. ISSN: 1861-6429. https://doi.org/10.1007/s11548-011-0603-3 (2012).

235. Lee, H.-C., Jung, C.-W. & Kim, H. C. Real-time endoscopic image orientation correction system using an accelerometer and gyrosensor. *PLOS ONE* **12,** 1–12. https://doi.org/10.1371/journal.pone.0186691 (2017).

236. Sodergren, M. H., Warren, A., Nehme, J., Clark, J., Gillen, S., Feussner, H., Teare, J., Darzi, A. & Yang, G.-Z. Endoscopic horizon stabilization in natural orifice translumenal endoscopic surgery: a randomized controlled trial. *Surgical innovation* **21,** 74–79. ISSN: 1553-3514 (Electronic) (2014).

237. Lee. *Identification and robust control of linear parameter-varying systems* PhD thesis (University of California at Berkeley, 1997), 166. http://citeseerx.ist.psu.edu/viewdoc/download?doi=10.1.1.55.2269{\&}rep=rep1{\&}type=pdf.

238. Apkarian, P. & Noll, D. Nonsmooth H_∞ synthesis. *IEEE Transactions on Automatic Control* **51,** 71–86. ISSN: 00189286 (2006).

239. Shamma, J. & Athans, M. Analysis of gain scheduled control for nonlinear plants. *IEEE Transactions on Automatic Control* **35,** 898–907 (1990).

240. Apkarian, P. Tuning controllers against multiple design requirements. *Proceedings of the American Control Conference,* 3888–3893. ISSN: 07431619 (2013).

241. Apkarian, P., Dao, M. N. & Noll, D. Parametric Robust Structured Control Design. *IEEE Transactions on Automatic Control* **60,** 1857–1869. ISSN: 00189286. arXiv: 1405.4202 (2015).

242. Onaizah, O., Koszowska, Z., Winters, C., Subramanian, V., Jayne, D., Arezzo, A., Obstein, K. L. & Valdastri, P. Guidelines for Robotic Flexible Endoscopy at the Time of COVID-19. *Frontiers in Robotics and AI* **8,** 20. ISSN: 2296-9144. https://www.frontiersin.org/article/10.3389/frobt.2021.612852 (2021).

243. Mitsala, A., Tsalikidis, C., Pitiakoudis, M., Simopoulos, C. & Tsaroucha, A. K. Artificial intelligence in colorectal cancer screening, diagnosis and treatment. A new era. *Current Oncology* **28,** 1581–1607. ISSN: 17187729 (2021).

244. Kumar, G. & Bhatia, P. K. *Comparative Analysis of Software Engineering Models from Traditional to Modern Methodologies* in *2014 Fourth International Conference on Advanced Computing & Communication Technologies* (2014), 189–196.